LUCAS FELIPE FERNANDES BITTENCOURT

REDUÇÃO NA EXPRESSÃO DA PROTEÍNA G3BP1 DE GRÂNULOS DE ESTRESSE SENSIBILIZA CÉLULAS DE GLIOBLASTOMA TRATADAS COM QUIMIOTERÁPICOS

Instituto de Ciências Biológicas

Universidade Federal de Minas Gerais

2019

LUCAS FELIPE FERNANDES BITTENCOURT

REDUÇÃO NA EXPRESSÃO DA PROTEÍNA G3BP1 DE GRÂNULOS DE ESTRESSE SENSIBILIZA CÉLULAS DE GLIOBLASTOMA TRATADAS COM QUIMIOTERÁPICOS

Tese apresentada ao Programa de Pós-Graduação em Biologia Celular do Departamento de Morfologia, do Instituto de Ciências Biológicas, da Universidade Federal de Minas Gerais, como requisito parcial para obtenção do título de Doutor em Ciências.
Área de concentração: Biologia Celular
Orientadora: Dra. Lucíola da Silva Barcelos

Instituto de Ciências Biológicas

Universidade Federal de Minas Gerais

2019

043 Bittencourt, Lucas Felipe Fernandes.
Redução na expressão da proteína G3BP1 de grânulos de estresse sensibiliza células de glioblastoma tratadas com quimioterápicos [manuscrito] / Lucas Felipe Fernandes Bittencourt. – 2019.

125 f. : il. ; 29,5 cm.

Orientadora: Dra. Lucíola da Silva Barcelos.
Tese (doutorado) – Universidade Federal de Minas Gerais, Instituto de Ciências Biológicas. Programa de Pós-Graduação em Biologia Celular.

1. Biologia Celular. 2. Apoptose. 3. Glioblastoma. 4. Bortezomib. 5. Etoposídeo. 6. Autofagia. I. Barcelos, Lucíola da Silva. II. Universidade Federal de Minas Gerais. Instituto de Ciências Biológicas. III. Título.

CDU: 576

Ficha elaborada pela Biblioteca do Instituto de Ciências Biológicas da UFMG

Universidade Federal de Minas Gerais - Instituto de Ciências Biológicas
Programa de Pós-Graduação em Biologia Celular

ATA DA DEFESA DE TESE DE DOUTORADO DE

LUCAS FELIPE FERNANDES BITTENCOURT

209/2019
entrada
2º/2015
2015710064

Às **treze horas** do dia **31 de maio de 2019**, reuniu-se, no Instituto de Ciências Biológicas da UFMG, a Comissão Examinadora da Tese, indicada pelo Colegiado do Programa, para julgar, em exame final, o trabalho final intitulado: **"REDUÇÃO NA EXPRESSÃO DA PROTEÍNA G3BP1 DE GRÂNULOS DE ESTRESSE SENSIBILIZA CÉLULAS DE GLIOBLASTOMA TRATADAS COM QUIMIOTERÁPICOS"**, requisito final para obtenção do grau de Doutor em Biologia Celular. Abrindo a sessão, a Presidente da Comissão, **Dra. Lucíola da Silva Barcelos**, após dar a conhecer aos presentes o teor das Normas Regulamentares do Trabalho Final, passou a palavra ao candidato, para apresentação de seu trabalho. Seguiu-se a arguição pelos examinadores, com a respectiva defesa do candidato. Logo após, a Comissão se reuniu, sem a presença do candidato e do público, para julgamento e expedição de resultado final. Foram atribuídas as seguintes indicações:

Prof./Pesq.	Instituição	Indicação
Dra. Lucíola da Silva Barcelos	UFMG	APROVADO
Dra. Maria Cristina Rodrigues Rangel	USP	APROVADO
Dra. Raquel Gouvêa dos Santos	CDTN	APROVADO
Dra. Elaine Maria de Souza Fagundes	UFMG	APROVADO
Dra. Catherine Maryvette Ropert	UFMG	APROVADO

Pelas indicações, o candidato foi considerado: APROVADO
O resultado final foi comunicado publicamente ao candidato pela Presidente da Comissão. Nada mais havendo a tratar, a Presidente encerrou a reunião e lavrou a presente ATA, que será assinada por todos os membros participantes da Comissão Examinadora. **Belo Horizonte, 31 de maio de 2019.**

Drª. Lucíola da Silva Barcelos (Orientadora) _____

Drª. Maria Cristina Rodrigues Rangel _____

Drª. Raquel Gouvêa dos Santos _____

Drª. Elaine Maria de Souza Fagundes _____

Drª. Catherine Maryvette Ropert _____

Obs: Este documento não terá validade sem a assinatura e carimbo do Coordenador

Prof. Erika Cristina Jorge
Coordenadora do Programa de Pós Graduação em Biologia Celular ICB/UFMG

Dedico esta tese a meus pais, Ana Maria e Valber, e a minha avó Francisca,

sem os quais este trabalho não seria possível.

Agradecimentos

Primeiramente não posso deixar de agradecer a minha orientadora, Drª Lucíola da Silva Barcelos por ter aberto as portas de seu laboratório e me dado a oportunidade de desenvolver este trabalho.

Agradeço aos colaboradores do artigo, Dra. Rosy Azambuja e suas alunas Ana Gabriela Silva e Isabela Brescia pelos ensaios de CAM. À Miriane Dutra e sua orientadora Dra Rafaela Silva pelos ensaios de Real-time. À Dra. Lirlândia Souza e sua aluna Graziele Negreiros-Lima pelos ensaios de Blotting e à Ana Carol Dias e professor Frederico Soriani pelo auxilio nos ensaios com siRNA.

Em seguida, agradeço com um grande carinho e aperto no coração meus incríveis colegas de laboratório, Alan, Mari, Gilmara, Marina, Helder (Hedden + Elder), Polly, Jousie, Camila e Leandro Barbosa. Vocês são pessoas únicas e foi uma honra dividir meus dias com vocês durante estes quatro anos. Muito obrigado!!

Gostaria de agradecer também alguns professores que me influenciaram e me ajudaram de diversas formas ao longo desta jornada, professor Greg, professor Aristóbolo e professora Waleska.

Agradeço também, a minha família belo Horizontina, com quem morei durante os melhores anos de doutorado, Rai, Jeff, André e Carlos Alberto. Nós criamos uma casa juntos e agora somos uma família, indissolúvel e eterna. Muito obrigado pelas experiências incríveis, por todo o apoio, conforto e risadas – e que venham muitas mais.

De coração aberto, agradeço meu namorado Ricardo Augusto, que me deu total suporte durante a escrita desta tese e contribuiu de forma expressiva para o meu bem-estar e felicidade neste último ano.

Saudosamente agradeço meus amigos de floripa, especialmente Rafael Paulo, por sempre me receberem de braços abertos nas férias, me ajudarem e ouvirem sempre que precisei nestes 4 anos.

Por último, mas nunca menos importante, agradeço imensamente meus pais, Ana Maria e Valber por seu incondicional apoio em todas as decisões da minha vida e por contribuírem massivamente para que eu

chegasse no ponto que estou. Vocês nunca mediram esforços em se tratando de educação, e agora, temos o primeiro doutor da família. Muito, muito obrigado por tudo. Amo vocês.

Agradeço também à CAPES, ao CNPq e à FAPEMIG pelo apoio financeiro.

Sumário

Resumo

O glioblastoma multiforme é uma enfermidade de baixa incidência, mas de alta letalidade. Um dos principais problemas no tratamento é a resistência deste tipo de tumor à quimioterapia. Nesta linha, esta tese teve como objetivo estudar uma via de resistência a fármacos, conhecida como formação de grânulos de estresse (GS). Os GS são pequenas organelas citoplasmáticas não membranosas que se formam quando uma célula está sujeita a estresse físico ou químico. Sua função é a de proteger mRNAs essenciais para a sobrevida da célula até que o fator estressor seja retirado ou metabolizado. Sua função fisiológica é clara, porém, em se tratando de tumores, esta resposta é corrompida e exacerbada, causando uma grande resistência aos tratamentos empregados no tratamento do câncer. Neste trabalho, então, utilizamos a metodologia de interferência por RNA para diminuir a expressão da principal proteína enucleadora destes grânulos, a G3BP1. Utilizando desta técnica, conseguimos com sucesso reduzir a formação de GS em células das linhagens tumorais T98G e U87MG quando expostas aos quimioterápicos Bortezomib (inibidor de proteassoma - BZM), Etoposídeo (inibidor da topoisomerase II) e Temozolomida (agente alquilante). Observamos redução na viabilidade de células submetidas à inibição de G3BP1 em relação às não inibidas, para todas as drogas. Para elucidar o que levava estas células a morte, focamos na linhagem U87MG e observamos um aumento nos níveis de apoptose pela técnica de citometria de fluxo utilizando marcação de anexina-V e 7-AAD. Este aumento estava presente em células tratadas com BZM e que haviam tido G3BP1 inibida. Confirmamos o aumento de apoptose pelo ensaio de imunoblotting de caspase 3 cliavada. Em seguida realizamos ensaios para determinar o nível de autofagia das células tratadas. Utilizamos o ensaio de acumulo de lisossomos e observamos aumento indireto de autofagia em U87 tratada com TMZ. Para elucidar este efeito usamos laranja de acridina (AO) em ensaio de vesículas acídicas por time-course, o que revelou aumento no acumulo destas vesículas para ETO e TMZ em 8H para U87 e 10-12H BZM/ETO e TMZ, respectivamente para T98. Como AO já marca lisossomos e autofagossomos maduros, queríamos observar se a expressão de LC3B havia sido modulada, anteriormente a maturação lisossomal. Por citometria de fluxo conseguimos observar aumento na expressão de LC3B para TMZ em 6 e 8H (U87 e T98, respectivamente). Paralelamente, observamos que a inibição de G3BP1 também leva à diminuição de angiogênese induzida por células U87 tratadas com BZM e essa diminuição não VEGF- dependente. Podemos concluir que, autofagia provavelmente tem um papel decisivo na redução de viabilidade de U87 com inibição de GS e tratamento com TMZ. Também concluímos que, a inibição de GS potencializa resposta apoptótica, reduzindo a viabilidade celular e diminui a angiogênese em células da linhagem U87MG tratadas com o quimioterápico BZM.

Palavras-chave: Apoptose, Glioblastoma multiforme, Bortezomib, Etoposiíeo, Temozolomida, Grânulos de estresse, G3BP1, U87MG, T98G, autofagia.

Abstract

Glioblastoma multiforme (GBM) is the most lethal form of gliomas. These astrocytic-derived pathologies have been studied for many years, yet, not actual cure was achieved with regular treatments. New therapies are currently in development to tackle treatment limitations. In this work, we aim to inhibit a stress-related cellular response triggered by chemotherapeutic agents. Thus, non-membranal organelles known as Stress Granules (SGs) allow cells to recruit and protect vital mRNAs during stress and, when conditions improve, release these mRNAs to resume cells normal activities. This SGs are composed of various proteins, being G3BP1, a core element that enucleates and therefore, results in SGs assembly. Interfering in G3BP1 mRNA and protein expression with short-interference RNA, we were able to successfully diminish SGs assembly. Using calculated IC50 of three chemotherapeutic agents (Bortezomib – proteasome inhibitor, Etoposide – Topoisomerase II inhibitor and Temozolomide – alkylating agent) we observed a reduced cell viability with MTT assay when comparing negative controls and G3BP1 knocked down cells. To elucidate how cells were losing viability in a G3BP1-dependent manner we performed the apoptotic hallmark assay Annexin V/7-AAD concerning phosphatidyl serine domains exposition (PS) and necrosis. Negative control BZM treated group displayed no increased apoptosis when comparing to control without drugs, however, G3BP1 silenced BZM group had a significative increased in apoptotic response. Through Caspase 3 protein quantification by immunoblotting confirmed BZM G3BP1 silenced effects, increasing protein quantity when compared to negative BZM treated group and control groups. In order to better comprehend cells viability loss, we performed a lysosomal accumulation assay which revealed increased autophagy in U87 cells treated with TMZ when SGs were impaired. Further on, we assayed a late stage autophagy assay with acridine orange in a time-course regimen, as results we obtained increased acidic vesicles at 8H for U87 treated with ETO and TMZ and 10-12H for T98 treated with BZM/ETO and TMZ, respectively. Based onobtained results we assesses cells LC3B expression, an early autophagic assay, in time-point prior to ones obtained with AO. Our results demonstrated a possible increase in LC3B expression in U87 cells treated TMZ for 6H and in T98 cells treated with ETO and TMZ for 8 hours. In parallel, we observed a reduced VEGF-independent angiogenesis in SG impaired U87 cells treated with BZM. We can conclude that autophagy probably has a pivotal role in reducing cellular viability in SG impaired U87 TMZ-treated cells All data obtained leads to a new and exciting phenomenon of apoptotic potentializing, anti-angiogenic effects in U87MG GBM cells with impaired SGs assembly.

Key words: Apoptosis, Glioblastoma multiforme, Bortezomib, Etoposide, Temozolomide, Stress granules, G3BP1, U87MG, T98G, autophagy

Lista de figuras

Lista de siglas

ANOVA – Analysis of Variance

APAF1 – Apoptotic protease-activating factor 1

BAK – Bcl-2 homologous antagonist killer

BAX – Bcl-2-associated X protein

BSA – Bovine serum albumine

BZM – Bortezomib

CAM – Chick Chorioallantoic Membrane

DISC – Death-inducing signaling complex

DMSO – Dimethyl sulfoxide

DTT – Dithiothreitol

EDTA – Ethylenediamine tetraacetic acid

EIF4E – Eukaryotic translation initiation factor 4E

ETO – Etoposide/Etoposídeo

FADD – FAS-associated protein with death domain

FBS – Fetal bovine sérum

G3BP1 – G3BP Stress Granule Assembly Factor 1

GBM – Glioblastoma multiforme

GNC – gibberellic acid mediated signaling pathway

GS – Grânulos de estresse

hgDMEM – High glucose Dulbecco's Modified Eagle Medium

HIF1 – Hypoxia-inducible factor 1

HSF – Heat-shock transcription factor

IC_{50} – Half maximal inhibitory concentration

ISR – Integrated stress response

miRNA – Micro RNA

mTOR – Mammalian target of rapamycin

MTT – 3-4,5 dimethylthiazol-2, 5 diphenyl tetrazolium bromide

NaF – Sodium fluoride

PBS – Phosphate-buffered saline

PERK – protein kinase RNA-like endoplasmic reticulum kinase pathway

PI – Propidium iodide

PMSF – Phenylmethylsulfonyl fluoride

qPCR – Quantitative PCR

RISC – RNA-induced silencing complex

RT-PCR – Reverse transcription polymerase chain reaction

SG – Stress granules

siRNA – Short interference RNA

TIA-1 – TIA1 Cytotoxic Granule Associated RNA Binding Protein

TMZ – Temozolomide/Temozolomida

VEGF – Vascular endothelial growth factor

Considerações iniciais

A presente tese é apresentada em inglês, com a introdução e parte dos resultados no formato de artigos. Mais precisamente, a tese é composta de (1) um artigo de revisão sobre dados na literatura envolvendo grânulos de estresse (GS), apoptose, autofagia e quimioresistência, (2) um artigo original descrevendo parte dos resultados obtidos durante o período de doutoramento do discente, (3) resultados e metodologia expandidos, contendo objetivos adicionais da tese, e (4) discussão global dos resultados obtidos.

Tendo em vista a grande letalidade do glioblastoma multiforme (GBM), este trabalho visa contribuir para o conhecimento científico crescente acerca de uma das principais vias de resistência a quimioterápicos, os GS. Utilizando a técnica de RNA de interferência, ferramenta que está sendo avaliada em ensaios clínicos para tratamento de pacientes com os mais diversos tipos de câncer, nosso alvo foi inibir a expressão da principal proteína enucleadora dos GS, a G3BP1, a fim de se obter uma possível inibição da formação dos GS em linhagens celulares de GBM e aumentar a sensibilidade das células a quimioterápicos.

Mesmo esta sendo uma enfermidade sem cura conhecida, melhorar a eficiência do tratamento quimioterápico nos pacientes, potencialmente aumentará a expectativa de vida em alguns meses ou anos, bem como permitirá possível remissão do tumor. Dessa forma, os resultados aqui obtidos poderão contribuir com descoberta de novos alvos que permitirão a busca por novos tratamentos e abordagens terapêuticas.

Assim, as hipóteses elaboradas a serem aceitas ou rejeitadas pelos dados experimentais são:

H0 – O *knockdown* da expressão de mRNA e, consequentemente, da expressão da proteína enucleadora de grânulos de estresse G3BP1 reduz a formação de GS e sensibiliza células das linhagens humanas de glioblastoma U87MG e T98G a quimioterápicos.

H1 – O *knockdown* da expressão de mRNA e, consequentemente, da expressão da proteína enucleadora de grânulos de estresse G3BP1 **não** reduz a formação de GS e **não** sensibiliza células das linhagens humanas de glioblastoma U87MG e T98G a quimioterápicos.

Gliomas are the most common type of primary brain tumors. Amongst different types and grades, the most lethal is known as Glioblastoma multiforme, a grade IV astrocyte derived cancer (FURNARI et al., 2007). Despite being relatively rare in comparison with breast or lung cancer, for instance, it is far more lethal (Figure 1). Patients diagnosed with this incurable disease are subjected to severe resection surgery and intense sessions of chemotherapy and radiotherapy. Still, survival rates are of 5% in 5 years post-diagnosis and median of survival is 14,6 months (OHGAKI, 2009). There has been intense research in the scientific community to improve patients further survival and quality of life (OSTROM et al., 2014).

Distribuição proporcional dos dez tipos de câncer mais incidentes estimados para 2018 por sexo, exceto pele não melanoma*

Localização Primária	Casos	%	Homens	Mulheres	Localização Primária	Casos	%
Próstata	68.220	31,7%			Mama Feminina	59.700	29,5%
Traqueia, Brônquio e Pulmão	18.740	8,7%			Cólon e Reto	18.980	9,4%
Cólon e Reto	17.380	8,1%			Colo do Útero	16.370	8,1%
Estômago	13.540	6,3%			Traqueia, Brônquio e Pulmão	12.530	6,2%
Cavidade Oral	11.200	5,2%			Glândula Tireoide	8.040	4,0%
Esôfago	8.240	3,8%			Estômago	7.750	3,8%
Bexiga	6.690	3,1%			Corpo do Útero	6.600	3,3%
Laringe	6.390	3,0%			Ovário	6.150	3,0%
Leucemias	5.940	2,8%			Sistema Nervoso Central	5.510	2,7%
Sistema Nervoso Central	5.810	2,7%			Leucemias	4.860	2,4%

*Números arredondados para múltiplos de 10.

Figure 1 – Cancer estimative in Brazil for the year 2018

Source: (INCA, 2017)

New therapies have been intensively studied and among them the small interfering RNA (siRNA), a common form of RNAi-based therapeutics. Silencing specific genes associated with cancer resistance to chemotherapeutic agents and cancer progression can potentially become a new form of therapy in the near future (KU et al., 2014). Despite clinical limitations such as the lack of specificity of siRNA delivery in tumor sites and its easy degradation during circulation, solutions are constantly being proposed (ALAGIA; ERITJA, 2016). Some of them include new delivery systems that protect siRNA from endogenous nucleases and site-specific injections (MALHOTRA; MITTAL, 2014).

Our research group has recently demonstrated that the inhibition of the phosphorylation of the eukaryotic translation initiation factor 2 *alpha* (eIF2-*alpha*) reduces stress granules (SG) assembly and sensitizes Glioblastoma (GBM) cell lines to the chemotherapeutic agents Bortezomib, a proteasome inhibitor, Etoposide, a topoisomerase II inhibitor, and Cisplatin, an alkylating agent, by enhancing apoptosis (VILAS-BOAS et al., 2016). These results prompt us to pursue the SG assembly as a potential target for new co-adjuvant therapies to treat gliomas. Therefore, we propose to evaluate if and how SG directly contributes to the chemotherapeutic resistance of brain tumor cell lines.

Stress granules have been studied for their role in cancer resistance to chemotherapeutic agents in many cell types (KEDERSHA et al., 1999), but glioma cells. SGs are non-membranous cytoplasmic *foci*, composed of non-translating messenger ribonucleoproteins (mRNPs) that rapidly aggregate in cells exposed to adverse environmental conditions such as chemical and physical stress (BUCHAN, 2014). The polysome disruption and transfer of polysome-released mRNA of housekeeping and stress-related genes into SGs play a resistance to stress role. As stressing factors fades away, SGs enter into a recovery phase by disassembling and all stored mRNAs escape and are selectively translated in polysomes, repairing stress-related cell damage (LAVUT; RAVEH, 2012). The Ras-GTPase-activating protein SH3 domain-binding protein 1 (G3BP1), used as siRNA target in the present work, is an essential RNA-binding protein that dephosphorylates at Ser-149 leading to multimerization and consequent initiation of SG assembly. It has been demonstrated that upon G3BP1 knockdown, SGs formation is essentially abolished (MATSUKI et al., 2013).

The autophagic pathway plays an essential role in the clearance of SGs (figure 2). Autophagy involves an autophagosome, a double-membrane bound structure that forms from extant membrane-bound organelles (CHAN; TANG, 2013). The autophagosome engulfs regions of the cytosol and fuses with the lysosome to become the autophagolysosome where its contents are catabolized (SCORRANO, 2013). Autophagy has been linked to the clearing of the large protein aggregates that feature prominently in several neurodegenerative diseases and SG clearance by diverse mechanisms, such as decapping SG mRNAs,

returning sequestered mRNAs to active translation, and direct 5′ to 3′ digestion of constituent mRNA molecules. The metabolic and homeostatic mechanisms of mRNA translation and degradation likely reflect a very dynamic, complex cycle, of which autophagy is a critical player

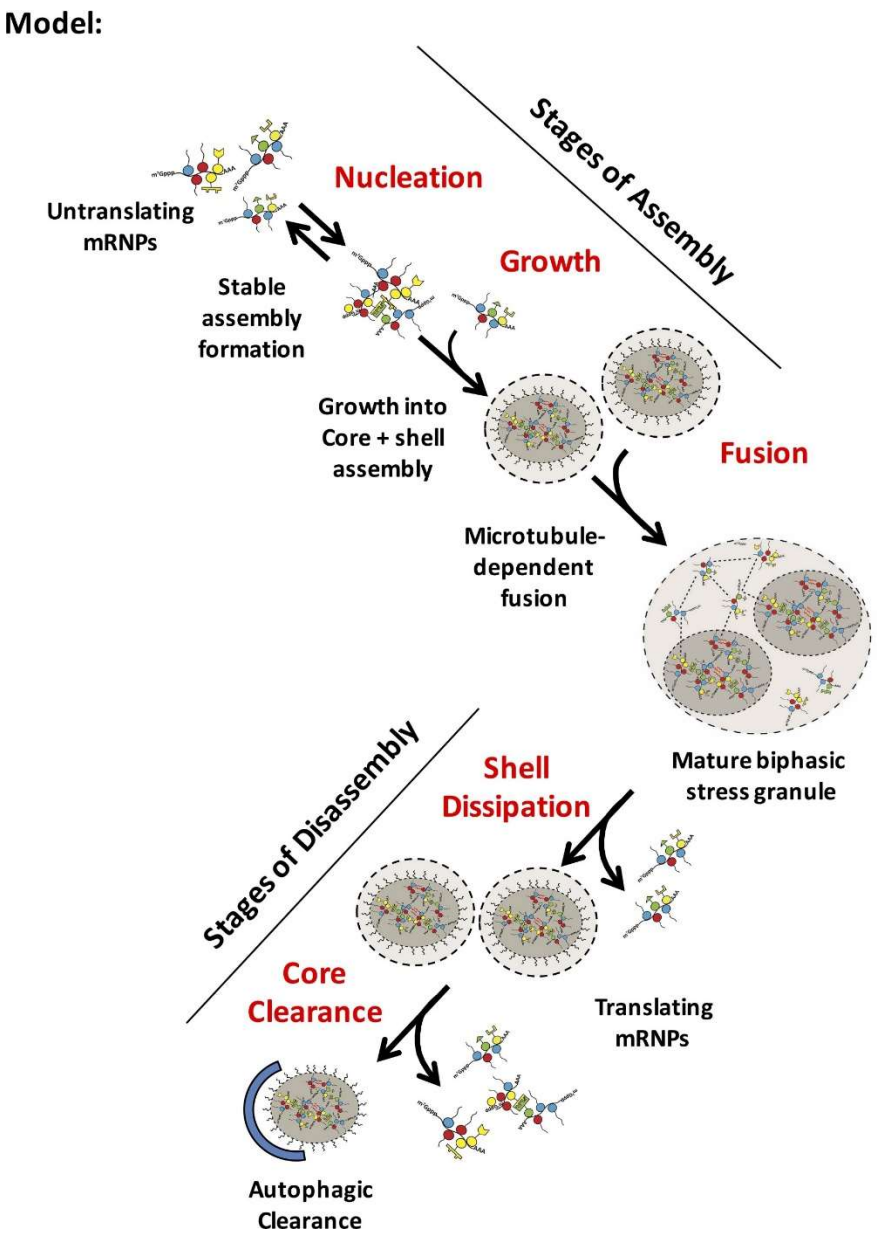

Figure 2. Stress granules dynamics

Source: (WHEELER et al., 2016)

Therefore, we propose to silence the G3BP1 gene to inhibiting SG assembly in human GBM cell lines and assess a possible effect on the sensitization of GBM cell lines to chemotherapeutic agents.

Introduction: The Stress Granule Tri-force, a mini review of a tiny organelle

[1]Bittencourt, L.F.F. and [1] *Barcelos, L.S.

[1]Departamento de Fisiologia e Biofísica, Instituto de Ciências Biológicas, Universidade Federal de Minas Gerais (UFMG), Minas Grais, Brasil.

*Address correspondence to:

Lucíola da Silva Barcelos

Departamento de Fisiologia e Biofísica

Instituto de Ciências Biológicas (ICB)

Universidade Federal de Minas Gerais (UFMG)

Av. Antônio Carlos, 6627 - Pampulha

31270-901 BELO HORIZONTE MG BRASIL

Phone # 55 31 3409 2955 (direct line)

e-mail: luciolasbarcelos@gmail.com

Abstract

The rise of scientific publications that include stress granules (SGs) is on the verge. New and more complex unfolding of SG dynamics influence in many pathologies are highlighting researchers worldwide to invest in the study of these tiny membrane-less organelle. In this mini-review we will discuss and learn from the latest and more prominent articles involving SGs dynamics, their links with apoptotic and autophagic pathways and, mainly, chemoresistance. We will tackle several aspects of SG assembly and how nuclear factors, mRNA binding proteins, cytokinetic inflammatory proteins and circadian cycle can augment or diminish it. The role of SGs in apoptotic response will be examined as we dive into how oxidative stress, cellular stemness, gene modulation Ca2+ and mitochondrial proteins are influenced. Genes related to ALS, glucocorticoids, Syk-binding proteins and valosin are a few of the factors modulated by SGs in autophagic events. These two events are vital in order to comprehend how SGs are utterly essential in cellular chemoresistance and what are the pathways involved and how can we use the in favor of medical advance. Understanding and visualizing this glimpse of literature, we hope to aid in the development of new therapies and drugs to treat those afflicted by cancer, ALS and many other pathologies.

Keywords: Stress granules; cancer; apoptosis; autophagy; inflammation; chemoresistance

Introduction

Stress granules (SGs) are a class of cytoplasmatic macromolecular RNA aggregates alongside with p-bodies (PB), germ granules and neuronal granules. Although many reviews tackled other types of granules [1–4], we will focus mainly on SGs and their role on key cellular events: apoptosis, autophagy and chemoresistance in cancer.

Translational shutdown as a response to stress exposure is a cellular tool that allows cells to survive. This inhibition of protein synthesis is mediated by a phosphorylation mechanism involving the eukaryotic initiation factor 2 (eIF2α) and assembly of the eIF4F complex. As translation arrest happens, small foci of SGs form in the cytoplasm. SGs comprise mRNAs from disassembled polysomes, translation initiation complexes, messenger ribonucleoproteins and RNA-binding proteins [5].

SGs assembly occurs in a very dynamic way, initiating with nanoscopic SG seeds that are formed and recruit nearby seeds via weak electrostatic interactions, interactions with neighboring SG seeds, and coalescence to form microscopically irregular visible SGs. Microscopically visible SGs can fuse to produce larger SGs and after stress release, events that promote SG disassembly may include increase in concentrations of ternary complexes; phosphorylation of eIF4E-binding protein 1 (4E-BP1) by mammalian target of rapamycin (mTOR), releasing the eIF4E block; and reactivation of eIF4A activities. As SGs shrink, the Laplace pressure increases to promote further fusion with adjacent SGs. Over time, fewer and larger SGs appear before they eventually disappear from the cytoplasm [6].

SGs form during acute stress and their presence correlates with the transient translational silencing. SG formation is fast, and it does not require transcription [7]. The stress response is auto-regulated, and the phosphorylation of elF2alpha triggered upon stress induction facilitates translation of proteins that mediate elF2alpha dephosphorylation. The mRNA encoding GADD34 / PPP1R15a, the regulatory subunit of protein phosphatase 1 (PP1), a phosphatase for elF2alpha reactivation that is found in SGs, contains

different uORFs (upstream Open Reading Frames) and therefore, enhances translation upon elF2alpha inactivation [8, 9].

Almost a hundred of translation factors and modulators, splicing factors, nucleases, and a few other molecular functions, are essential SG components. SG composition can be varied according to the nature of the stress stimulus and also change, progressively, during the response. In addition, SGs are not homogenous, and some components can concentrate in microdomains [10, 11]. An example was reported for the endonuclease PMR1, which is normally associated to polysomes. PMR1 interacts with TIA1 (TIA1 Cytotoxic Granule Associated RNA Binding Protein) and is recruited to arsenite-induced SGs in a mature phase [12]. The incorporation of an endonuclease at late stages is compatible with the idea that SGs serve as reparation sites to reactivate translation, and that mRNAs that fail to be reused for translation are destroyed. Virus-induced SGs may show a progressive change in composition, as a consequence of viral activity. Initially, poliovirus-induced SGs contain G3BP, PABP and 4G. However, during later phases of the infection these molecules are cleaved and no longer detected in SGs, which still contain polyadenylated RNA and TIA1 [7]. Finally, SGs may incorporate PBs or PB components at later stages. PBs are mainly composed of Lsm4/CCR4/Dhh1p [13], EDC3 [14], GW182 [15], EDC4 [16], and SGs have mostly TIA1/TIAR [17], MNL51 [10], Pumilio 2 [18],Caprin [19], TDP43[20] and G3BP [21]. Differences in the composition of SGs triggered by distinct stimuli, as well as changes observed along the response undoubtedly reflect distinct physiological conditions that may affect mRNA metabolism and other functions that remain to be unveiled.

Stress granules current knowledge

Even though PubMed lists as many as 235 entries for “stress granules” + “cancer”, we are only scratching the surface on the importance of these aggregates in cancer hallmarks. As no specific cancer is known to mainly depend on SGs to survive, cancer research as a hole is benefiting from all new information about SGs role in tumor progression. As an example, one of the most lethal types of cancer, gliomas, are a rising

hot-spot of studies. Narrowing the criteria to “stress granules” + “glioma” we get only 10 results. Amongst these results, only 5 articles do describe SGs in their content. Thus, the importance of more research on SGs on these types of cancer is evidenced and exalted. Our group is responsible for one of these publications, in which we described the importance of eukaryotic translation initiation factor (eIF2α) in SGs assembly as well as in chemoresistance response in U87MG and C6 cells in vitro (Fabrício de Almeida Souza Vilas-Boas et al. 2016).

Nuclear factors regulate SGs dynamics

As knowledge around SGs evolve, many new publications describe novel molecules, proteins and nuclear factors that regulates positively or negatively SGs assembly/disassembly. The recent discovery of Ataxin-2-like protein (ATXN2L) as a SG down-regulator in gastric cancer (GC) is an example of the evolving knowledge around this subject. Examining clinical follow-ups of GC patients Lin et al., 2019 found that ATXN2L was upregulated in patients with poor prognosis, diminishing survival and increasing tumor recurrence. These findings were supported with in vitro ATXN2L knockdown leading to promoted GC cell migration and invasion via epithelial to mesenchymal transition.

Many other factors influence SGs assembly, including nuclear factors who indirectly affects SGs. The DEAD-Box Helicase 3 X-Linked (encoded by DDX3X gene) has been associated with cell cycle control, apoptosis, and tumorigenesis [24]. By using medulloblastoma single-cell resolution to assess translation efficiency link with DDX3X, researchers revealed that SG hyper-assembly correlated precisely with impaired global translation. SG hyper-assembly and translation impairment driven by mutant DDX3X were rescued by a genetic approach that limited SG assembly and by deletion of the N-terminal low complexity domain within DDX3X. Thus, in addition to a primary defect at the level of translation initiation caused by DDX3X mutation, SG assembly itself contributes to global translation inhibition. These findings a context-dependent survival advantage that must be considered as a possible contributor to tumorigenesis [25, 26].

Another nuclear factor that plays a role in SGs assembly are the adenylate-uridylate-rich elements binding proteins (AUBPs), which controls mRNA stability or translation through their binding to AU-rich elements enriched in the three prime untranslated regions (3'-UTR) of inflammation- and cancer-associated mRNA transcripts. Thus, AUBPs influence mRNAs recruitment into SGs. Altered expression of AUBPs Alterations in the expression and activities of AUBPs and SG assembly have been observed to occur with colorectal cancer (CRC) progression, indicating the significant role AUBP-dependent post-transcriptional regulation plays in controlling gene expression during CRC tumorigenesis. Accordingly, these alterations contribute to the pathological expression of many early-response genes involved in prostaglandin biosynthesis and inflammation, along with key oncogenic pathways. One of these AUBPs, HuR (ELAVL1), that belongs to the Embryonic-Lethal Abnormal Vision in Drosophila (ELAV) family of RBPs [27] can directly bind to miRNAs (such as microRNA-21) and thus prevent the downregulation of their targets [28]. HuR is frequently upregulated in most human cancers and exerts oncogenic functions [29].

Following nuclear factors that influence on mRNA, there is the nucleoporin GLE1, a highly conserved, essential modulator of RNA-dependent DEAD-box proteins that exists as at least two distinct isoforms in human cells. Gle1A is required for proper SG formation, whereas Gle1B functions in mRNA export at the nuclear pore complex. Since Gle1A is required for SG function, it is hypothesized that SG-dependent survival responses are also be Gle1-dependent. Gle1A is required for the sodium arsenite (SA) survival response, and overexpression of Gle1A supports survival response. Overexpression of the SG-component G3BP1 enables a similar response [30].

Inflammatory response is modulated and modulates SGs

Considering that tumors imply in a general inflammatory niche, cytokinetic proteins epithelial cell transforming 2 and Aurora kinase B (AurkB) are localized to stress granules in human astrocytoma cells. Chemical (AZD1152-HQPA) and siRNA inhibition of AurkB results in fewer and smaller stress granules when analyzed using high-throughput fluorescent-based cellomics assays. Using RNA

immunoprecipitation with the known stress granule aggregates enucleating proteins TIA1 and G3BP on astrocytoma cells, revealed that astrocytoma stress granules harbor unique mRNAs for various cellular pathways, including those of cancer hallmarks: cellular migration, metabolism (proliferation), translation, and transcriptional regulation. RNA stress granules are a novel form of epigenetic regulation in astrocytoma cells, which may be targetable by chemical inhibitors and enhance astrocytoma susceptibility to conventional therapy, such as radiation and chemotherapy [31]. Taken in consideration tumor cell populations heterogenicity, it is vital to consider stem cells role in the scenario. The mitotic serine/threonine-protein kinase 6 (Aurora A), has recently been identified to regulate alternative functions like cell polarity, asymmetric cell division, and epithelial to mesenchymal transition in glioma stem cells [32].

One important concept to introduce is the Integrated stress response (ISR), which is activated in different forms of neurodegeneration. Since neuroinflammation is common to many neurodegenerative diseases – including cancer, the endogenously produced product of inflammation, 15-Deoxy-Δ12,14-prostaglandin J2 (15-d-PGJ2), triggers eIF2α phosphorylation thereby activating the ISR, repressing bulk translation, and triggering SG formation [33].

Stress granule formation is important for stress response in normal cells and could lead to chemotherapy resistance in cancer cells. Aberrant SGs dynamics are also known to disrupt proteostasis, affect RNA metabolism, and contribute to neuronal cell death [34]. Formation of SGs varied by zeitgeber time in mouse liver. Moreover, altering circadian regulation by silencing the core circadian gene Brain and Muscle ARNT-Like 1 (BMAL1) significantly increased stress granule dynamics, while the overexpression of Bmal1 decreased them. Increased SG dynamics and formation by transient decrease of BMAL1 coincided with increased resistance to stress-induced cell death. The circadian regulation of SGs was mediated by oscillating eIF2α expression. At zeitgeber time when BMAL1 and eIF2α were at nadir, reduction of unphosphorylated eIF2α could significantly alter the ratio of phosphorylated/total eIF2α and quickly lead

to increased formation of stress granules. Therefore, diurnal oscillating eIF2α connects the circadian cue to a cellular stress response mechanism that is vital for both neurodegeneration and cancer [35].

The pivotal role of SGs in tumor progression becomes more evident as new studies link various previously known molecules and factors with SGs expression. As the influence of multiple actors over SGs expression are brought to light, it is also vital to understand how SGs themselves influence tumor hallmarks.

SGs x Apoptosis

Concerning how SG dynamics influence cellular death, some works describe an increased apoptotic response when chemotherapeutic and other stress agents are employed [36]. Depending on the intensity of physical or chemical stress, cells can activate defense mechanisms or rather activate the apoptotic default program. One of the possible defense mechanisms induced by oxidative stress is the formation of cytoplasmic SGs, a multimolecular aggregate that manifests an arrest of mRNA translation and might avoid the generation of misfolded proteins. Although the execution of apoptotic cell death and SG formation are mechanistically unrelated, AIF (apoptosis induction factor) can be placed in the intersection of the two phenomena. AIF determines the balance between NAD(P)H and glutathione (GSH) under stress conditions and maintains the levels of non-oxidized GSH, which indirectly determines SG formation. When localized in the nucleus, AIF actively participates in DNA digestion [37, 38] utterly resulting in cellular death. When present in mitochondria, AIF catalyzes redox reactions whose optimal and physiologically relevant electron donors and acceptors remain elusive. Both functions of AIF, the pro-apoptotic function and the redox-active, SG-modulatory one, can be separated because they rely on distinct molecular domains [39].

Not only by tempering with SGs core proteins influence in apoptotic response, as the siRNA-knockdown of apoptosis-inducing factor AIF, a mitochondrial protein involved in regenerating intracellular, reduced GSH levels ended up causing a general augmented oxidative stress in the cell and up-regulating eIF2α. Thus, leading to an increased SG-positive cell number in BHK (Baby hamster kidney 21, strain WI2)

infected with West Nile flavivirus, thusly demonstrating a again, a connected pathway between apoptosis and SGs [40].

Stress response relationship with SGs

Using hydrogen peroxide (H202) an oxidative agent, the TIA1 SG-enucleating protein is oxidized, impairing SG assembly in U2OS osteosarcoma cells. Also, when ER-stress is induced with thapsigargin or sodium arsenite SG assembly is up-regulated due eIF2α phosphorylation. Combined, H2O2 and thapsigargin also lead to SG impaired assembly, demonstrating that even though cellular redox imbalance is an important trigger for SG assembly, the lack of functional SG core proteins such as TIA1, affects SGs dynamics. This impairment led to a significative increase in apoptosis in comparison to non-oxidized TIA1 cells thus, linking directly SGs absence to increased cell death [41].

Besides cytosolic events affecting apoptosis, there are nuclear events than influence cell death in a SG-dependent manner. A mutation in progranulin (PGRN) gene exon 1 that introduces a charged amino acid in the hydrophobic core of its signal peptide at residue 9 (named PGRN A9D) causes a mis-sorting in the protein angiogenin (ANG) a stress-response factor and neurodegenerative disease-related protein, from nucleus to cytoplasmic SGs, interacting with each other and activating its cytoprotective stress-response program by cleaving transfer RNAs (tRNAs) to tiRNAs (tRNA-derived, stress-induced small RNAs), thus promoting PGRN A9D cell survival and preventing apoptotic response [42].

Interestingly, not directly related actors like some stem cell maintaining-phenotype factors like Musashi1 (MSI1) gene in CRCs. When up-regulated, MSI1 displays a positive correlation with SGs, therefore, promoting an anti-apoptotic effect [43].

Apoptotic response to chemotherapeutic agents affects SGs

Correlating with drug treatments, the study of Comba et al. 2018, described the relationship of arginylated calreticulin (R-CRT) in apoptosis of human glioma cell lines (HOG, MO59K) treated with Bortezomib

(BZM). The two cell lines had distinctive susceptibility to apoptosis and BZM efficiency was found to be correlated with a subcellular distribution of R-CRT. In MO59K (apoptosis-resistant), R-CRT was confined to SGs formed following BZM treatment. In contrast, HOG (apoptosis-susceptible) treated with BZM showed lower SG formation and higher levels of cytosolic and plasma membrane R-CRT. Increased R-CRT level was associated with enhanced mobilization of intracellular Ca2+ and with sustained apoptosis activation via upregulation of cell death receptor 5 (DR5). R-CRT overexpression in the cytoplasm of MO59K rendered the cells susceptible to BZM-induced cell death.

One another work also demonstrated an increase in apoptotic response when using quercetin and temozolomide (TMZ) in T98 glioblastoma (GBM) cells. These findings were not linked to SGs as TIA1 or G3BP1 proteins were not stained. However, the authors described presence of several cytoplasmatic granules in treated cells. As they relate theses unknown granules to endoplasmic reticulum (ER)-stress we can propose the idea that they were indeed SGs [45].

Similarly, our group demonstrated an apoptotic potentializing (annexin V and cleaved caspase 3) when knocking down G3BP1 enucleating protein in U87 cells treated with the chemotherapeutic agent BZM.

Together, these findings reveal how apoptosis can and is influenced directly and indirectly by SG trigger and impairment.

SGs x Autophagy

The studies involving autophagy and stress granules are recent (less than 10 years) and not very elusive. Case reports about up-regulated SG and autophagic proteins (valosin-containing protein – VCP – CDC48) already suggested an SG clearance-role of autophagy [46].

Exploratory experiments attempt to elucidate autophagic influence in SGs dynamics. Using baker's yeast, 125 genes were identified in a genetic screen that affected the dynamics of SGs. Analyses of mutants,

including CDC48 alleles, provided evidence that SGs can be targeted to autophagic vacuoles, a process named granulophagy. Moreover, stress granule clearance in mammalian cells is reduced by inhibition of autophagy or by depletion or pathogenic mutations in VCP, the human ortholog of CDC48 [47].

Concerning the role of autophagy in SGs clearance, proteomic analyses of Syk-binding (spleen tyrosine kinase) proteins identified several interacting partners also found to be recruited to stress granules. Treating cells with SGs inducers resulted in Syk recruitment to SGs. This recruitment required the phosphorylation of Syk on tyrosine and resulted in the phosphorylation of proteins at or near the stress granule, like the growth factor receptor-bound protein 7 (Grb7). This recruitment promotes the formation of autophagosomes and the clearance of stress granules from the cell once the stress is relieved, enhancing the ability of cells survival [48].

Diseases, stress and autophagy – a SG correlation

As autophagy is knowingly linked to cellular stress, chronic environmental stress and high glucocorticoid trigger mTOR-dependent inhibition of autophagy, leading to Tau (microtubules stabilization proteins) aggregates accumulation and utterly, cell death in P301L-Tau expressing mice and cells. The disturbed cellular homeostasis triggers insoluble accumulation of different RNA binding proteins (RBPs), such as Poly(A)-binding protein (PABP), G3BP1, TIA-1, and FUS, forming SGs and Tau aggregation. An mTOR-driven pharmacological stimulation of autophagy attenuates the high glucocorticoid-driven accumulation of Tau and SG-related proteins as well as the related cell death, suggesting a critical interface between autophagy and the response of the SG-related protein in the neurodegenerative potential of chronic stress and high glucocorticoid [49]. Most observations of SGs involvement with autophagy were described in diseases. One of the most studied pathologies is the amyotrophic lateral sclerosis (ALS). ALS-causing genes, including TARDBP (Transactive DNA-binding protein 43 - TDP-43), FUS (fused in sarcoma gene), MATR3 (Matrin-3), chromosome 9 open reading frame 72 (C9ORF72) and several others fall into two functional categories: RNA-binding/homeostasis and protein-quality control (i.e. autophagy and

proteasome). The RNA-binding proteins tend to be aggregation-prone with low-complexity domains similar to the prion-forming domains of yeast. Mutant forms of TDP-43 and FUS perturb SG dynamics, lengthening their cytoplasmic persistence. Persistent SGs may give rise to intractable aggregates that disrupt neuronal homeostasis, thus failure to clear SGs by autophagic processes may promote ALS pathogenesis [50].The expression of ALS-linked FUSR521C impairs the disassembly of SG under oxidative stress conditions. As FUS-positive SGs colocalize with the classical autophagy marker LC3, up-regulating autophagic dynamics reduced the number of SGs, including FUSR521C positive ones. This augmented clearance attenuated the neurotoxic consequences of mutant FUS expression under oxidative stress conditions that induced SG assembly in neurons. Specifically, neurite fragmentation and cell death were ameliorated in these cells [51].

Very interesting questions that remain not entirely answered were risen by Lee, 2015 :How do cells regulate and harmonize formation/disassembly/autophagic degradation of SGs in response to different stresses in physiology and pathology? Which signals induce autophagic clearance of physiological or pathological SGs as opposed to disassembly of SGs? How are transient or persistent SGs recognized by autophagy machineries? Unravelling the pathways around these questions could lead to new strategies of treatment for ALS and other diseases, such as cancer.

SGs x Chemoresistance

Being able to resist cytotoxic effects of the broad arsenal of chemotherapeutic agents is a main challenge when fighting cancer. Tumors use all sorts of escape routes to dampen pharmacological effects and avoid cellular death. A variety of genes and proteins have their expression modulated in cancer. Previously mentioned ATXN2L, promotes cell invasiveness and oxaliplatin resistance and can be upregulated by epidermal growth factor (EGF) via PI3K/Akt signaling. ATXN2L may be an indicator and therapeutic target in GC, especially for oxaliplatin-based chemotherapy [23].

When considering chemotherapy regimen, it is important to know they affect and target DNA or RNA. Receptor for activated C kinase 1 (RACK1) a protein mediating cell survival and apoptosis, is a component of 5-fluorouracil-induced stress granules. Analysis of 5-fluorouracil metabolites led to the conclusion that SG assembly is caused by RNA, not DNA incorporating 5-fluorouracil metabolites. Incorporation of chemotherapeutics into RNA may result in stress granule assembly with potential significance in chemoresistance [53].

Chemotherapeutics vs SGs

Chemotherapeutic agents' effects are often lessened by SGs formation. When C6 and U87MG cells were exposed to BZM, cisplatin, or etoposide SG formation peaked. However, when forced expression of a dominant negative mutant of eIF2α (eIF2α(DN)) was employed to block this pathway, SG assembly was impaired. Less SGs enhanced chemotherapeutically-induced cell death for all three drugs [54].

Another protein that is directly linked to anti-cancer drugs is MSI1, that promotes human GBM stem cells and enhances chemoresistance when exposed to sublethal stress. The overexpression of MSI1 leads to a protective effect in mitigating drug-induced cell death, thus facilitating the formation of chemo resistant SGs in response to arsenic trioxide (ATO) treatment. SG components, such as protein kinase RNA-activated (PKR) and eIF2α, are dominantly activated and assembled, in cells treated with ATO. The activated PKR and eIF2α contribute to downstream enhancements in stem cell genes, thereby promoting the progression of GBM. By silencing MSI1, the effect was abolished. Thus, MSI1 plays an important role in SG dynamics that grants cancer stem cells chemo resistant stress granules in GBM, in response to stressful conditions (Chen et al., 2018). Intracellular MSI1 SGs also enhances the chemoresistance of CRCs by promotion of stemness phenotype. An analysis of clinical CRC samples indicated that MSI1 expression was prominent in CRC stage IIA and IIB. By critically modulating and promoting development of CD44+ (surface adhesion receptor) stem cells phenotype and also enhancing CRC chemoresistance via formation of SGs [43].

Chemoresistance is a multi-factor phenomenon that thrives with complexity. Cell ability to resist drug treatment is surprising, and, with the pathways and actors being discovered and elucidated, we are on a path to overcome it.

Concluding remarks

Stress granules studies have been arising in the domain of publications. Not only they are been described as mechanisms of chemoresistance but their influence in autophagic and apoptotic pathways is undeniable. As many factors modulate SG dynamics of assembly and disassembly, we can only wonder how influential are these little membrane-less organelles in a variety of pathologies. The answer is being constructed by science, brick by brick and as knowledge is formed, new therapies can be developed and lives, saved.

References

1. De Graeve F, Bessé F (2018) Neuronal RNP granules: From physiological to pathological assemblies. Biol. Chem.

2. Anderson P, Kedersha N (2006) RNA granules. J. Cell Biol. 172:803–808

3. Bassell GJ, Gitler AD, Warren ST, et al (2011) Local RNA Translation at the Synapse and in Disease. J Neurosci. https://doi.org/10.1523/jneurosci.4105-11.2011

4. Voronina E, Seydoux G, Sassone-Corsi P, Nagamori I (2011) RNA granules in germ cells. Cold Spring Harb. Perspect. Biol.

5. Aulas A, Fay MM, Lyons SM, et al (2017) Stress-specific differences in assembly and composition of stress granules and related foci. J Cell Sci. https://doi.org/10.1242/jcs.199240

6. Panas MD, Ivanov P, Anderson P (2016) Mechanistic insights into mammalian stress granule dynamics. J. Cell Biol.

7. Piotrowska J, Hansen SJ, Park N, et al (2010) Stable Formation of Compositionally Unique Stress Granules in Virus-Infected Cells. J Virol. https://doi.org/10.1128/jvi.01320-09

8. Holcik M, Sonenberg N (2005) Translational control in stress and apoptosis. Nat. Rev. Mol. Cell Biol.

9. Gebauer F, Hentze MW (2004) Molecular mechanisms of translational control. Nat Rev Mol Cell Biol. https://doi.org/10.1038/nrm1488

10. Baguet A, Degot S, Cougot N, et al (2007) The exon-junction-complex-component metastatic lymph node 51 functions in stress-granule assembly. J Cell Sci. https://doi.org/10.1242/jcs.009225

11. Tsai NP, Wei LN (2010) RhoA/ROCK1 signaling regulates stress granule formation and apoptosis. Cell Signal. https://doi.org/10.1016/j.cellsig.2009.12.001

12. Yang F, Peng Y, Murray EL, et al (2006) Polysome-Bound Endonuclease PMR1 Is Targeted to Stress Granules via Stress-Specific Binding to TIA-1. Mol Cell Biol. https://doi.org/10.1128/mcb.00090-06

13. Reijns MAM, Alexander RD, Spiller MP, Beggs JD (2008) A role for Q/N-rich aggregation-prone regions in P-body localization. J Cell Sci. https://doi.org/10.1242/jcs.024976

14. Decker CJ, Teixeira D, Parker R (2007) Edc3p and a glutamine/asparagine-rich domain of Lsm4p function in processing body assembly in Saccharomyces cerevisiae. J Cell Biol. https://doi.org/10.1083/jcb.200704147

15. Eulalio A, Tritschler F, Izaurralde E (2009) The GW182 protein family in animal cells: New insights into domains required for miRNA-mediated gene silencing. RNA

16. Jinek M, Eulalio A, Lingel A, et al (2008) The C-terminal region of Ge-1 presents conserved structural features required for P-body localization. RNA. https://doi.org/10.1261/rna.1222908

17. Buchan JR, Muhlrad D, Parker R (2008) P bodies promote stress granule assembly in Saccharomyces cerevisiae. J Cell Biol. https://doi.org/10.1083/jcb.200807043

18. Vessey JP, Vaccani A, Xie Y, et al (2006) Dendritic Localization of the Translational Repressor Pumilio 2 and Its Contribution to Dendritic Stress Granules. J Neurosci. https://doi.org/10.1523/jneurosci.0649-06.2006

19. Khong A, Matheny T, Jain S, et al (2017) The Stress Granule Transcriptome Reveals Principles of mRNA Accumulation in Stress Granules. Mol Cell. https://doi.org/10.1016/j.molcel.2017.10.015

20. Colombrita C, Zennaro E, Fallini C, et al (2009) TDP-43 is recruited to stress granules in conditions of oxidative insult. J Neurochem. https://doi.org/10.1111/j.1471-4159.2009.06383.x

21. Tourrière H, Chebli K, Zekri L, et al (2003) The RasGAP-associated endoribonuclease G3BP assembles stress granules. J Cell Biol. https://doi.org/10.1083/jcb.200212128

22. Vilas-Boas F de AS, da Silva AM, de Sousa LP, et al (2016) Impairment of stress granule assembly via inhibition of the eIF2alpha phosphorylation sensitizes glioma cells to chemotherapeutic agents. J Neurooncol 127:253–260. https://doi.org/10.1007/s11060-015-2043-3

23. Lin L, Li X, Pan C, et al (2019) ATXN2L upregulated by epidermal growth factor promotes gastric cancer cell invasiveness and oxaliplatin resistance. Cell Death Dis. https://doi.org/10.1038/s41419-019-1362-2

24. Chen CY, Chan CH, Chen CM, et al (2016) Targeted inactivation of murine Ddx3x: Essential roles of Ddx3x in placentation and embryogenesis. Hum Mol Genet. https://doi.org/10.1093/hmg/ddw143

25. Valentin-Vega YA, Wang YD, Parker M, et al (2016) Cancer-associated DDX3X mutations drive stress granule assembly and impair global translation. Sci Rep. https://doi.org/10.1038/srep25996

26. Zhang J, Gilbertson RJ, Wang Y-D, et al (2016) Cancer-associated DDX3X mutations drive stress granule assembly and impair global translation. Sci Rep. https://doi.org/10.1038/srep25996

27. Lin NY, Lin CT, Chen YL, Chang CJ (2007) Regulation of tristetraprolin during differentiation of 3T3-L1 preadipocytes. FEBS J 274:867–878. https://doi.org/10.1111/j.1742-4658.2007.05632.x

28. Poria DK, Guha A, Nandi I, Ray PS (2016) RNA-binding protein HuR sequesters microRNA-21 to prevent translation repression of proinflammatory tumor suppressor gene programmed cell death 4. Oncogene. https://doi.org/10.1038/onc.2015.235

29. Legrand N, Dixon DA, Sobolewski C (2019) AU-rich element-binding proteins in colorectal cancer. World J Gastrointest Oncol 11:71–90. https://doi.org/10.4251/wjgo.v11.i2.71

30. Glass L, Wente SR (2019) Gle1 mediates stress granule-dependent survival during chemotoxic stress. Adv Biol Regul. https://doi.org/10.1016/j.jbior.2018.09.007

31. Weeks A, Agnihotri S, Lymer J, et al (2016) Epithelial Cell Transforming 2 and Aurora Kinase B Modulate Formation of Stress Granule-Containing Transcripts from Diverse Cellular Pathways in Astrocytoma Cells. Am J Pathol 186:1674–1687. https://doi.org/10.1016/j.ajpath.2016.02.013

32. Willems E, Lombard A, Dedobbeleer M, et al (2017) The Unexpected Roles of Aurora A Kinase in Gliobastoma Recurrences. Target Oncol. https://doi.org/10.1007/s11523-016-0457-2

33. Tauber D, Parker R (2019) 15-Deoxy-Δ 12,14 -prostaglandin J2 promotes phosphorylation of eukaryotic initiation factor 2α and activates the integrated stress response . J Biol Chem 2:jbc.RA118.007138. https://doi.org/10.1074/jbc.ra118.007138

34. Anderson P, Kedersha N (2002) Visibly stressed: The role of eIF2, TIA-1, and stress granules in protein translation. Cell Stress Chaperones

35. Wang R, Jiang X, Bao P, et al (2019) Circadian control of stress granules by oscillating EIF2α. Cell Death Dis 2019 103 10:215. https://doi.org/10.1038/s41419-019-1471-y

36. Buchan JR, Parker R (2009) Eukaryotic Stress Granules: The Ins and Outs of Translation. Mol. Cell

37. Zhu C, Wang X, Deinum J, et al (2007) Cyclophilin A participates in the nuclear translocation of apoptosis-inducing factor in neurons after cerebral hypoxia-ischemia. J Exp Med. https://doi.org/10.1084/jem.20070193

38. Candé C, Vahsen N, Kouranti I, et al (2004) AIF and cyclophilin A cooperate in apoptosis-associated chromatinolysis. Oncogene. https://doi.org/10.1038/sj.onc.1207279

39. Cande C (2004) Regulation of cytoplasmic stress granules by apoptosis-inducing factor. J Cell Sci. https://doi.org/10.1242/jcs.01356

40. Basu M, Courtney SC, Brinton MA (2017) Arsenite-induced stress granule formation is inhibited by elevated levels of reduced glutathione in West Nile virus-infected cells. PLoS Pathog. https://doi.org/10.1371/journal.ppat.1006240

41. Arimoto-Matsuzaki K, Saito H, Takekawa M (2016) TIA1 oxidation inhibits stress granule assembly and sensitizes cells to stress-induced apoptosis. Nat Commun 7:1–10. https://doi.org/10.1038/ncomms10252

42. Li S, Chen Y, Sun D, et al (2018) Angiogenin Prevents Progranulin A9D Mutation-Induced Neuronal-Like Cell Apoptosis Through Cleaving tRNAs into tiRNAs. Mol Neurobiol. https://doi.org/10.1007/s12035-017-0396-7

43. Chiou GY, Yang TW, Huang CC, et al (2017) Musashi-1 promotes a cancer stem cell lineage and chemoresistance in colorectal cancer cells. Sci Rep. https://doi.org/10.1038/s41598-017-02057-9

44. Comba A, Bonnet L V., Goitea VE, et al (2018) Arginylated Calreticulin Increases Apoptotic Response Induced by Bortezomib in Glioma Cells. Mol. Neurobiol.

45. Jakubowicz-Gil J, Langner E, Bądziul D, et al (2013) Apoptosis induction in human glioblastoma multiforme T98G cells upon temozolomide and quercetin treatment. Tumor Biol. https://doi.org/10.1007/s13277-013-0785-0

46. Mori F, Watanabe Y, Miki Y, et al (2014) Ubiquitin-negative, eosinophilic neuronal cytoplasmic inclusions associated with stress granules and autophagy: An immunohistochemical investigation of two cases. Neuropathology. https://doi.org/10.1111/neup.12075

47. Buchan JR, Kolaitis RM, Taylor JP, Parker R (2013) XEukaryotic stress granules are cleared by autophagy and Cdc48/VCP function. Cell. https://doi.org/10.1016/j.cell.2013.05.037

48. Krisenko MO, Higgins RL, Ghosh S, et al (2015) Syk is recruited to stress granules and promotes their clearance through autophagy. J Biol Chem 290:27803–27815. https://doi.org/10.1074/jbc.M115.642900

49. Silva JM, Rodrigues S, Sampaio-Marques B, et al (2018) Dysregulation of autophagy and stress granule-related proteins in stress-driven Tau pathology. Cell Death Differ.

50. Monahan Z, Shewmaker F, Pandey UB (2016) Stress granules at the intersection of autophagy and ALS. Brain Res 1649:189–200. https://doi.org/10.1016/j.brainres.2016.05.022

51. Ryu HH, Jun MH, Min KJ, et al (2014) Autophagy regulates amyotrophic lateral sclerosis-linked fused in sarcoma-positive stress granules in neurons. Neurobiol Aging. https://doi.org/10.1016/j.neurobiolaging.2014.07.026

52. Lee J-A (2015) Autophagy manages disease-associated stress granules. Oncotarget. https://doi.org/10.18632/oncotarget.5902

53. Kaehler C, Isensee J, Hucho T, et al (2014) 5-Fluorouracil affects assembly of stress granules based on RNA incorporation. Nucleic Acids Res. https://doi.org/10.1093/nar/gku264

54. Vilas-Boas F de AS, da Silva AM, de Sousa LP, et al (2016) Impairment of stress granule assembly via inhibition of the eIF2alpha phosphorylation sensitizes glioma cells to chemotherapeutic agents. J Neurooncol. https://doi.org/10.1007/s11060-015-2043-3

Graphical abstract

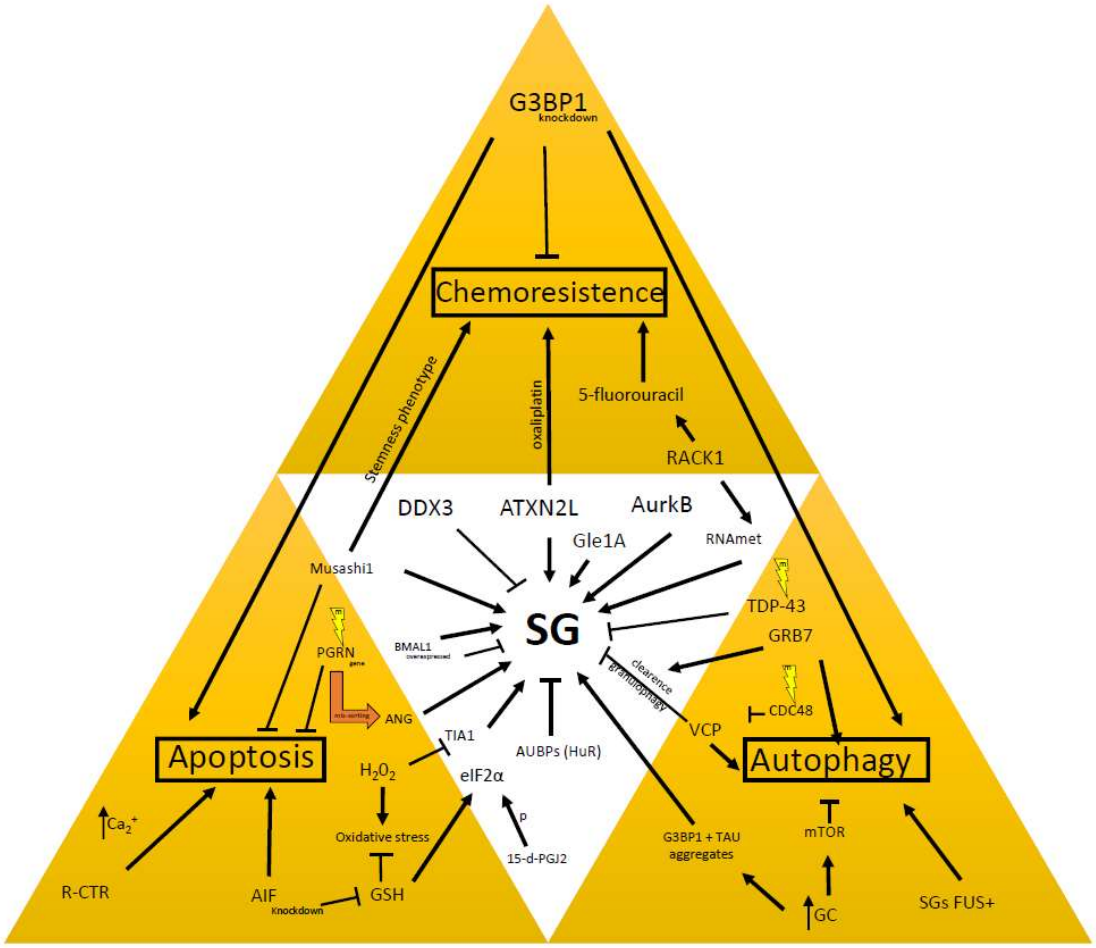

Objetivos

Objetivo geral

Avaliar os efeitos da redução da expressão do mRNA e, consequentemente, da expressão da proteína enucleadora de grânulos de estresse G3BP1 sobre a formação de GS e sobre a sensibilização de células das linhagens humanas de glioblastoma U87MG e T98G aos quimioterápicos Bortezomib (BZM), Etoposídeo (ETO) e Temozolomida (TMZ).

Objetivos específicos

1. Definir a concentração de inibição de 50% (*half maximal inhibitory concentration* - IC_{50}) para os quimioterápicos BZM, ETO e TMZ;
2. Avaliar a dinâmica temporal de formação de GS durante a exposição às drogas BZM, ETO e TMZ;
3. Definir qual é a melhor sequência (dentre três possibilidades) capaz de reduzir a expressão do RNAm de G3BP1 com a técnica de silenciamento por RNA de interferência;
4. Avaliar o efeito da redução da expressão do RNAm de G3BP1 na viabilidade celular da linhagem U87MG tratada com BZM, ETO e TMZ;
5. Avaliar o efeito da redução da expressão do RNAm de G3BP1 no ciclo celular da linhagem U87MG tratada com BZM, ETO e TMZ;
6. Avaliar o efeito da redução da expressão do RNAm de G3BP1 na morte celular induzida pelos quimioterápicos BZM, ETO e TMZ na linhagem U87MG;
7. Avaliar o efeito da redução da expressão do RNAm de G3BP1 na autofagia após tratamento das células da linhagem U87MG com BZM, ETO e TMZ;
8. Avaliar o efeito da redução da expressão do RNAm de G3BP1 na angiogênese induzida pelas células da linhagem U87MG tratadas com BZM, ETO e TMZ.

Methodology

Cell culture

Cells from two glioblastoma multiforme lines (U-87 MG [ATCC® HTB-14™] and T98G [ATCC® CRL-1690™]) were cultured in high-glucose Dulbecco's modified Eagle's medium (hgDMEM) supplemented with antibiotics (Penicillin-Streptomycin, SigmaAldrich®), L-glutamine (GlutaMAX™, ThermoFisher Scientific®) and 10% fetal bovine serum at 37°C in 5% CO2.

Chemotherapeutic treatment

GBM cells were exposed to three different chemotherapeutic agents: Bortezomib (BZM), Etoposide (ETO) and Temozolomide (TMZ) (All from Sigma-Aldrich®, 0,05% in DMSO) diluted in hgDMEM 1% FBS.

Cell viability

Cellular drug resistance was tested with MTT assay. In both cell lines, 10^4 cells were plated on 96-well plates and kept in hgDMEM supplemented with 10% FBS for 24 hours and then subjected to drug treatment in hgDMEM supplemented with 10% FBS for additional 24 hours in cell incubator. The concentrations tested ranged from 5nM - 500µM. After treatment, cells were washed with PBS and added MTT ((3-(4,5-dimethylthiazol-2-yl)-2,5-diphenyl tetrazolium bromide, Sigma-Aldrich®) in a final concentration of 0,2mg/mL for two hours. The solution was withdrawn, and the formed formazan crystals were dissolved in DMSO and read on a plate reader (Versamax™, Molecular Devices®) using a reference wavelength of 570nM (AMERICAN TYPE CULTURE COLLECTION, 2011).

Immunofluorescence assay

Cells from U87MG and T98G cell lines were plated over round glass coverslips in 24-well plates at a concentration of 10^5 cells/well and kept in hgDMEM supplemented with 10% FBS for 24 hours. Briefly, after the desired drug incubation time (4,6,8,10,12,14,16 or 24 hours) in hgDMEM 1% FBS and siRNA transfection (when applicable), cells were washed with PBS and fixed with paraformaldehyde 4% for 10 minutes. Fixed cells were permeabilized and blocked with a 3% Triton X-100 (Sigma-Aldrich®), 10% bovine serum albumin (BSA) PBS solution for 1 hour. Then, cells were incubated with primary anti-G3BP1 antibody (1:150, TT-Y:sc-81940, Santa Cruz Biotechnology®) and/or TIA-1 antibody (1:20, C-20:sc-1751, Santa Cruz Biotechnology®) diluted in staining solution (3% Triton X-100, 1% BSA) overnight at 4°C and Alexa Fluor 488/594 fluorescent secondary antibodies (1:200, Abcam™) for 2 hours at room temperature. We analyzed the DAPI-counterstained slides using confocal microscope (Zeiss™ Axiovert LSM 880, Carl Zeiss, Jena, Germany) equipped with a Plan-APOCHROMAT 63X/1.40 oil DICII objective (Zeiss™, Carl Zeiss, Jena, Germany) and determined the overlap between these proteins as described previously [15]. We analyzed the DAPI-counterstained slides by using filter sets that provide an excitation of 364, 488 and 633 nm with emission band pass (BP) of 437 to 490 nm, 515 to 534 nm and 651 to 704 nm to detect the fluorescence of DAPI, Alexa Fluor® 488 (A-11034) and Alexa Fluor® 633 (A-21050), respectively. Foci analysis was carried out considering de following scores: 4 – 75-100% cells harboring SGs, 3 – 50-75%, 2 – 25-50% and 1 – 0-25%.

Small interference RNA

Cultured U87 cells were plated in a density of 10^5 cells per well in 6-well plate (blotting) or 10^4 in 24-well plates (immunofluorescence and annexin) or 10^3 in 96-well plates (MTT). Cells were kept in hgDMEM supplemented with 10% FBS for 24 hours. Transfection was carried out using specific siRNA for human G3BP1 (TriFecta™ kit, IDT®) and universal negative control - SCRAMBLE at a final concentration of

10pmol with transfection reagent FuGENE 6 (Promega®) in hgDMEM 10% FBS, according to product's manual, for 48 hours.

Real-time PCR

Total ribonucleic acid (RNA) from siRNA transfected cells was isolated with TRIzol (Invitrogen, USA) and treated with DNAse I Amplification Grade (Sigma, USA) following the manufacturer's specifications before quantification using a spectrophotometer (NanoDrop® ND-1000, Thermo Scientific, USA). For reverse transcription polymerase chain reaction (RT-PCR), we used a standard. First, 250 ng of RNA were added on a mix 1 with 300 ng/ul of random primers and 7 µL of MiliQ water up to a final volume of 10 µL. The mix 1 was heated at 70° C for 10 minutes and immediately chilled on ice. Then, another mix was prepared and added to the mix 1, containing 4 µL of 5x buffer solution, 1,25 µL of Deoxynucleotide (10mM), 2 µL of Dithiothreitol, 1 µL of TR4 enzyme and 1,75 µL of MiliQ water. For the RT-PCR, we performed the following program: heating at 42° C for 60 minutes, 70° C for 15 minutes and cooling at 4° C for 10 minutes before a new quantification.

The expression level of the G3BP1 marker was analyzed by quantitative real-time polymerase chain reaction (qPCR) on Life Viia 7 PCR System (Applied Biosystems, USA) using Power up SyBr Green Master Mix (Thermo Fisher Scientific, USA) following all manufacturers' specifications, running 50 cycles in the fast mode. We used the QuantStudio Real-Time PCR Software (Applied Biosystems, USA) and the ΔΔCt method in order to obtain the relative G3BP1 gene expression in RNAi-treated and control human glioblastoma cells. Glyceraldehyde 3-phosphate dehydrogenase (GAPDH) and 18s ribosomal RNA (18s) were used as endogenous controls and control group (CT) as the reference sample. Primer sequences are: G3BP1 Forward CTT TGG GTT TGT CAC TGA GC, Reverse GGT GTT TGC TGT CTT TCT TCA GGT TCC, 18S Forward CGT TCC ACC AAC TAA GAA CG, Reverse CTC AAC ACG GGA AAC CTC AC

and GAPDH Forward GG AGT CCA CTG GCG TCT TCA C, Reverse GAG GCA TTG CTG ATG ATC TTG AGG.

Cell cycle analysis by hypotonic solution of propidium iodide

As previously described (RICCARDI; NICOLETTI, 2006), 10^4 cells were plated in 24-well plates, kept at hgDMEM 10%FBS for 24 hours, transfected with siRNA in hgDMEM 10% FBS for 48 hours and treated with chemotherapeutic agents IC50 in hgDMEM 1% FBS for further 24 hours. Then, cells were harvested with trypsin (0,05%), resuspended in PBS, centrifuged at 200g for 5 minutes and stained with hypotonic PI solution for 1 hour. Stained nuclei were evaluated by flow cytometer at PI-A channel. Data was analyzed by FlowJo.

Annexin V - 7AAD

Platted, siRNA transfected and IC50 drug in hgDMEM 1% FBS treated cells were harvested with trypsin (0,05%) from 24-well plates at 10^4 density, resuspended in 500µl of binding buffer. Incubated with 1µl Annexin V-FITC (BD Biosciences) and 2µl 7AAD (BD Biosciences) for 15 min at 37 °C in cell incubator. Cells were analyzed by flow cytometer. Dot plots were analyzed by FlowJo.

Immunoblotting

Cleaved and total caspase 3 expression in U87 glioblastoma siRNA transfected and IC50 drug treated cells was evaluated by Western blot. Whole cell extracts were obtained 6-well cultured cells seeded at 105 density, kept for 24 hours in hgDMEM 10% FBS and transfected with siRNA in hgDMEM 10% FBS for 48 hours, by using a lysis buffer (0.5% Triton X-100, 100 mM Tris/HCl, pH 8.0, 10% glycerol, 5 mM EDTA, 200 mM NaCl, 1 mM DTT, 1 mM PMSF, 25 mM NaF, 2,5µg/ml leupeptin, 5µg/ml aprotinin, and

1 mM sodium orthovanadate) on ice. Lysates were centrifuged at 13,000g for 10 min at 4 °C and quantified using the Bradford assay reagent (Bio-Rad Hercules). Extracts (20μg) were separated by electrophoresis on a denaturing 10% polyacrylamide-SDS gel and transferred onto nitrocellulose membranes. Membranes were blocked overnight at 4 °C with PBS containing 5% (w/v) nonfat dry milk and 0.1% Tween-20, washed three times with PBS containing 0.1% Tween-20, and then incubated with Caspase 3 and Caspase 3 – cleaved antibody (Cell signaling - 1:1000 final dilution) in phosphate-buffered saline containing 5% (w/v) BSA and 0.1% Tween-20. After washing, membranes were incubated with horseradish peroxidase-conjugated secondary antibody (Santa Cruz Biotechnology - 1:3000 final dilution). Immunoreactive bands were visualized through an enhanced chemiluminescence detection system (GE Healthcare). Cleaved and total caspase 3 levels were quantified by using a densitometric analysis software (ImageJ, Image Processing and Analysis in Java), and these values were normalized to the values of β-actin (1:10000) in the same sample and expressed in arbitrary units (PIETRANI et al., 2018).

Chick chorioallantoic membrane (CAM) assay

The CAM is immunodeficient and highly vascularized, making it a natural in vivo model of tumor growth and angiogenesis. CAM begins to develop by day 3 after fertilization and matures by day 14. The CAM is naturally immunodeficient and highly vascularized, making it an ideal system for implantation of. Briefly, fertilized chicken eggs (*Gallus gallus*) were purchased from Incubator Rivelli (Mateus Leme, MG, Brazil) and maintained in a 37° C incubator under a moist atmosphere with 70% humidity. After three days, a hole was cut in the egg shell, following sealing with tape and incubation of eggs at 37°C. On the 10th day a silicone ring was placed in each CAM and BZM IC50 siG3BP1 and siSCRAMBLE conditioned U87MG media was added. After three days the silicone ring with CAM was removed from the eggs and fixed aldehyde fixation 4% (w/v) in PBS pH 7.4. Then, the CAMs were dehydrated, paraffin embedded and stained with hematoxylin-eosin. Images of forty areas were obtained and blood vessels were quantified

using Zen BLUE software. Histological images were obtained using a 20x objective in Axio Lab A1 (Zeiss, Carl Zeiss) confocal microscope (OLIVEIRA et al., 2012).

Stem cell quantification

Platted U87 cells were harvested with trypsin (0,05%) from 24-well plates at 10^4 density, resuspended in 200µl of binding buffer. Incubated with CD133 antibody (1:200 Miltenyl Biotec®) for 2 hours. Then, cells were stained with secondary antibody AlexaFluor 488 (1:200, Abcam™) for 2 hours. Cells were analyzed by flow cytometer. Dot plots and histograms of total fluorescence were analyzed by FlowJo.

Determination of lysosomal accumulation by cytochemical-staining (AAU)

Determination of Autophagy Arbitrary Units (AAU) is based on three different assays combined. In order to observe lysosomal accumulation caused by drug treatment, cells are subjected to a recovery phase after drug treatment and then experimented. The first assay is Neutral red (NR), used to stain lysosomes. Then. After washes and fixation, MTT and violet crystal (CVS) assays are performed in order to correct and normalize cell quantity.

G3BP1 knocked down and siSCRAMBLE U87 cells were treated with BZM, ETO and TMZ for 24 hours with hgDMEM 1% FBS (v/v) in a 37 °C incubator at a moist atmosphere of 5% carbon dioxide. After treatment, and 48H recovery phase in hgDMEM 10%, cells were stained with 30 µg/mL NR (Sigma-Aldrich) at 37 °C for 2 hours and washed twice with PBS. Next, NR was eluted with a 1% (v/v) alcoholic-based acetic acid fixing solution for 10 min at room temperature and measured at 540 nm using a plate reader (Versamax™, Molecular Devices®), with a wavelength correction set at 800 nm for subtraction of backgrounds. Cell survival rates were normalized to the absorbance values of untreated cells and represented as percentage. Lysosomal accumulation was characterized by the uptake of lysosomotropic dye NR. To calculate AAU, the NRU survival rate was normalized to the mean of the MTT and CVS survival rates according to the formula:

$$AAU = \left\{ \frac{x_a}{\left[x_b + x_c \right] / 2} \right\}$$

where x_a, x_b, and x_c were respectively the survival rates measured by NRU, CVS, and MTT assays. (MARTINS et al., 2013).

Acidic vesicles detection by acridine orange staining and flow cytometry

Measurement of indirect autophagy by acidic vesicles detection was performed by platting 10^5 cells (T98 and U87) and in hgDMEM 10% FBS. On the next day, cells were treated with chemotherapeutic agents (BZM, ETO and TMZ) in hgDMEM 1% FBS, at a time-course regimen (2,4,6,8,10,12,14 and 16 hours). After incubation cells were washed in PBS and a solution of acridine orange hemi(zinc chloride) salt (1µg/mL, Sigma-Aldrich®) was added for 15 minutes, than withdrawn and replaced with DMEM 1% FBS. Positive control was rapamycin (1µM, Sigma-Aldrich®). Images were quickly acquired with EVOS FL Cell Imagining System™ (ThermoFisher Scientific®) and cells were detached and resuspended in FACS buffer for flow cytometry analysis (BD Accuri™ C6 Plus, BD Biosciences®). Images were analyzed by quantification of green/red channels using ImageJ®. Flow cytometry data was analyzed by FL3(PE)/FL1(FITC) ratio mean on fluorescence intensity of positive events in FlowJo VX® software.

LC3 protein detection

Cells were plated on round glass coverslips in 24-well plates at concentration of 10^5 cells (T98 and U87) and kept in hgDMEM 10% FBS. Briefly, after the desired incubation time (4,6,8,10,12,14 and 16 hours), cells were washed in PBS, fixed with paraformaldehyde 4% for 10 minutes and cold-ice methanol for additional 10 minutes. Prior to antibody phase, cells were permeabilized with a 3% PBS solution of Triton X-100 (Sigma-Aldrich®) for 10 minutes and blocked with BSA for 1 hour. Microtubule-associated protein 1A/1B-light chain 3 (LC3) was detected using a primary antibody anti-LC3 (1:100, Anti-LC3B 1mg/ml, L7543 SIGMA, Sigma-Aldrich®) overnight at 4°C and secondary antibody Alexa 488 (1:200, ThermoFisher Scientific®) for 2 hours at room temperature. After staining, cells were resuspended in FACS

buffer for flow cytometry analysis (BD Accuri™ C6 Plus, BD Biosciences®). Flow cytometry data was analyzed by obtaining mean of FITC fluorescence of gated cells with FlowJo® VX software

Statistical analysis

Statistical analysis was performed using GraphPad Prism® or SPSS Statistics version 20. The strength of linear correlation analysis was calculated by Pearson's coefficient (r). To perform comparative statistical analysis, we first analyzed the normal distribution of data according to Kolmogorov-Smirnoff test. Next, we performed pair-wise comparisons for independent samples using the parametric or non-parametric tests T-student or Mann-Whitney, respectively. Outliers were removed by ROUT method (Q = 1)(BROWN; MOTULSKY, 2006). In case of multiple comparisons, we performed one-way analysis of variance (ANOVA) with Dunnett's T3, Tukey or Bonferroni post-hoc tests, depending on homogeneity of variance. We analyzed data obtained from at least 3 independent experiments and expressed as mean values ± error standard. As statistically significant, we considered P values lower than 0.05. The significance levels relative to control were described with asterisks above bars and for multiple or pair comparisons according to what is indicated by lines.

Results - G3BP1 knock-down sensitizes U87 glioblastoma cell line to Bortezomib by inhibiting stress granules assembly and potentializing apoptosis

[1]Bittencourt, L.F.F., 1Dutra, M.F., [2]Negreiros-Lima, G.L., [3]Silva, A.G., [3]Brescia, A., [1]Dias, A.C.F., [1]Silva, R.F., [2]Sousa, L.P., [3]Ribeiro, R.I.M.A., [4]Martins, W.K., [1]Barcelos, L.S.

[1]Departamento de Fisiologia e Biofísica, Instituto de Ciências Biológicas, Universidade Federal de Minas Gerais (UFMG), Minas Grais, Brasil. [2]Faculdade de Farmácia, Universidade Federal de Minas Gerais, Minas Grais, Brasil. [3]Laboratório de Patologia Experimental, Universidade Federal de São João del-Rei (UFSJ), Minas Gerais, Brasil. [4]Universidade Anhanguera de São Paulo, Pós-graduação Stricto-sensu e Pesquisa, São Paulo, Brasil.

Address correspondence to:

Lucíola da Silva Barcelos

Departamento de Fisiologia e Biofísica

Instituto de Ciências Biológicas (ICB)

Universidade Federal de Minas Gerais (UFMG)

Av. Antônio Carlos, 6627 - Pampulha

31270-901 BELO HORIZONTE MG BRASIL

Phone # 55 31 3409 2955 (direct line)

e-mail: luciolasbarcelos@gmail.com

ABSTRACT

Glioblastoma multiforme (GBM) is the most lethal form of gliomas. New therapies are currently in development to tackle treatment limitations such as chemotherapy resistance. One mechanism of resistance may be the stress granules (SG) assembly, a stress-related cellular response that allows cells to recruit and protect mRNAs during stress. SG are composed of various proteins, being G3BP1 a core element that enucleates and results in SG assembly. Here, we aimed to evaluate the effects of inhibiting the G3PB1 expression in the chemotherapeutical-induced cell death of the U87 glioblastoma cell line. Interfering in G3BP1 mRNA and protein expression with short-interference RNA, we were able to diminish SG assembly successfully. Using Bortezomib (BZM), a proteasome inhibitor, we observed reduced cell viability in the MTT assay when compared to the vehicle control. By staining cells with Annexin V/7-AAD and analyzing by flow cytometry, we observed that when G3BP1 was knocked-down, the BZM-treated cells had a significant increase in the apoptotic response. Corroborating this data, we observed increased Caspase-3 activation in the BZM-treated and G3BP1-knocked-down cells when compared to vehicle-treated and scramble-transfected cells, as evaluated by immunoblotting. Worth mentioning, the conditioned culture medium of G3BP1-knocked-down cells inhibited the angiogenesis in the chorioallantoic membrane in vivo assay when compared to controls. Our data suggest G3BP1 knock-down diminishes SG formation and stimulates BZM-induced apoptosis of U87 in vitro, in addition to inhibiting glioblastoma-induced angiogenesis in vivo.

Keywords: Stress granules, G3BP1, Glioblastoma multiforme, Bortezomib, Apoptosis, Angiogenesis.

INTRODUCTION

Gliomas are the most common type of human primary brain tumors. The most lethal form is the glioblastoma multiforme (GBM), a class IV astrocyte-derived cancer which ranges in age-adjusted incidence rate from 0.59 to 3.69 per 100,000 persons depending on reporting country/organization [1].

Despite being relatively rare in comparison to breast or lung cancer, it is far more lethal. Survival rates in 5 years post-diagnosis are 5% with a survival median of 5 to 8 months [2]. New therapies, such as the small interfering RNA (siRNA), a common form of RNAi-based therapeutics, have been intensively investigated [3]. Silencing specific genes associated with cancer chemotherapy resistance and tumor progression can be potentially used as a novel antitumoral strategy in the near future [4, 5].

The stress granules (SG) have been studied for their role in cancer resistance to chemotherapy [6]. They are non-membranous cytoplasmic foci, composed of mRNA-protein complexes (mRNP), that rapidly aggregate in cells exposed to adverse environmental conditions, such as chemical and physical stresses, by then inhibiting protein synthesis [7]. Our research group has recently demonstrated the rat C6 and human U87 cell lines when exposed to Bortezomib, Cisplatin, or Etoposide assembly SG in an eIF2α-dependent manner. The forced expression of a dominant negative mutant of eIF2α enhanced the chemotherapeutically-induced cell death [8]. Worth mentioning, the knock-down of core SG enucleating proteins, such as G3BP1 or TIA-1, has been shown to impair SG assembly and diminishes tumor aggressiveness of some cancer cells [9, 10, 11]. However, there is no current data in the literature about the effect of knocking-down SG enucleating proteins on GBM.

In the present study, we aimed to evaluate the effects of knocking-down the G3BP1 expression by siRNA strategy towards SG assembly using U87 GMB cell line, which were exposed to the chemotherapeutic Bortezomib (BZM). BZM is a selective proteasome inhibitor approved by the United States Food and Drug Administration for treating several types of tumors [12], induces growth arrest and apoptosis in glioma cell lines [13] and ovarian, prostate, and head and neck squamous cell cancers [14]. However, the effect of BMZ on GBM seems to be quite restricted, limiting its application to the association with Temozolomide in the clinical practice [15].

We hypothesized that the inhibition of SG assembly by silencing the expression of the core enucleating protein G3BP1 potentializes BZM-induced cell death in U87 cells. Also, as angiogenesis is an important hallmark of GBM aggressiveness [16], we also hypothesized that SG inhibition disrupts GBM-induced

angiogenesis. If we are correct, direct inhibition of SG formation could be a good adjuvant strategy to be considered to overcome the chemoresistance observed for GBM.

MATERIALS AND METHODS

Cell culture

Human glioblastoma multiforme cell line U87 [ATCC® HTB-14™] was cultured in high-glucose Dulbecco's modified Eagle's medium (DMEM), supplemented with antibiotics (Penicillin 1000 units – Streptomycin 0.1 mg/L, Sigma-Aldrich®), L-glutamine (GlutaMAX™, ThermoFisher Scientific®) and 10% (v/v) fetal bovine serum (FBS, Cultilab®) in a humidified atmosphere containing 5% CO2 at 37°C .

Chemotherapeutic treatment

GBM cells were exposed to Bortezomib (CAS 179324-69-7 Sigma-Aldrich®) dissolved in DMSO (0.05 M - Sigma-Aldrich®) and diluted in DMEM (Sigma-Aldrich□) supplemented with 1% (v/v) FBS, 1000 units of penicillin and 0.1 mg/L of streptomycin. Of note, in contrast to our previous work where the culture media was supplemented with 10% (v/v) FBS [8], in the present study, U87 cells were exposed to BZM diluted in such a starvation media aiming to better mimicking the low perfused scenario of GBM dysregulated growth [17].

Cell viability and IC50 determination

After 24 h of seeding 104 U87 cells per well in a 96-well plate, we treated cells with BZM at increasing concentrations (10-10 to 10-4 M) and incubated for further 24 hours in a humidified atmosphere containing 5% CO2 at 37°C . To quantify viability, we performed the MTT colorimetric assay, as previously described [18]. Absorbance values were read at 550 nm, using the microplate reader (Versamax™, Molecular Devices®) and a reference wavelength of 570 nm. The IC50 was calculated through linear regression after ROUT outlier exclusion method [19].

Small interference RNA

After seeding U87 cells in DMEM supplemented with 10% (v/v) FBS for 24 hours in a humidified atmosphere containing 5% CO2 at 37°C , the transfection was carried out using specific siRNA for human G3BP1 (TriFecta™ kit, IDT®) and universal negative SCRAMBLE control at a final concentration of 10pmol with transfection reagent FuGENE 6 (Promega®) for 48hours, in DMEM 10% (v/v), according to manufacturer's instructions. After that, the wells were washed, and cells were exposed to BZM or DMSO vehicle diluted in DMEM 1% FBS for the required time depending on the purpose.

Immunofluorescence assay

U87 cells were seeded at 105 cells per well in 24-well plate containing round cover glass and treated with BZM (20nM). Supernatants were washed out, and adherent cells were immunoassayed after aldehyde fixation 4% (w/v) in PBS pH 7.4 for 10 minutes. After washing and blocking, we incubated cells with primary monoclonal antibodies against G3BP1 (clone TT-Y) and TIA-1 (clone C-20) (both from Santa Cruz Biotechnology®) according to manufacturer's instructions, and then with goat Alexa Fluor-coupled antibodies (Molecular Probes) against mouse IgG (Alexa 633) or rabbit IgG (H+L) (Alexa 488), respectively. We analyzed the DAPI-counterstained slides using confocal microscope LSM 880 equipped with a Plan-APOCHROMAT 63X/1.40 oil DICII objective (Carl Zeiss). The overlap between target proteins was determined as described previously [19]. The foci quantity score was carried out considering: 4 – 75-100% cells harboring SGs, 3 – 50-75%, 2 – 25-50% and 1 – 0-25%.

Real-time PCR

Total RNA from G3BP1 and SCRAMBLE siRNA-transfected U87 cells (seeded at 106 cells per well in 6-well plates) was isolated with TRIzol (Invitrogen®) and treated with DNAseI (Sigma Aldrich®) following the manufacturer's specifications. The expression level of the G3BP1 was analyzed by quantitative real-time polymerase chain reaction (qPCR) on Life Viia 7 PCR System (Applied

Biosystems®) using Power up SyBr Green Master Mix (Thermo Fisher Scientific®) following manufacturers' specifications. We used the QuantStudio Real-Time PCR Software (Applied Biosystems®) and the ΔΔCt method in order to obtain the relative G3BP1 gene expression. GAPDH and 18s ribosomal RNA were used as endogenous controls, and scramble control group (CT) as the reference sample. Primer sequences were: G3BP1 Forward CTTTGGGTTTGTCACTGAGC, Reverse GGTGTTTGCTGTCTT TCTTCAGGTTCC, 18S Forward CGTTCCACCAACTAAGAACG, Reverse CTCAAC ACGGGAAACCTCAC, and GAPDH Forward GGAGTCCACTGGCGTCTTCAC, Reverse GAGGCATTGCTGATGATCTTGAGG.

Annexin V / 7-AAD staining and flow cytometry

G3BP1 and SCRAMBLE siRNA-transfected U87 cells (seeded at 104 cells per well in 24-well plate) were treated with BZM (20nM) for 24 hours. Two-color flow cytometry was applied to detect the Annexin V-FITC binding and the exclusion of 7-AAD. The cells Annexin V+ and 7-AAD- represented the early apoptotic cells, whereas the cells positive for both markers represented the late apoptotic cells. After the treatment, cells from the supernatant and the adhered ones were collected and washed twice with PBS. A total of 1 µL of Annexin V-FITC and 7 µL of 7-AAD (both from BD Biosciences®) were added in 500 µL binding buffer, and samples were maintained at room temperature for 15 min in the dark. At least 10,000 events were acquired (BD FACS CANTO II™) and data was analyzed using the FlowJo® VX software.

Immunoblotting

Pro- and cleaved caspase-3 expression was evaluated by western blot in siG3BP1 and siSCRAMBLE U87 cells (106 cells per well in 6-well plate) treated with BZM (20nM) for 24 h. Whole cell extracts were lysed in buffer □0.5% (v/v) Triton X-100, 100 mM Tris/HCl, pH 8.0, 10% (v/v) glycerol, 5 mM EDTA, 200 mM NaCl, 1 mM DTT, 1 mM PMSF, 25 mM NaF, 2.5 µg/mL leupeptin, 5 µg/mL aprotinin, and 1

mM sodium orthovanadate on ice. Lysates were centrifuged at 13,000g for 10 min at 4°C and quantified using the Bradford assay reagent (Bio-Rad Hercules). Extracts (20 μg) were fractionated by electrophoresis on a denaturing 10% polyacrylamide-SDS gel and transferred onto nitrocellulose membranes. Membranes were blocked overnight at 4 °C with PBS containing 5% (w/v) nonfat dry milk and 0.1% (v/v) Tween-20 (Sigma-Aldrich), washed three times with PBS containing 0.1% (v/v) Tween-20, and then incubated with primary antibodies against total and cleaved caspase-3 (Cell signaling®) or β-actin (Sigma Aldrich®) diluted 1:1000 and 1:10000 in phosphate-buffered saline containing 5% (w/v) BSA and 0.1% (v/v) Tween-20, respectively. After washing, membranes were incubated with horseradish peroxidase-conjugated secondary antibody (Santa Cruz Biotechnology® - 1:3000 final dilution). Immunoreactive bands were visualized through an enhanced chemiluminescence detection system (GE Healthcare®), and were quantified by using densitometric analysis software (ImageJ®). Values were normalized to the β-actin in the same sample and expressed as arbitrary units [20].

Chick chorioallantoic membrane (CAM) assay

The CAM is immunodeficient and highly vascularized, making it a natural in vivo model of angiogenesis [21]. CAM begins to develop by day 3 after fertilization and matures by day 14. Fertilized chicken eggs (Gallus gallus) were purchased from Incubator Rivelli (Mateus Leme, MG, Brazil) and maintained in a 37C incubator under 70% humidity. After three days, a hole was cut in the eggshell, following sealing with tape and incubation of eggs at 37C. On the 10th day, a silicone ring was placed in each CAM, and BZM siG3BP1 and siSCRAMBLE conditioned U87 media was added. After three days, the silicone ring with CAM was removed from the eggs and submitted to aldehyde fixation 4% (w/v) in PBS pH 7.4. Then, the CAMs were dehydrated, paraffin embedded and stained with hematoxylin-eosin. Images of forty areas were obtained, and blood vessels were quantified using Zen BLUE software. Histological images were obtained using a 20x objective in Axio Lab A1 (Carl Zeiss) confocal microscope. The analysis was carried out blindly by two different researchers.

Statistical analysis

Statistical analysis was performed using GraphPad Prism® 6 or IBM SPSS Statistics version 20. The strength of linear correlation analysis was calculated by Pearson's coefficient (r). The normal distribution of data was analyzed according to the Kolmogorov-Smirnoff test. Next, we performed pair-wise comparisons for independent samples using the parametric or non-parametric tests T-student or Mann-Whitney, respectively. In the case of multiple comparisons, we performed one-way analysis of variance (ANOVA) with Dunnett's T3, Tukey or Bonferroni post-hoc tests, depending on the homogeneity of variance. We analyzed data obtained from at least 3 independent experiments and expressed as mean values ± error standard. As statistically significant, we considered P values lower than 0.05. The significance levels relative to control were described with asterisks above bars and for multiple or pair comparisons according to what is indicated by lines.

RESULTS

Bortezomib treatment leads to transiently SG formation in U87 cells

Before to evaluate SG assembly/disassembly dynamics, we first performed a concentration-response curve of U87 cells exposed to BZM (10-10 to 10-4 M). The IC50 calculated through linear regression after ROUT outlier exclusion method [22] for BZM was 20 nM (Fig. 1 – A and B). This IC50 was employed in all other experiments as a standard concentration.

We attributed not assembled SG or assembled SG depending on G3BP1 cytoplasmic staining in a diffuse or punctuative-foci manner, respectively (Fig. 1C). By analyzing the dynamic of SG formation, we observed rising SG assembly after 2h to a peak of observed assembly at 6h of BZM exposure. Interestingly, this assembly was transient and is not observed anymore at the 8h time-point. However, a lower number of cells transiently reassembled SG between after 8h. No more SG assembly was observed after 12h of BZM exposure (Fig. 1C, bottom panel). Corroborating this data, by flow cytometry analysis,

we observed the cell granularity was significantly increased after BZM treatment compared to vehicle control for both 4h and 6h time-points (Fig. 1D). These findings suggest BZM transiently induces SG assembly.

G3BP1 down-regulation increases U87 cells sensitivity to chemotherapy: apoptosis activation

By down-regulating the G3BP1 expression through siRNA technology we could evaluate the biological response of U87 cells regarding to the induction of stress-related granules (Fig. 2). siRNA transfection allowed us to significantly decrease the G3BP1 expression by almost 80% in U87 cells (Fig. 2A). Accordingly, by decreasing G3BP1 expression, the recruitment of the other known SG core protein TIA-1 to forming foci was remarkably decreased in siG3BP1 transfected cells compared to siSCRAMBLE control (Fig. 2B). Note that in BZM-treated cells there was a remarkable co-localization between TIA-1 and G3BP1, which was lost after G3BP1 silencing.

Since the accumulation of SG is known to be associated with tumor chemoresistance [23], we investigated its relation with apoptosis. Upon BZM treatment there was a significant increase in plasma membrane permeabilization (7-AAD positive cells) as revealed by flow cytometry analysis (Fig. 3A). The proportion of apoptotic cells, characterized by the presence of negatively charged lipids that bind to Annexin V (AV) without losing cytoplasmic membrane integrity, and therefore avoiding cellular incorporation 7-AAD (AV+/7-AAD-), did not increase after BZM treatment in U87 siSCRAMBLE cells. However, by silencing G3BP1, after BZM treatment there was a significant increase in the AV+/7-AAD- population compared to siSCRAMBLE control. Corroborating this data, the expression of cleaved caspase-3 by the treatment with BZM for 24 h. Interestingly, we observed a further significant increase in the cleaved caspase-3 levels in G3BP1-silenced cells treated with BZM (Fig. 3B).

G3BP1 down-regulation induces anti-angiogenic effect of U87 cells

In order to evaluate the effects of G3PB1 knock-down on U87-induced angiogenesis, we collected the U87 cells conditioned culture media (CCM) after 24 h of BZM exposure and applied it onto the chorioallantoic membrane (CAM) of 10-days-fertilized chicken eggs. We observed BZM siSCRAMBLE U87 cells CCM promotes angiogenesis in the CAM in vivo model (Fig. 4). However, we observed a significant decrease in angiogenesis when G3BP1 was silenced, suggesting the down-regulation of G3BP1 and the consequent SG formation in U87 cells impair its ability to induce angiogenesis.

DISCUSSION

SG a part of the integrated stress response (ISR), which combines information from stress sensors and coordinates adaptation to stress. The ISR detects several stressing factors such as amino acids deprivation via GCN2, reticulum stress via PERK [24] and oxidative stress via HRI [17]. Therefore, tumor adapts to this aggressive microenvironment in order to maintain cell growth and resistance to chemotherapeutics [25].

Considering cell growth, some cellular aspects such as hypoxia, hyperosmolarity, and starvation are countered by inefficient and disorganized neovascularization of the peritumoral area [26]. Starved cells alternative is to uncouple glycolysis from oxidative phosphorylation to reduce dysregulation of protein synthesis that causes reticulum stress, an apoptotic trigger [27]. However, uncoupling glycolysis pathway from oxidative phosphorylation causes a marked increase in oxidative stress, activating several antioxidative defense pathways such as NRF2/KEAP1, HIF1, and HSF [28]. Therefore, working with therapy-mimicking cell media (1% FBS) allowed us to better evaluate chemotherapeutic response as well as the SG role in a model closer to actual clinic reality.

Different chemotherapeutic agents such as Bortezomib, Etoposide, and Cisplatin were previously described to cause SG assembly [29]. Also, it has been described some cells such as HeLa, Calu-1, and

MCF-7 cancer cells, can modulate a drug-induced resistance to apoptosis in an SG dependent-manner [30]. In fact, tumor resistance is a severe problem for patients as it renders chemotherapy not as potent as it should be. In this context, inhibiting the SG formation may provide insights into the tumoral chemotherapeutic resistance.

SG assembly occurs in a very dynamic way, initiating with nanoscopic SG seeds that are formed and recruit nearby seeds via weak electrostatic interactions, interactions with neighboring SG seeds, and coalescence to form microscopically irregular visible SG. Microscopically visible SG can fuse to produce larger SG, and after stress release, events that promote SG disassembly may include an increase in concentrations of ternary complexes; phosphorylation of 4E-BP by mTOR, releasing the eIF4E block; and reactivation of eIF4A activities. As SG shrink, the Laplace pressure increases to promote further fusion with adjacent SG. Over time, fewer and larger SG appear before they eventually disappear from the cytoplasm [31]. The assembly and disassembly of SG are controlled by several intracellular events such as the inhibition of RNA helicase eIF4A [32], oxidative stress-promoting binding of 4EBP1 to eIF4E [33] and situations where both eIF4F complex– and eIF2α–mediated translation inhibition contribute to SG assembly [34].

Herein, we time-related SG dynamics with the chemotherapeutic agent BZM. U87 showed a crescent and great SG assembly stress response followed by disassembly. The granularity analysis is indicative of protein aggregates that might translate to stress granules and was used to support that find.

As SG assembly is related to inhibition of apoptosis by diminishing oxidative stress in vivo [35], we asked if by regulating the G3BP1 expression, GBM cells would become more sensitive to BZM. Our results demonstrate an increase in death after BZM treatment in G3BP1 silenced U87 cells. Such an increase in cell death was associated with caspase-3 activation. Caspase-3 is present both in intrinsic and extrinsic apoptotic pathways: Intrinsic apoptosis is induced by cellular stress, leading to the activation of the Bcl-2 family of proteins. The extrinsic apoptosis pathway is stimulated via ligand binding to corresponding death receptors and recruitment of FADD, leading to the formation of a death-inducing

signaling complex that culminates in cellular death [36] [37]. It is well-known that BZM modulated death through both extrinsic and intrinsic pathways in prostate cancer [38], myeloma [39], cervical cancer [40] and glioma [41]. By silencing G3BP1, we could improve this apoptosis associated cell death triggered by BZM. Therefore, the SG impairment-strategy may be a promisor therapeutic approach to improve BMZ-induced cell death. Accordingly, by knocking down the G3BP1 expression, the tumor cells-induced angiogenesis was substantially impaired. Although an anti-angiogenic effect of BZM was described in myeloma cells [42] and myeloma microvesicles [43], a pro-angiogenic effect of BZM was observed in glioma stem cells [44]. Taken together, our results indicate a new paradigm concerning the fate of integrated stress response in the U87 cell line. Whether it will cause cell rescue or cell death, it seems to depend on the extent of SG formation. The harmful effects of BMZ relate to an SG axis of stress-related cellular response, which will end up causing tumor resistance in U87. This paradigm explains the cell resistance to BZM cytotoxicity [45] and may help in the search for a new anti-tumoral approach based on SG impairment. We hope this paper contributes to future work in this direction.

CONFLICT OF INTEREST

The authors state that there are no competing interests.

ACKNOWLEDGMENTS

The microscopic data shown in this work was obtained using the microscopes and equipment in the Centro de Aquisição e Processamento de Imagens (CAPI- ICB/UFMG).This work was supported by Pró-Reitoria de Pesquisa da UFMG (PRPq-UFMG), Coordenação de Aperfeiçoamento de Pessoal de Nível Superior (CAPES), Conselho Nacional de Pesquisa (CNPq), Fundação de Amparo à Pesquisa do estado de Minas Gerais (FAPEMIG), and FAPESP (Fundação de Amparo à Pesquisa do Estado de São Paulo) grants 2013/07937-8 and 2016/07642-6. LFFB holds a CAPES PhD Scholarship. LSB, and LPS hold CNPq Research Fellowships.

REFERENCES

1. Ostrom QT, Bauchet L, Davis FG, et al (2014) The epidemiology of glioma in adults: A state of the science review. Neuro Oncol 16:896–913. https://doi.org/10.1093/neuonc/nou087.

2. Ohgaki H, Kleihues P (2009) Genetic alterations and signaling pathways in the evolution of gliomas. Cancer Sci 100:2235–41. https://doi.org/10.1111/j.1349-7006.2009.01308x

3. Wittrup A, Lieberman J (2015) Knocking down disease: A progress report on siRNA therapeutics. Nat. Rev. Genet. https://doi.org/10.1038/nrg3978

4. Ku SH, Kim K, Choi K, et al (2014) Tumor-targeting multifunctional nanoparticles for sirna delivery: Recent advances in cancer therapy. Adv Healthc Mater 3:1182–1193. https://doi.org/10.1002/adhm.201300607

5. Malhotra A, Mittal BR (2014) SiRNA gene therapy using albumin as a carrier. Pharmacogenet Genomics 24:582–587. https://doi.org/10.1097/FPC.0000000000000094

6. Kedersha NL, Gupta M, Li W, et al (1999) eIF-2 □ to the Assembly of Mammalian Stress Granules. J Cell Biol 147:1431–1441. https://doi.org/10.1083/jcb.147.7.1431

7. Buchan JR (2014) mRNP granules. Assembly, function, and connections with disease. RNA Biol 11:1019–30. https://doi.org/10.4161/15476286.2014.972208

8. Vilas-Boas F de AS, da Silva AM, de Sousa LP, et al (2016) Impairment of stress granule assembly via inhibition of the eIF2alpha phosphorylation sensitizes glioma cells to chemotherapeutic agents. J Neurooncol. https://doi.org/10.1007/s11060-015-2043-3

9. Zhang H, Ma Y, Zhang S, et al (2015) Involvement of Ras GTPase-activating protein SH3 domain-binding protein 1 in the epithelial-to-mesenchymal transition-induced metastasis of breast cancer cells via the Smad signaling pathway. Oncotarget. https://doi.org/10.18632/oncotarget.3636

10. Xu C, Wang P, Liu Y, et al (2013) Integrative Genomics in Combination with RNA Interference Identifies Prognostic and Functionally Relevant Gene Targets for Oral Squamous Cell Carcinoma. PLoS Genet. https://doi.org/10.1371/journal.pgen.1003169

11. Zhang H, Zhang S, He H, et al (2012) GAP161 targets and downregulates G3BP to suppress cell growth and potentiate cisplaitin-mediated cytotoxicity to colon carcinoma HCT116 cells. Cancer Sci. https://doi.org/10.1111/j.1349-7006.2012.02361.x

12. Bao X, Ren T, Huang Y, et al (2017) Bortezomib induces apoptosis and suppresses cell growth and metastasis by inactivation of Stat3 signaling in chondrosarcoma. Int J Oncol 50:477–486. https://doi.org/10.3892/ijo.2016.3806

13. Styczynski J, Olszewska-Slonina D, Kolodziej B, et al (2006) Activity of bortezomib in glioblastoma. Anticancer Res. https://doi.org/10.3892/ol.2017.5585

14. Adams J (2003) Potential for proteasome inhibition in the treatment of cancer. Drug Discov. Today. https://doi.org/10.1016/S1359-6446(03)02647-3

15. Kong XT, Nguyen NT, Choi YJ, et al (2018) Phase 2 Study of Bortezomib Combined With Temozolomide and Regional Radiation Therapy for Upfront Treatment of Patients With Newly Diagnosed Glioblastoma Multiforme: Safety and Efficacy Assessment. Int J Radiat Oncol Biol Phys. https://doi.org/10.1016/j.ijrobp.2018.01.001

16. Yao ZG, Li WH, Hua F, et al (2017) LBH589 inhibits glioblastoma growth and angiogenesis through suppression of HIF-1α expression. J Neuropathol Exp Neurol. https://doi.org/10.1093/jnen/nlx088

17. McEwen E, Kedersha N, Song B, et al (2005) Heme-regulated inhibitor kinase-mediated phosphorylation of eukaryotic translation initiation factor 2 inhibits translation, induces stress granule

formation, and mediates survival upon arsenite exposure. J Biol Chem 280:16925–16933. https://doi.org/10.1074/jbc.M412882200

18. American Type Culture Collection (2011) MTT Cell Proliferation Assay Instruction Guide. Components 6597:1–6. https://doi.org/ATCC 30-1010K

19. Bolte S, Cordelières FP (2006) A guided tour into subcellular colocalization analysis in light microscopy. J Microsc 224:213–32. https://doi.org/10.1111/j.1365-2818.2006.01706.x

20. Pietrani NT, Ferreira CN, Rodrigues KF, et al (2018) Proresolving protein Annexin A1: The role in type 2 diabetes mellitus and obesity. Biomed Pharmacother 103:482–489. https://doi.org/10.1016/j.biopha.2018.04.024

21. Oliveira AG de L, Silva RS, Alves EN, et al (2012) Chorioallantoic membrane assays (HET-CAM and CAM-TBS): alternative tests for performing toxicological evaluation of products with low potential for ocular irritation. Rev Inst Adolfo Lutz 71:153–159

22. Brown R, Motulsky H (2006) Detecting outliers when fitting data with nonlinear regression - a new method based on robust nonlinear regression and the false discovery rate. BMC Bioinformatics 7:1–20. https://doi.org/10.1186/1471-2105-7-123

23. Arimoto-Matsuzaki K, Saito H, Takekawa M (2016) TIA1 oxidation inhibits stress granule assembly and sensitizes cells to stress-induced apoptosis. Nat Commun 7:1–10. https://doi.org/10.1038/ncomms10252

24. Harding HP, Zhang Y, Bertolotti A, et al (2000) Perk is essential for translational regulation and cell survival during the unfolded protein response. Mol Cell 5:897–904. https://doi.org/10.1016/S1097-2765(00)80330-5

25. Avgeropoulos NG, Batchelor TT (1999) New treatment strategies for malignant gliomas. Oncologist 4:209–224

26. Fischer I, Gagner J-P, Law M, et al (2010) Angiogenesis in Gliomas: Biology and Molecular Pathophysiology. Brain Pathol. https://doi.org/10.1111/j.1750-3639.2005.tb00115.x

27. Porporato PE, Dhup S, Dadhich RK, et al (2011) Anticancer targets in the glycolytic metabolism of tumors: A comprehensive review. Front Pharmacol AUG: https://doi.org/10.3389/fphar.2011.00049

28. Gorrini C, Harris IS, Mak TW (2013) Modulation of oxidative stress as an anticancer strategy. Nat Rev Drug Discov 12:931–947. https://doi.org/10.1038/nrd4002

29. Fournier M-J, Gareau C, Mazroui R (2010) The chemotherapeutic agent bortezomib induces the formation of stress granules. Cancer Cell Int 10:12. https://doi.org/10.1186/1475-2867-10-12

30. Gareau C, Fournier MJ, Filion C, et al (2011) P21waf1/cip1 upregulation through the stress granule-associated protein CUGBP1 confers resistance to bortezomib-mediated apoptosis. PLoS One 6:. https://doi.org/10.1371/journal.pone.0020254

31. Panas MD, Ivanov P, Anderson P (2016) Mechanistic insights into mammalian stress granule dynamics. J. Cell Biol. https://doi.org/10.1083/jcb.201609081

32. Kim WJ, Kim JH, Jang SK (2007) Anti-inflammatory lipid mediator 15d-PGJ2 inhibits translation through inactivation of eIF4A. EMBO J. https://doi.org/10.1038/sj.emboj.7601920

33. Emara MM, Fujimura K, Sciaranghella D, et al (2012) Hydrogen peroxide induces stress granule formation independent of eIF2α phosphorylation. Biochem Biophys Res Commun. https://doi.org/10.1016/j.bbrc.2012.06.033

34. Szaflarski W, Fay MM, Kedersha N, et al (2016) Vinca alkaloid drugs promote stress-induced translational repression and stress granule formation. Oncotarget. https://doi.org/10.18632/oncotarget.8728

35. Arimoto K, Fukuda H, Imajoh-Ohmi S, et al (2008) Formation of stress granules inhibits apoptosis by suppressing stress-responsive MAPK pathways. Nat Cell Biol 10:1324–1332. https://doi.org/10.1038/ncb1791

36. Boland K, Flanagan L, Prehn JHM (2013) Paracrine control of tissue regeneration and cell proliferation by Caspase-3. Cell Death Dis. https://doi.org/10.1038/cddis.2013.250

37. Choudhary GS, Al-harbi S, Almasan A (2014) Caspase-3 activation is a critical determinant of genotoxic stress-induced apoptosis. In: Apoptosis and Cancer: Methods and Protocols: Second Edition

38. Zheng RP, Wang W, Wei CD (2015) Bortezomib inhibits cell proliferation in prostate cancer. Exp Ther Med 10:1219–1223. https://doi.org/10.3892/etm.2015.2617

39. Turan T, Şanli-Mohamed G, Baran Y (2013) Changes in protein profiles of multiple myeloma cells in response to bortezomib. Leuk Lymphoma 54:1061–1068. https://doi.org/10.3109/10428194.2012.735668

40. Cui H, Qin Q, Yang M, et al (2015) Bortezomib enhances the radiosensitivity of hypoxic cervical cancer cells by inhibiting HIF-1α expression. Int J Clin Exp Pathol

41. Zhang Y, Zhu X, Hou K, et al (2015) Mcl-1 downregulation sensitizes glioma to bortezomib-induced apoptosis. Oncol Rep. https://doi.org/10.3892/or.2015.3875

42. Kim C, Kasuya J, Jeon J, et al (2015) A quantitative microfluidic angiogenesis screen for studying anti-angiogenic therapeutic drugs. Lab Chip. https://doi.org/10.1039/c4lc00866a

43. Guo HM, Sun L, Yang L, et al (2018) Microvesicles shed from bortezomib-treated or lenalidomide-treated human myeloma cells inhibit angiogenesis in vitro. Oncol Rep. https://doi.org/10.3892/or.2018.6395

44. Bota DA, Alexandru D, Keir ST, et al (2013) Proteasome inhibition with bortezomib induces cell death in GBM stem-like cells and temozolomide-resistant glioma cell lines, but stimulates GBM stem-like cells' VEGF production and angiogenesis. J Neurosurg. https://doi.org/10.3171/2013.7.JNS1323

45. Atkinson JM, Shelat AA, Carcaboso AM, et al (2011) An integrated in vitro and in vivo high-throughput screen identifies treatment leads for ependymoma. Cancer Cell. https://doi.org/10.1016/j.ccr.2011.08.013

FIGURES and LEGENDS

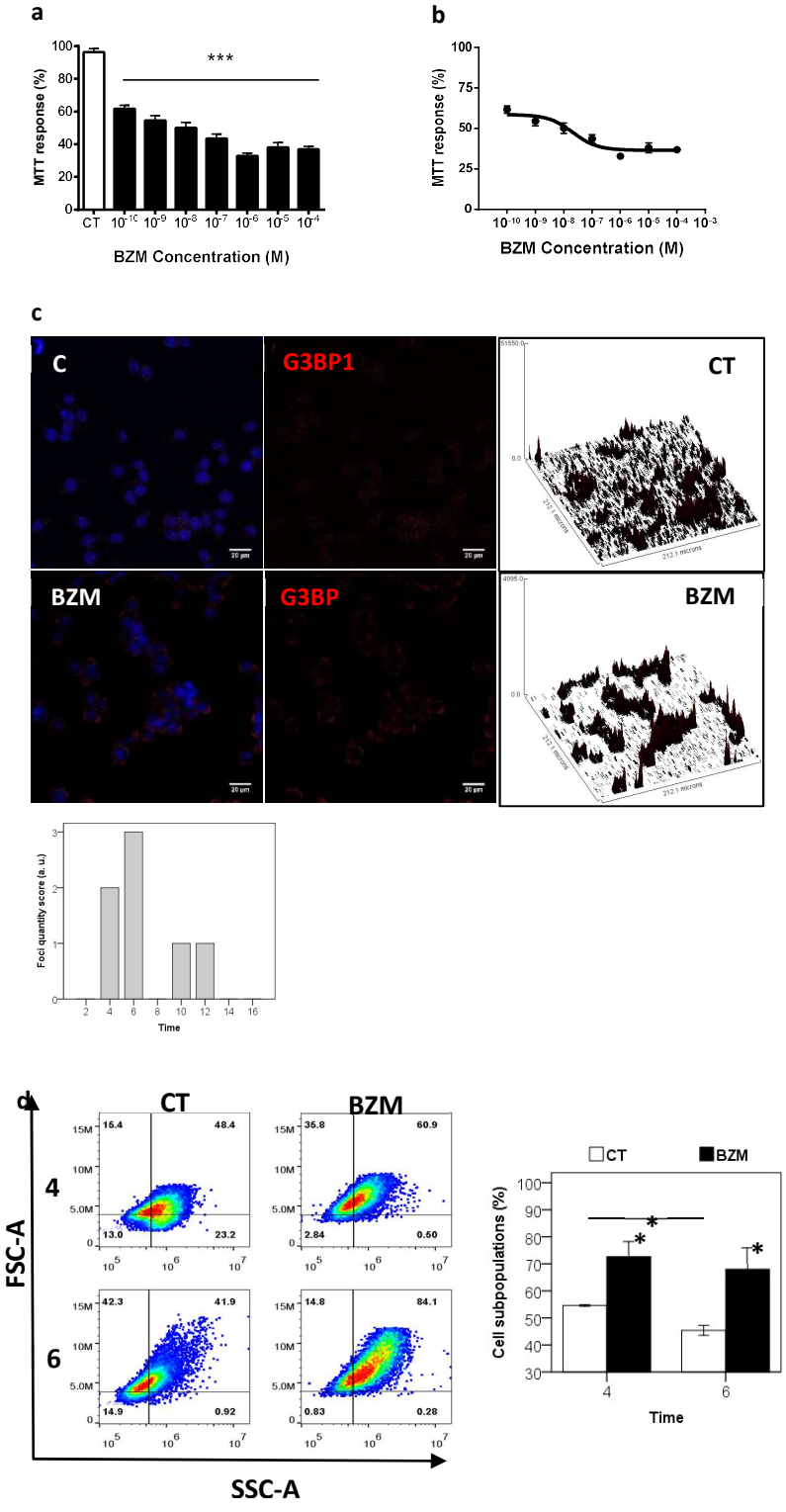

Figure 1. BZM IC50 increases cell granularity and causes SG assembly.

A – Graphical representation of tested BZM concentrations by MTT assay. All tested doses were significantly different when compared to control. B – Sigmoid curve obtained from linear regression of calculated IC50. C – Graphical representation of foci score at 2, 4, 6 and 8h time-points. D – Representative Immunofluorescence images and surface-plots of U87 cells, stained for G3BP1 (RED). Overlaid images are composed of nuclei DAPI staining (BLUE). E – Representative dot-plots from FACS analysis of cell granularity and size. F – Graphical representation of FACS data for 4 and 6hours of control and BZM treatment. One-way ANOVA test was used, where * stands for $p < 0.05$ and *** $p < 0.001$

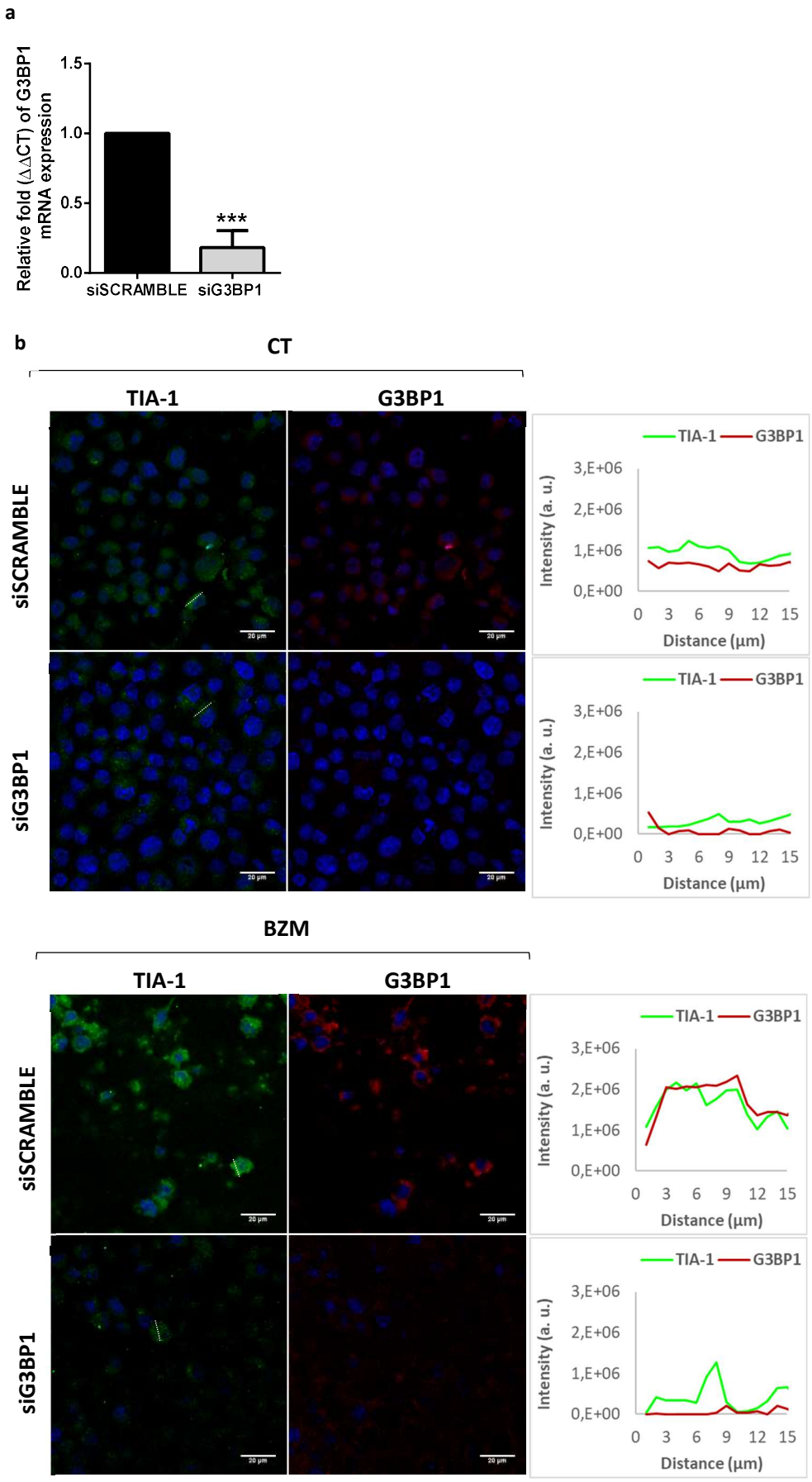
a
Relative fold (ΔΔCT) of G3BP1 mRNA expression
1.5
1.0
0.5
0.0
***
siSCRAMBLE
siG3BP1
b
CT
TIA-1
G3BP1
siSCRAMBLE
siG3BP1
TIA-1
G3BP1
Intensity (a. u.)
3,E+06
2,E+06
1,E+06
0,E+00
0 3 6 9 12 15
Distance (µm)
BZM
TIA-1
G3BP1
siSCRAMBLE
siG3BP1
TIA-1
G3BP1
Intensity (a. u.)
3,E+06
2,E+06
1,E+06
0,E+00
0 3 6 9 12 15
Distance (µm)

Figure 2. Knockdown of G3BP1 mRNA by siRNA reduces G3BP1 and TIA protein expression.

Representative Immunofluorescence images and surface-plots of U87 cells, stained for TIA-1 (GREEN) and G3BP1 (RED). Overlaid images are composed of nuclei DAPI staining (BLUE). A – siSCRAMBLE control. B – siG3BP1 control. C – siSCRAMBLE BZM (6hours). D – siG3BP1 BZM (6hours). E – Graphical representation of real-time PCR results (relative to control ΔΔCT). One-way ANOVA test was used, where *** stands for $p < 0.001$.

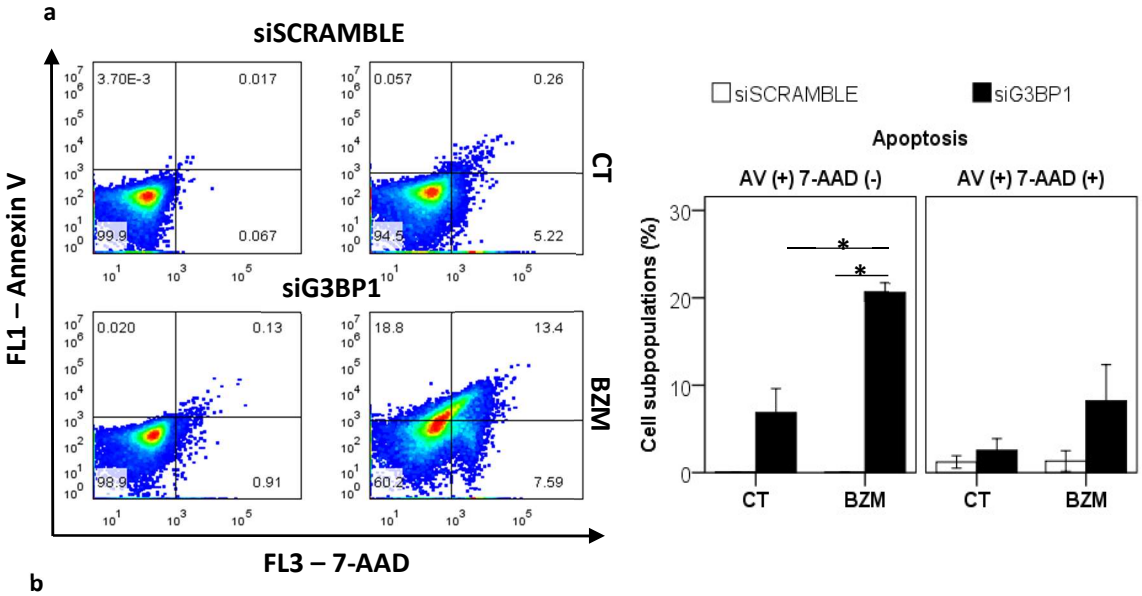
a
siSCRAMBLE
siG3BP1
CT
BZM
FL1 – Annexin V
FL3 – 7-AAD
3.70E-3
0.017
99.9
0.067
0.057
0.26
94.5
5.22
0.020
0.13
98.9
0.91
18.8
13.4
60.2
7.59
siSCRAMBLE
siG3BP1
Apoptosis
AV (+) 7-AAD (-)
AV (+) 7-AAD (+)
Cell subpopulations (%)
30
20
10
0
CT
BZM
CT
BZM
*
*

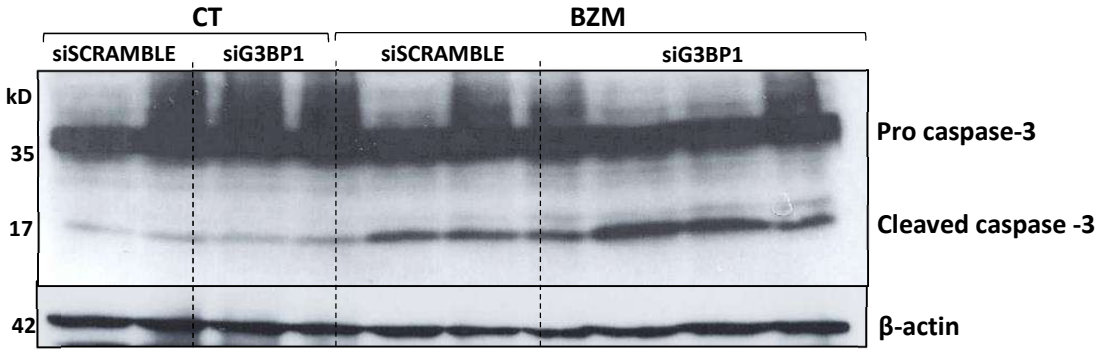
b
CT
BZM
siSCRAMBLE
siG3BP1
siSCRAMBLE
siG3BP1
kD
35
17
42
Pro caspase-3
Cleaved caspase -3
β-actin

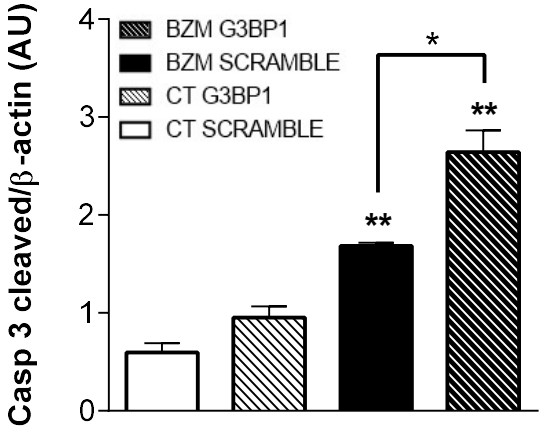
Casp 3 cleaved/β-actin (AU)
BZM G3BP1
BZM SCRAMBLE
CT G3BP1
CT SCRAMBLE
4
3
2
1
0
*
**
**

Figure 3. BZM apoptotic effect is potentialized by G3BP1 knock-down.

A – Graphical representation of MTT assay of siSCRAMBLE and siG3BP1 control and BZM treated (24 hours) groups. B – Representative dot-plots of Annexin-V and 7-AAD FACS analysis of siSCRAMBLE and siG3BP1 control and BZM treated (24 hours) groups C – Graphical representation of FACS obtained data in Annexin-V/7-AAD apoptosis/necrosis assay of siSCRAMBLE and siG3BP1 control and BZM treated (24 hours) groups. D – Immunoblotting of cleaved ad total caspase-3 expressions of siSCRAMBLE and siG3BP1 control and BZM treated (24 hours) groups. E – Graphical representation of cleaved caspase-3, normalized by β-actin expression in siSCRAMBLE and siG3BP1 control and BZM treated (24 hours) groups. One-way ANOVA test was used, where * stands for $p < 0.05$; ** $p < 0.01$ and *** $p < 0.001$.

a

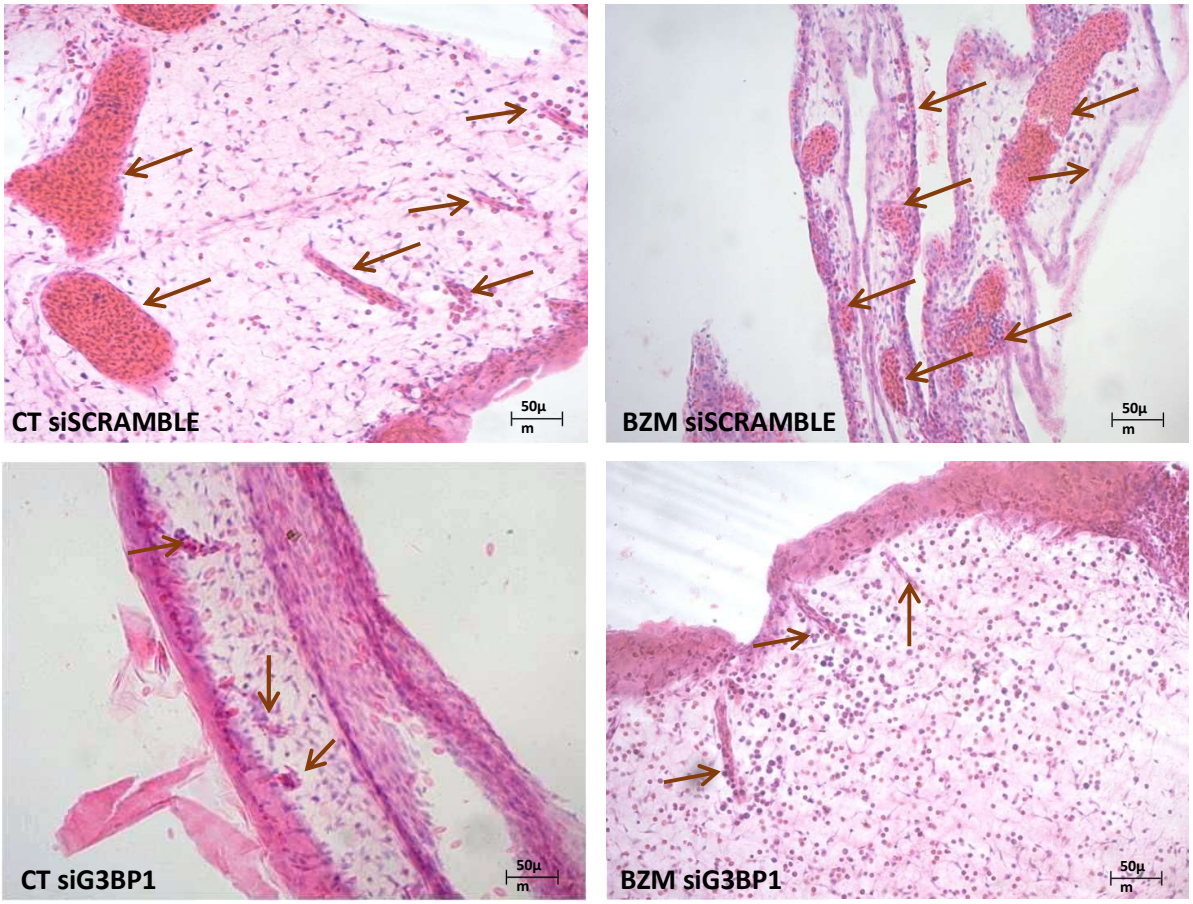
CT siSCRAMBLE
50µm
BZM siSCRAMBLE
50µm
CT siG3BP1
50µm
BZM siG3BP1
50µm

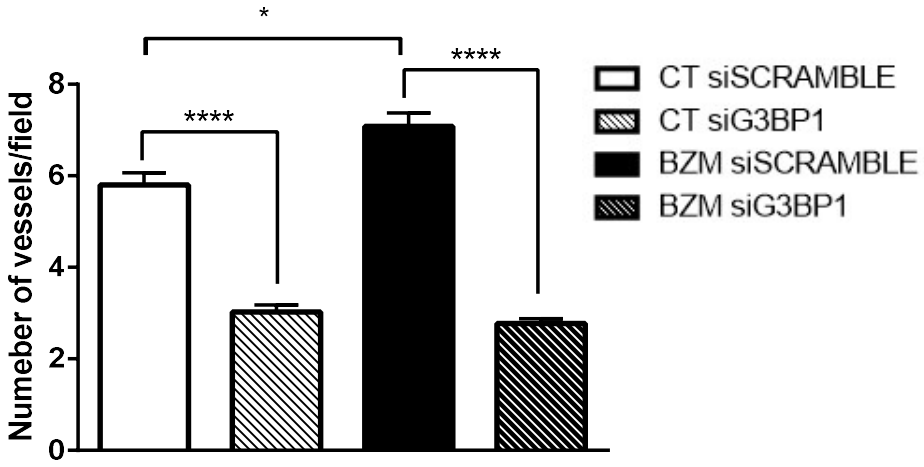
*
****
****
Numeber of vessels/field
0
2
4
6
8
CT siSCRAMBLE
CT siG3BP1
BZM siSCRAMBLE
BZM siG3BP1

Figure 4. G3BP1 knockdown has an anti-angiogenic effect and prevents BZM angiogenic role.

A – Representative hematoxylin-eosin stained histological images of CAMs incubated with conditioned media from siSCRAMBLE, and siG3BP1 control and BZM treated (24 hours) cells. Arrows indicate blood vessels. B – Graphical representation of counted blood vessels per field. One-way ANOVA test was used, where * stands for $p < 0.05$; and *** $p < 0.001$.

Expanded results

Cell viability and calculation of IC_{50} curves

MTT viability assay was used to test the effect of each chemotherapeutic agent, BZM, ETO and TMZ, in both cell lines U87MG and T98G in order to calculate the half maximal inhibitory concentration (IC50), which is a measure of the potency of a substance in inhibiting a specific biological or biochemical function (Figure 1). Results show that, among tested chemotherapeutics, BZM is the most potent in reducing cells viability at the 24 hours time-point (calculated IC50 = 4 x10-9 ± 0.1 M for T98 and 2 x10-8 ± 0.3 M for U87) and TMZ the least effective among the three chemotherapeutics (calculated IC50 = 9 x10-5 ± 0.2 M for T98 and 1.2 x10-4 ± 0.2 M for U87). The calculated IC50 for ETO was 5 x10-6 ± 0.4 M for T98 and 1.3 x10-6 ± 0.3168 M for U87.

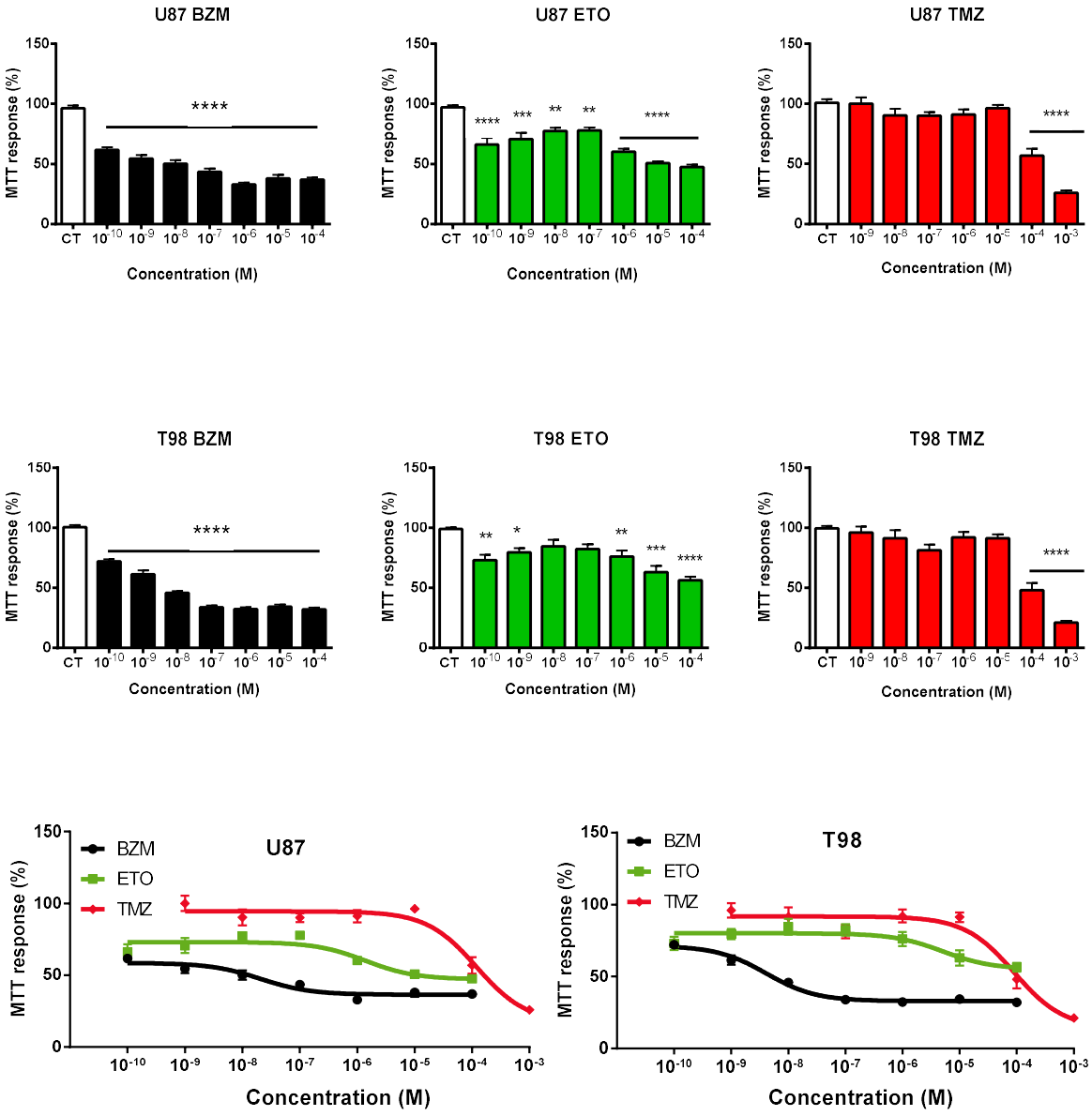

Figure 1.Cell viability and calculated IC50 curves.

Graphical representations of relative to control MTT assay results and calculated IC50 from U87 and T98 cell lines treated with BZM, ETO and TMZ. Results are show and mean ± SEM n=3. One-way ANOVA test was used, where * stands for $p < 0,05$; ** $p < 0,01$ and *** $p < 0,001$.

Determination of SGs dynamics by immunofluorescence assays

To establish drugs IC_{50} influence on SGs assembly/disassembly dynamics, U87 and T98 cells were exposed to chemotherapeutic agents in 8 different time points (2, 4, 6, 8, 10, 12, 14 and 16 hours). The anti-G3BP1 monoclonal antibody was used to demonstrate differences between cytoplasm-spread G3BP1 (not assembled SGs) and G3BP1 cytoplasmic foci (assembled SGs). In figure 2 and 3 we can observe cells behavior when exposed to drug treatments. We notice a pattern difference in SGs assembly of T98 and U87. Stress granules assembly occur earlier on U87 cell line, showing the first score peak at 6 hours when treated with BZM and at 4 hours when treated with ETO and TMZ.

Comparatively to T98 which shows later peaks at 8 hours for BZM and ETO. Temozolomide peak, however, occurred at the same time in both cell lines, indicating that despite the intrinsic differences between cell lines, TMZ activates stress response at the same time. Dynamically speaking, both cell lines showed a first fast and intense SGs assembly stress response followed by a minor later one.

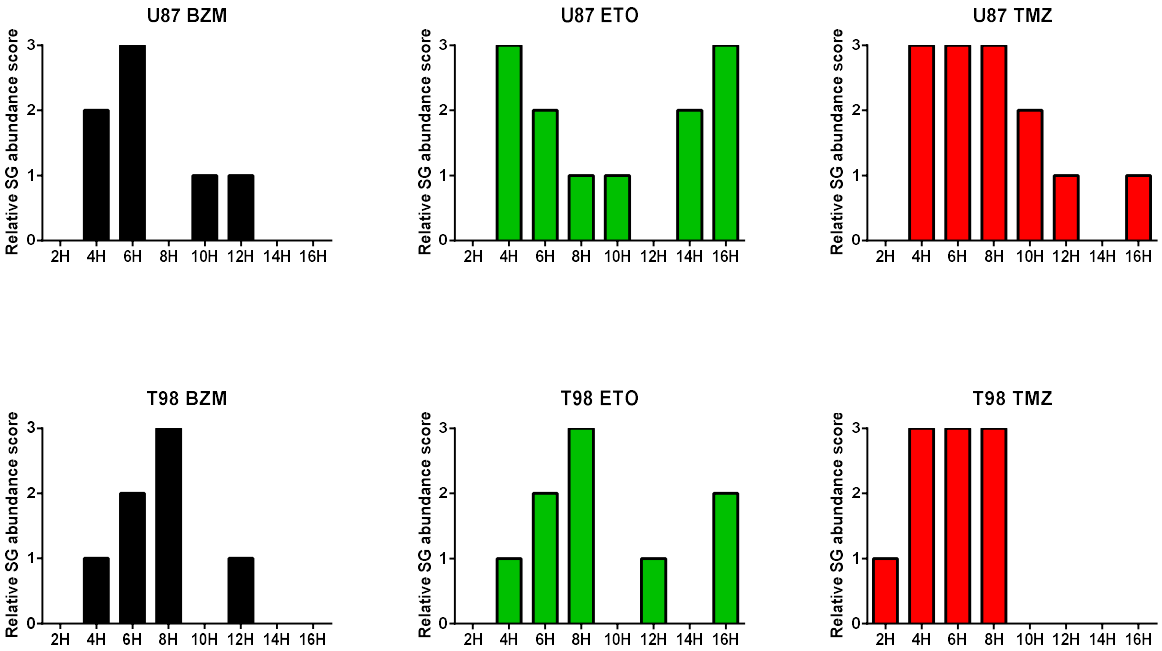

Figure 2. Stress Granules dynamics by focci qualitative score

Qualitative focci score from 2, 4, 6, 8, 10, 12, 14 and 16 hours time-points of U87 and T98 cell lines treated with BZM, ETO and TMZ.

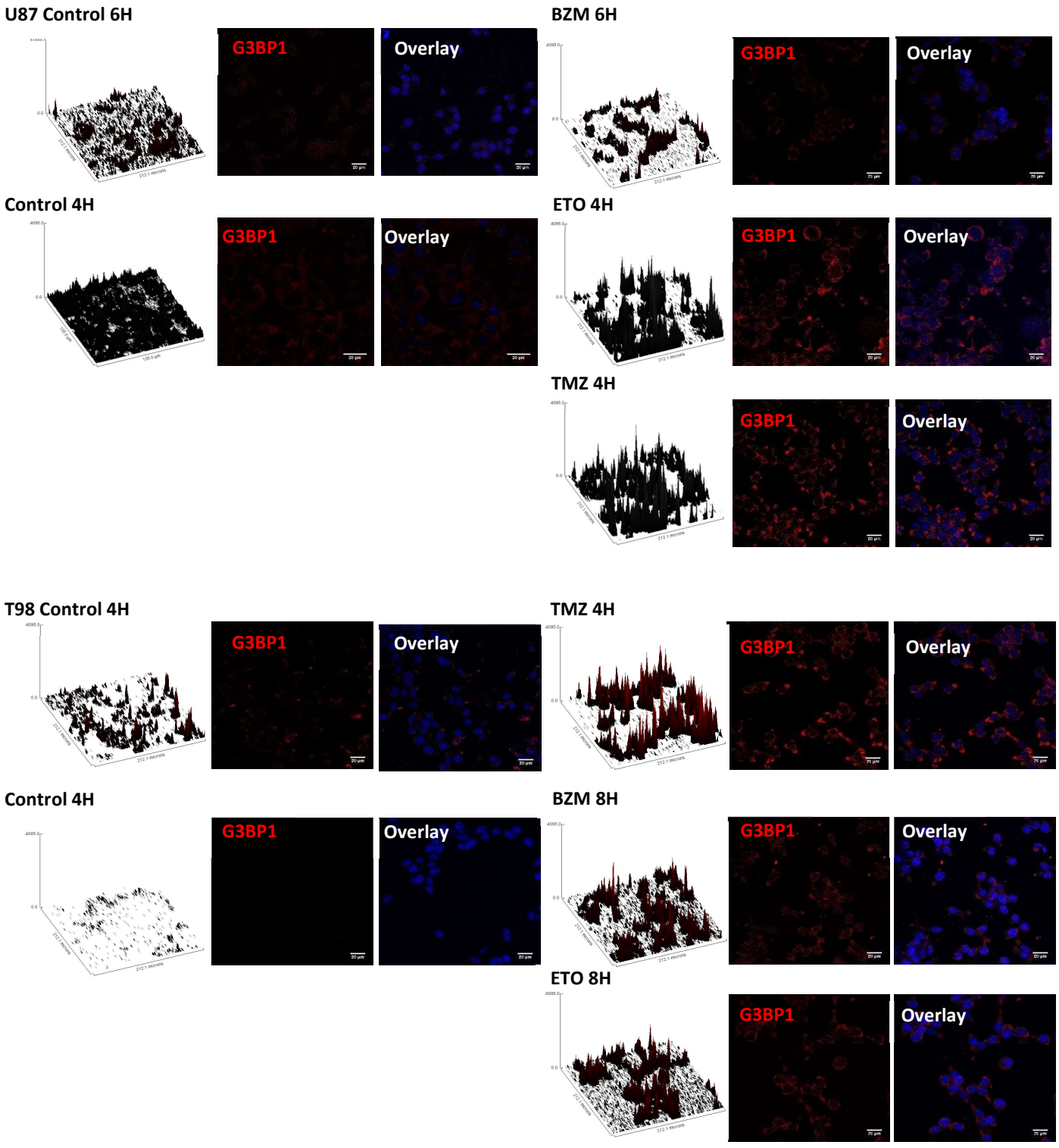

Figure 3. Stress granules representative immunofluorescence of G3BP1 expression peaks

Representative Immunofluorescence images and surface-plots of U87MG cells, stained for G3BP1 (RED). Overlaid images are composed with nuclei DAPI staining (BLUE).

SGs impairment by G3BP1 knockdown with siRNA technique

In order to achieve a reduction in G3BP1 expression, specific siRNA was employed. We tested three different sequences of siRNA to choose better which would have the desired effect in both cell lines (Figure 4). Obtained data from real-time PCR demonstrates that siRNA sequence 2 reduced G3BP1 mRNA expression by 43% on U87 and 90% on T98 when compared to the universal negative control (scrambled sequence). Two endogenous genes were used for normalization (18S and Hprt) as results were more accurate employing them.

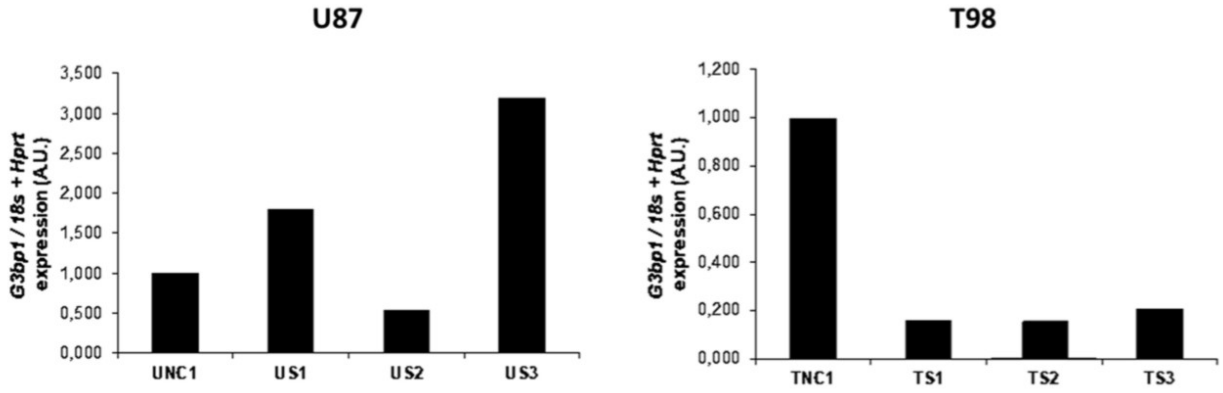

Figure 4. Real-time analysis of siRNA sequences 1, 2 and 3. Chosen sequence is number 2.

Graphical representation of real-time PCR experiment using three different siRNA sequences on U87 and T98 cell lines.

Even though siRNA sequence 2 performed in an acceptable manner for U87, further experiments were made to better understand low siRNA efficiency and high cell death. To address these issues the transfection reagent was changed from Lipofectamine to Fugene 6, a gentler transfection agent. By analyzing the results, we made some observations. Transfection with Fugene6 did not work on T98 cells (Figure 5) as positive reaction control TYE-565 did not penetrate cells.

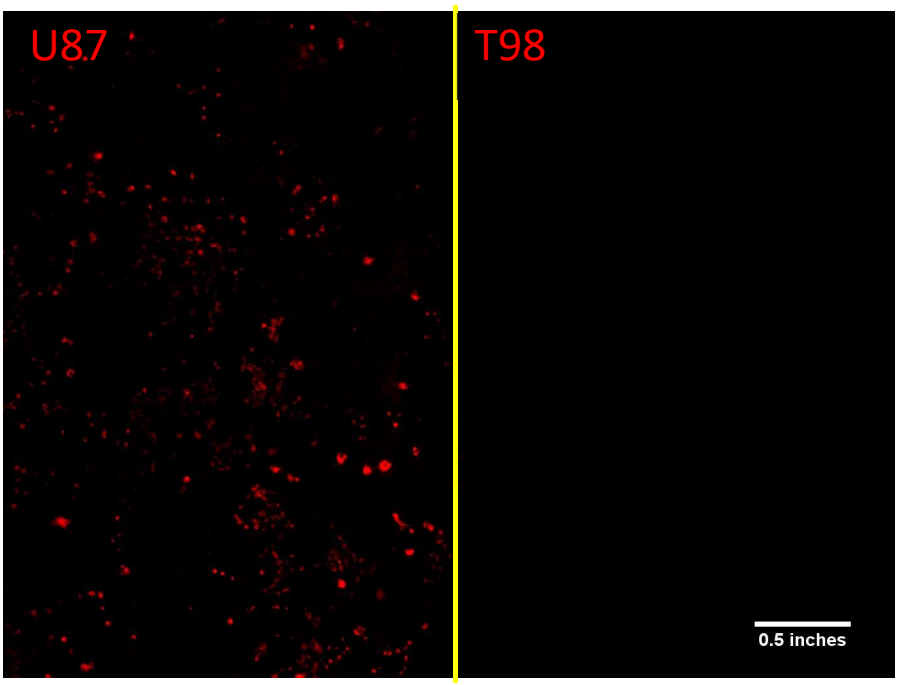

Figure 5. Fluorescent control of transfection for U87 and T98 cells. T98 cells are not transfected with Fugene 6 reagent.

Representative image of fluorescent positive transfection control TYE-565 on U87 and T98 cell lines. Transfection was carried out with FIugene6, according to manufactures instructions, for 48 hours.

On U87 cells, transfection worked but upon real-time analysis we observed that siRNA sequence 2 was not only inefficient but surprisingly, increased G3BP1 mRNA (Figure 6). Upon literature review (LI, Ping et al., 2010), we decided to test other siRNA concentrations and discovered that using less siRNA produced the desired effect, augmenting siRNA efficiency and inhibiting G3BP1 mRNA by more than 80% (Figure 7).

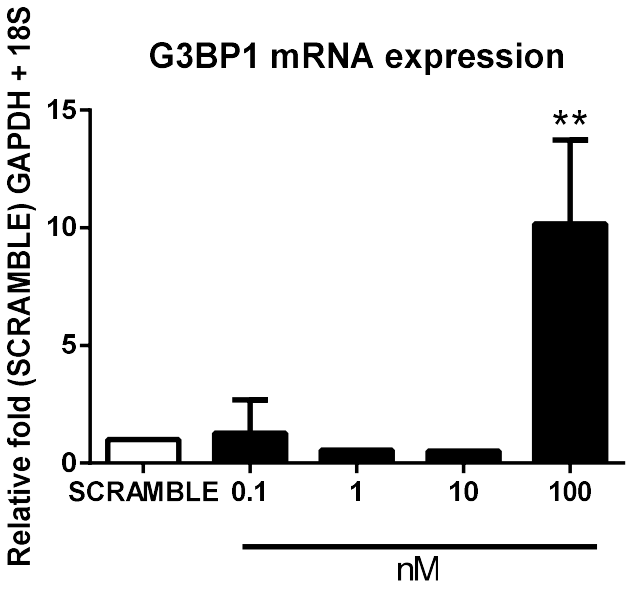

Figure 6. Real-time analysis of different concentrations of siRNA, revealing varied expression with changing concentrations

Graphical representation of real-time PCR results with Fugene 6 transfection and varying concentrations of siRNA 2 against G3BP1 mRNA in U87 cell lines. Results are show and mean ± SEM n=3. One-way ANOVA test was used, where ** stands for $p < 0,01$.

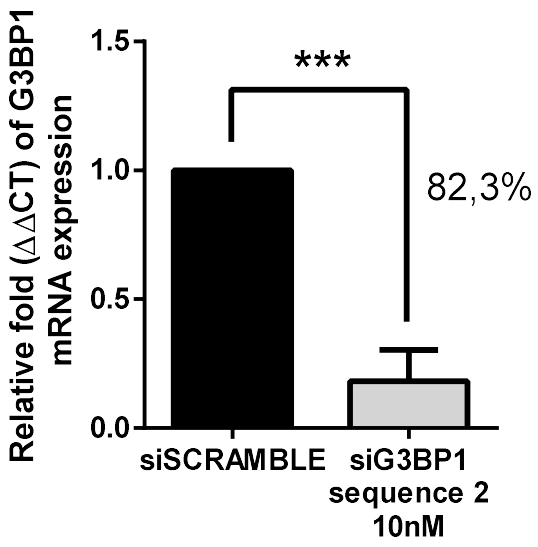

Figure 7. Real-time analysis of siRNA 2 at 10nM reduces mRNA of G3BP1 by 82,3%

Graphical representation of real-time PCR results of U87 cells transfected with Fugene 6 and 10nM of siRNA sequence 2. Results are show and mean ± SEM n=3. One-way ANOVA test was used, where *** stands *** $p < 0{,}001$.

Cell viability G3BP1-dependent sensitization to chemotherapeutic agents

After demonstrating viable knockdown of G3BP1 protein expression, we tested our hypothesis of cell sensitization in a G3BP1-dependent manner. Our results show a significative difference between cells transfected with siSCRAMBLE and siG3BP1 (Figure 8). Data is plotted as ratio between siSCRAMBLE:siG3BP1 groups, evidencing a reduction in the absorbance assessed by MTT assay. Thus, we observed a negative ratio when comparing chemotherapeutic-treated groups to control group, suggesting the G3BP1 knockdown further reduces cell viability in response to BZM, ETO, and TMZ in U87 cells.

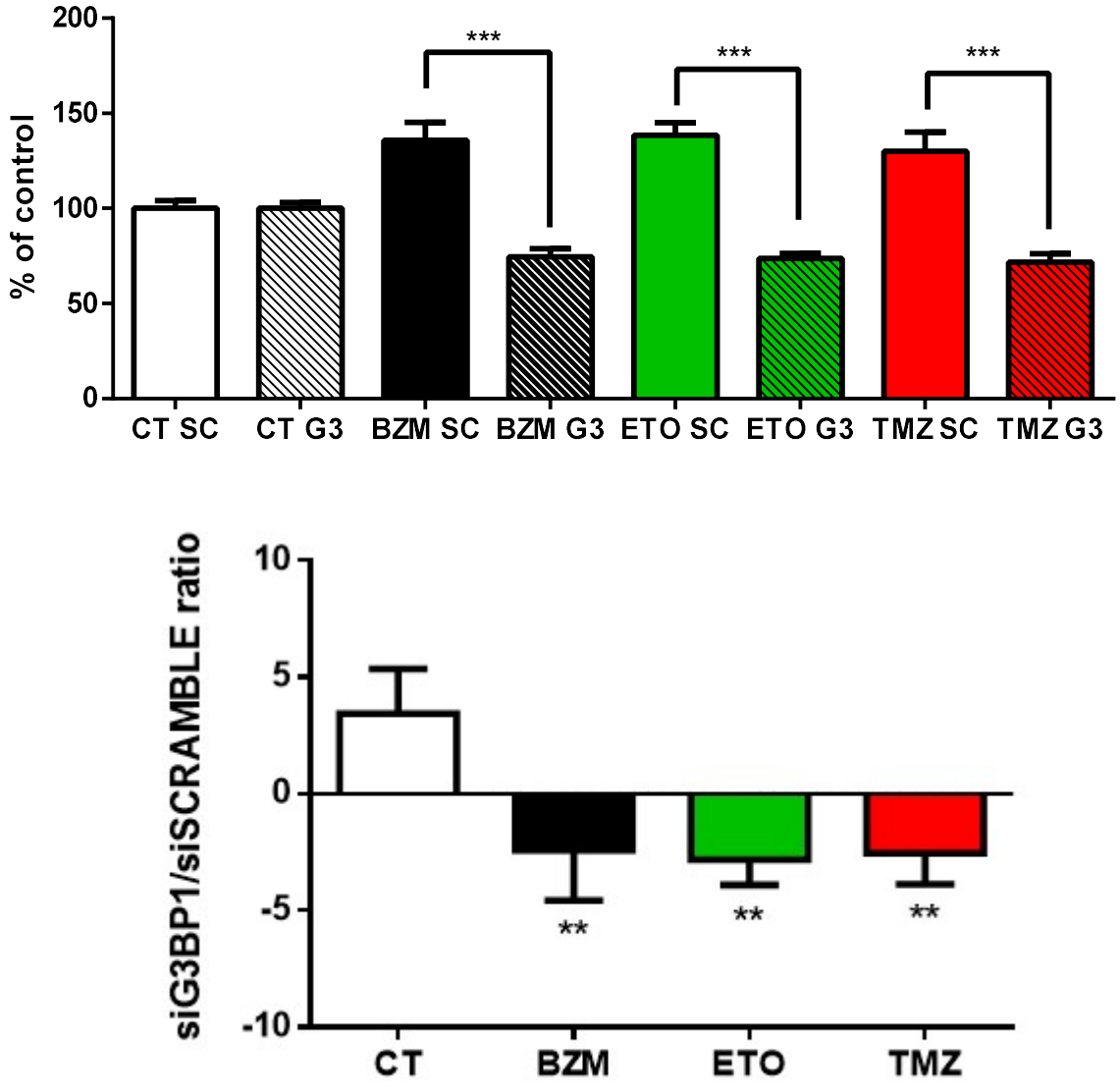

Figure 8. MTT comparative ratio analysis of transfected cells reveals sensibilization and negative ratio for all tested drugs

TOP - Graphical representation of siSCRAMBLE and siG3BP1 control, BZM, ETO and TMZ groups. BOTTOM - Calculated siG3BP1: siSCRAMBLE ratio obtained by MTT assay. Values obtained from MTT assay were used in order to calculate each drug (BZM, ETO and TMZ) siG3BP1: siSCRAMBLE ratio at 24 hours. Results are show and mean ± SEM n=3. One-way ANOVA test was used, where ** stands for $p < 0,01$.

Cell cycle modulation by Etoposide is not influenced by SGs impairment

Using propidium iodide hypotonic solution, we assessed U87 cell cycle status with 24 hours of chemotherapeutic treatment. By analyzing siSCRAMBLE and siG3BP1 treated cells, we found no statistic difference between control and BZM/TMZ treated groups (Figure 9). However, we did find a reduction in cell number at G0/G1 phase with further increased cells at G2/M phase upon ETO treatment.

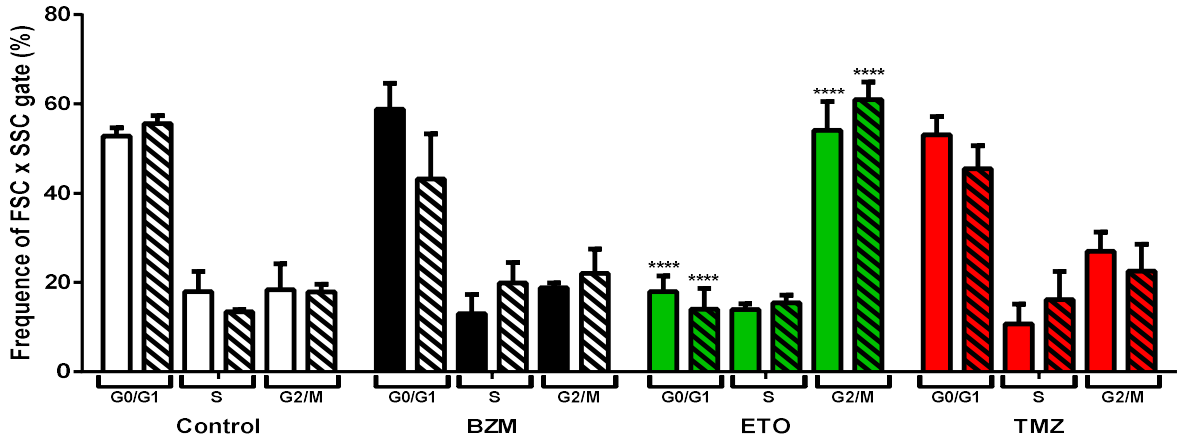

Figure 9. Cell cycle analysis reveals ETO's influence on U87 cells in a G3BP1-independent manner

Percentage of cells distributed in cell cycle phases. Values obtained from annexin cell cycle assay are shown separated for each drug (BZM, ETO and TMZ) and transfected siRNA (siSCRAMBLE and siG3BP1) at 24 hours. Hatched bars represent siG3BP1 transfected cells while regular bars represent siSCRAMBLE transfected cells. Results are show and mean ± SEM n=3. One-way ANOVA test was used, where **** stands for $p < 0{,}0001$.

Annexin V- 7AAD apoptotic staining: a BZM – G3BP1 relation

Since the enhanced expression of G3BP1 and TIA1 are intrinsically associated with tumor chemoresistance (ARIMOTO-MATSUZAKI; SAITO; TAKEKAWA, 2016; MATSUKI et al., 2013), we investigated their relation with apoptosis. Under BZM there was a significant increase in plasma membrane permeabilization (7-AAD positive cells) as revealed by cytofluorometric analysis (Figure 11). The proportion of apoptotic cells, characterized by the presence of negatively charged lipids that bind to Annexin V (AV) without losing cytoplasmic membrane integrity and therefore avoiding cellular incorporation 7-AAD, did not increase after chemotherapy in GBM U87 cells. However, by silencing G3BP1 after BZM treatment there was significant difference for AV+/7-AAD- populations compared to siSCRAMBLE control ($p = 0.001$). Note that upon BZM G3BP1 silenced-cells revealed an apoptotic phenotype compared to ETO and TMZ ($p = 0.007$).

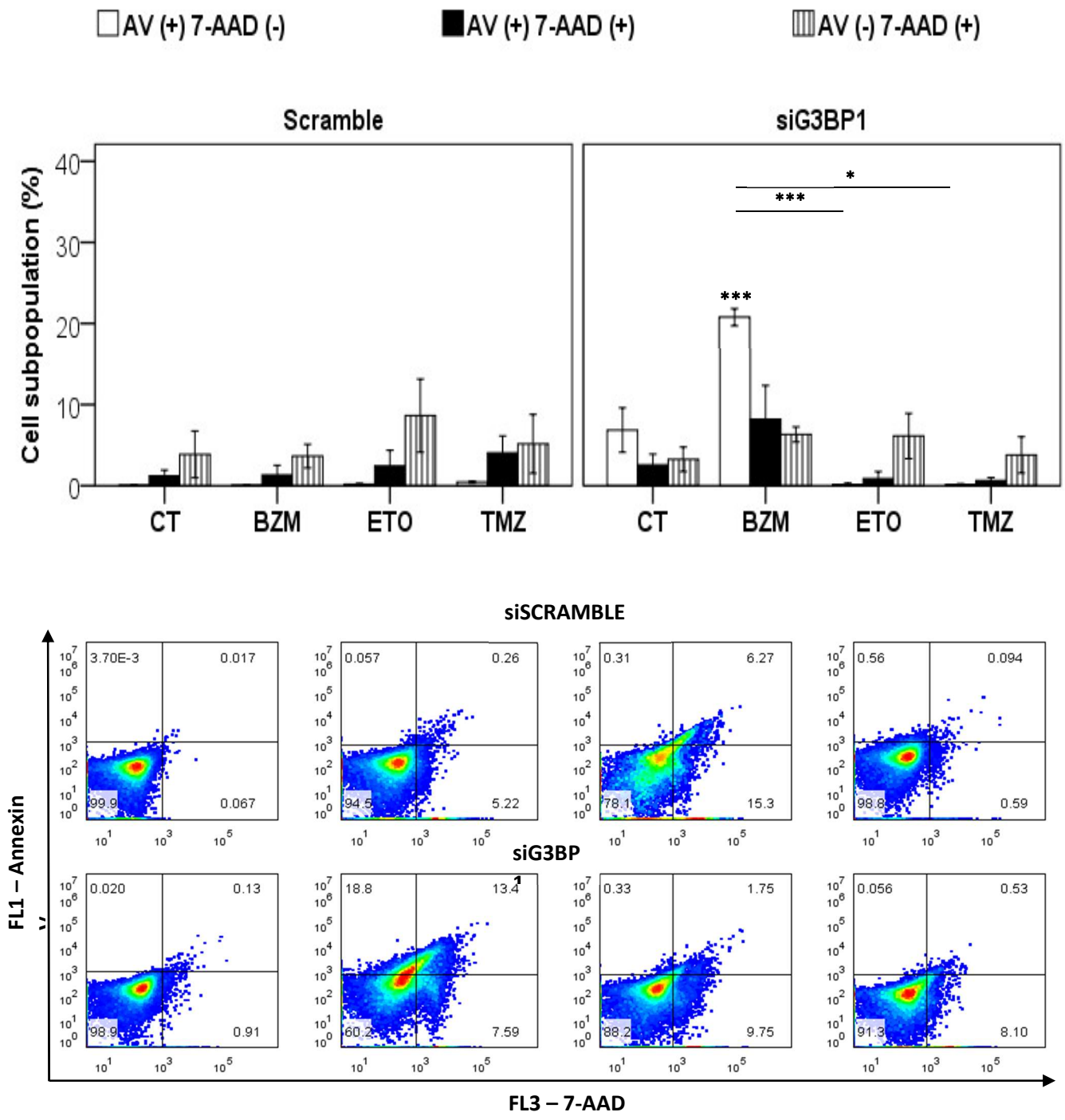

Figure 10. Annexin V and 7-AAD analysis. Increased apoptosis observed in siG3BP1 BZM treated cells.

Percentage of cells annexin V + / 7AAD -, annexin V - / 7AAD + and total 7AAD +. Values obtained from annexin V/7AAD assay are shown separated for each drug (BZM, ETO and TMZ in hgDMEM 1%FBS) and transfected siRNA (siSCRAMBLE and siG3BP1) at 24 hours. Hatched bars represent siG3BP1 transfected cells while regular bars represent siSCRAMBLE transfected cells. Results are show and mean ± SEM n=3. One-way ANOVA test was used, where * stands for $p < 0,05$; ** $p < 0,01$ and *** $p < 0,001$

Acidic vesicles peaks detection by acridine orange time-course

To assess cells autophagic state, we performed an assay with acridine orange (A.O.), a vital staining reagent that when spread, displays a green fluorescence and when aggregated, displays a red fluorescence. By calculation a ratio between red fluorescence and green fluorescence obtained from fluorescent images we were able to plot a time-course graph for all three drugs in both U87 and T98 cell lines. We can clearly observe and increase in RG ratio at 8 hours for ETO and TMZ. As for T98, the RG ratio shows a peak at 10 hours for BZM/ETO and at 12/16 hours for TMZ.

To refine our understanding of A.O. dynamic observed in U87 cells, we assayed through a time-course, A.O. red (FL3) staining. As BZM and ETO had no significant difference among all tested times, TMZ revealed and increased cell population from 8 to 12 hours of treatment.

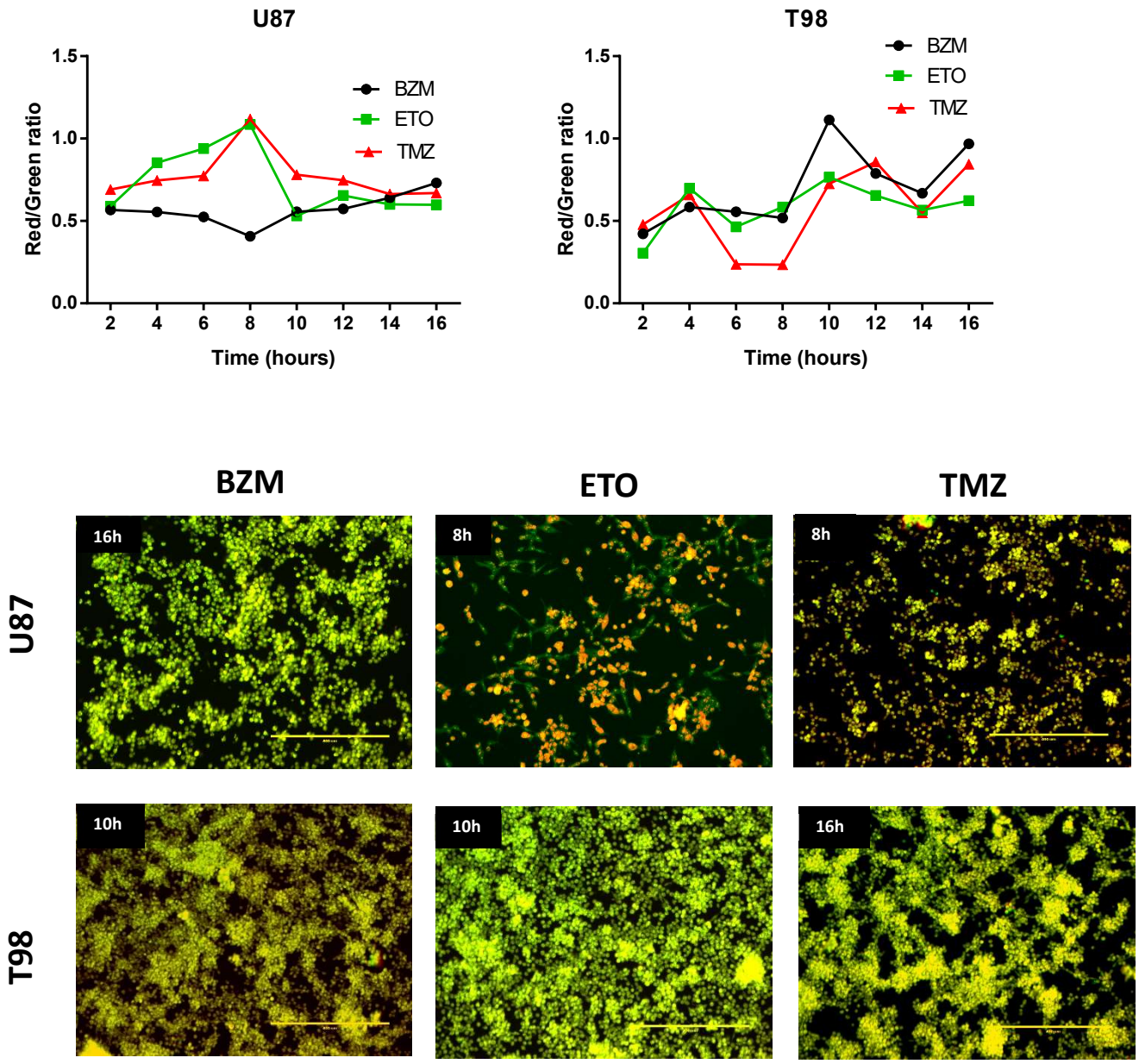

Figure 11. Red/Green ratio of measured fluorescence with acridine orange peaks at 8H for U87 and 10/12H for T98

TOP – Representative graph of U87 and T98 cell lines treated with BZM, ETO and TMZ for a time-course period. Data is shown as a ratio between red and green fluorescence (n =1). BOTTOM – Representative overlaid fluorescent acridine orange images of peak RG ratio. Green fluorescence represents spread A.O. and red fluorescence represents aggregated A.O. Overlaid images display orange as the superposition of red and green.

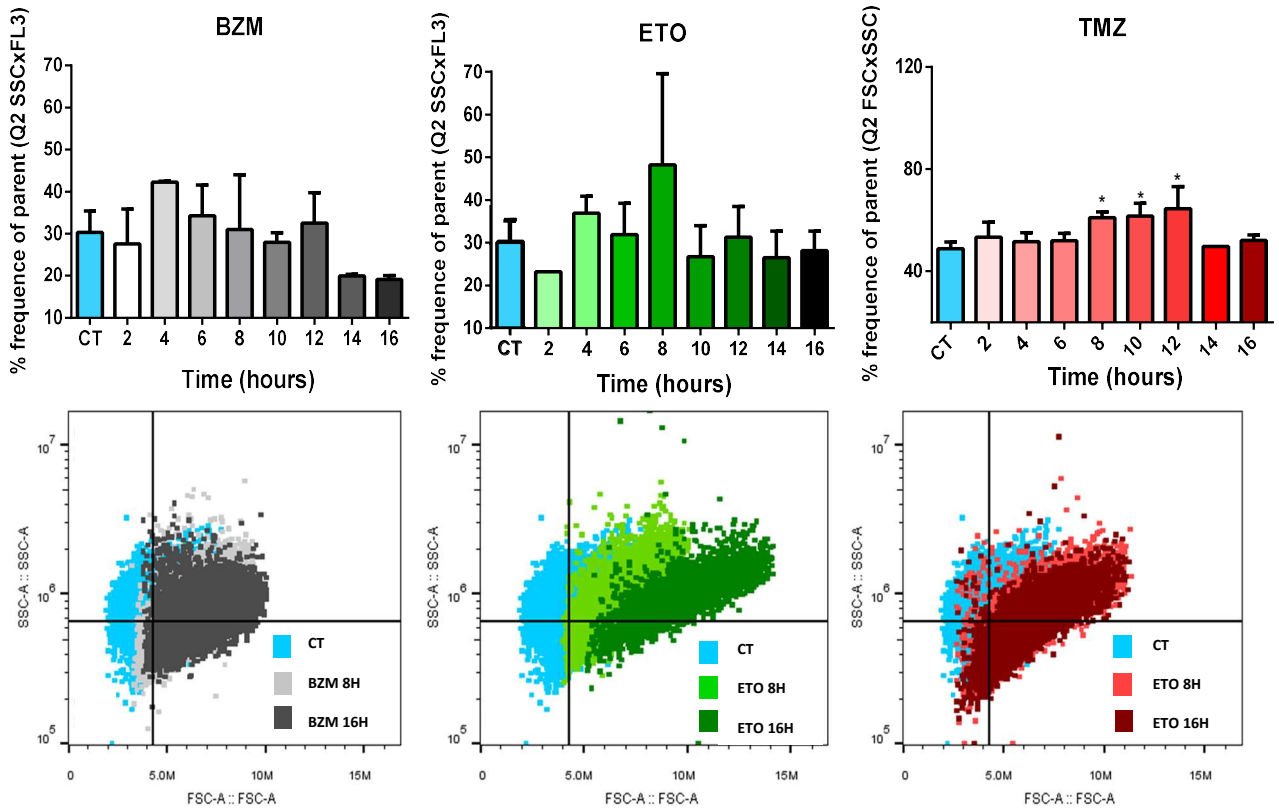

Figure 12. Acridine orange flow cytometry results show increased granularity and A.O. staining ate 8-12H for TMZ

TOP – Representative graphs of U87 cell line treated with BZM, ETO and TMZ in a time-course regimen. Data is shown as percentage of frequency of parent gated population (SSCxFL3). One-way ANOVA test was used, where * stands for $p < 0,05$. BOTTOM – Representative comparative-to-control dot-plots of 8 and 16 hours of treatment with all drugs.

AAU – Autophagy detection by lysosomal accumulation is modulated by G3BP1 knockdown

Lysosomal accumulation was used to detect autophagy levels on U87 G3BP1-knockdown cells, treated with BZM, ETO and TMZ. We used chloroquine (CQ), which is a medication used to prevent and treat malaria that also acts as an autophagy inhibitor. Our results show that our positive control betulinic acid (BA) indeed induced autophagy and had its effects reverted when CQ as employed. Interestingly, TMZ also had a significative increase in lysosomal accumulation but its effects were not reverted upon CQ usage.

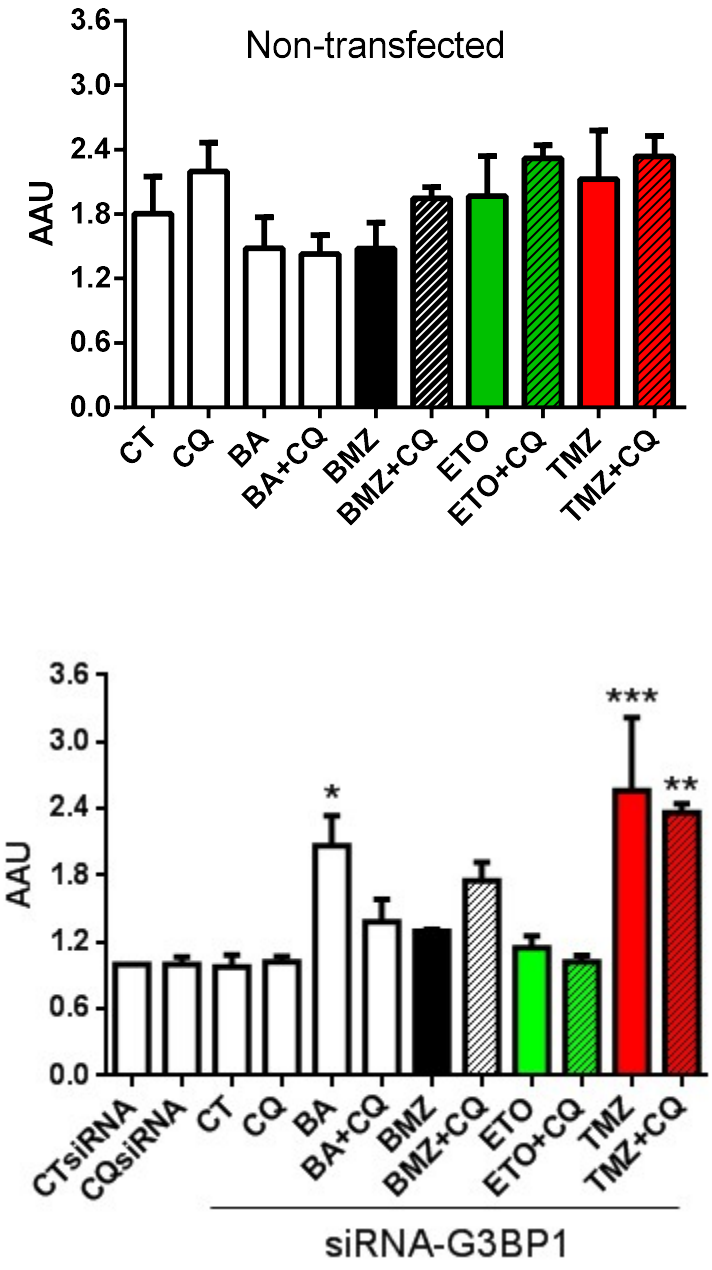

Figure 13.Increased AAU lysosomal accumulation in TMZ-treated siG3BP1 cells.

Graphical representation of lysosomal accumulation assay of U87 non-transfected (TOP) and transfected (BOTTOM) cells, treated with BZM, ETO, TMZ, BA and CQ. Data is shown as calculated AAU. Plain bars represent no transfection, striped bars represent G3BP1 knockdown and square bars represent CQ treatment. One-way ANOVA test was used, where ** stands for $p < 0,01$; and *** $p < 0,001$. Ns = not-significative.

LC3B protein detection as an early-autophagic marker

As A.O. results demonstrated “hot-spot” times of treatment of late-stage autophagy, we decided to take a step back and analyze LC3B (as an early autophagic state) status. We assessed by flow cytometry the mean of fluorescence of stained total LC3B proteins (FL1) to better comprehend the relation between them. Our results display increased total LC3B staining for TMZ U87 (6 hours) and T98 (8 hours) cells (Figure 16 TOP). Histograms show two distinctive fluorescence peaks of cells (Figure 16 BOTTOM).

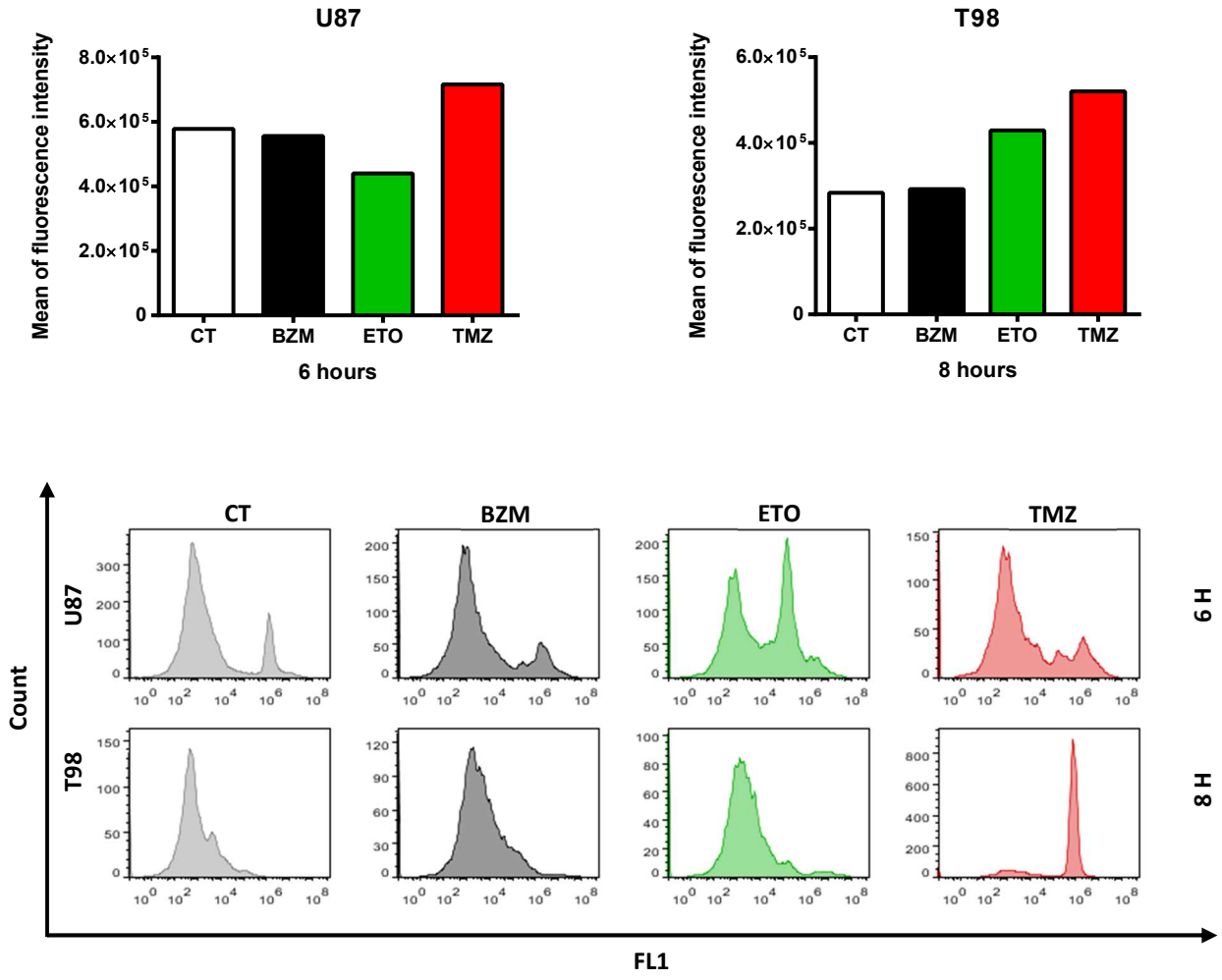

Figure 14. LC3B protein detection by flow cytometry reveals increased fluorescence in U87 TMZ-treated cells and in ETO and TMZ T98-treated cells

TOP –Graphical representation of U87 and T98 cell lines treated for 6 and 8 hours respectively with BZM, ETO and TMZ. Data is shown as mean of fluorescence intensity of FL1 channel (n=1). BOTTOM – Representative histograms of FL1 fluorescence.

Cultured media in CAM angiogenic histological assay

By silencing the G3BP1 expression in U87 GBM cells, the capacity of inducing angiogenesis was remarkably decreased in both vehicle control and BZM-treated cells when compared to siSCRAMBLE. Considering the siSCRAMBLE condition, upon BZM there was a slight enhance compared to control, but that significantly decreases when G3BP1 was silenced (Figure 13).

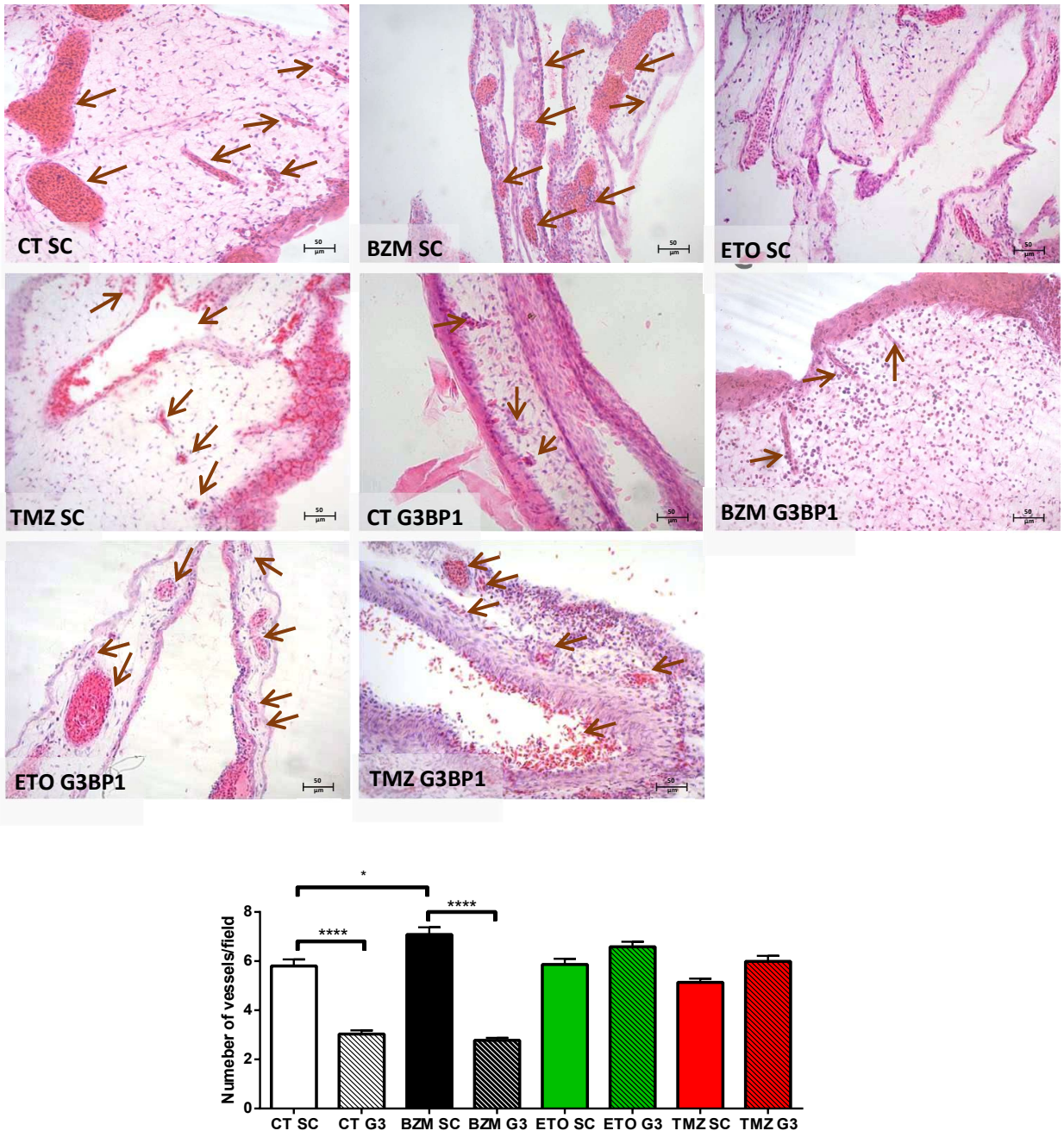

Figure 15. Increased angiogenesis caused by BZM treatment is reverted by G3BP1 knockdown in CAM assay

TOP - Representative hematoxylin-eosin stained histological images of CAMs incubated with conditioned media from siSCRAMBLE and siG3BP1 control and BZM, ETO and TMZ treated (24 hours) cells. Arrows indicate blood vessels. BOTTOM - Graphical representation of counted blood vessels per field. One-way ANOVA test was used, where * stands for $p < 0,05$; and **** $p < 0,0001$.

Angiogenic effects are VEGF-independent

Since we observed a decrease in angiogenesis, VEGF was quantified by ELISA with the same cultured media used in the CAM assay. Results were corrected with from MTT cell viability data in order to obtain a more accurate measure. No statistical difference was found between groups.

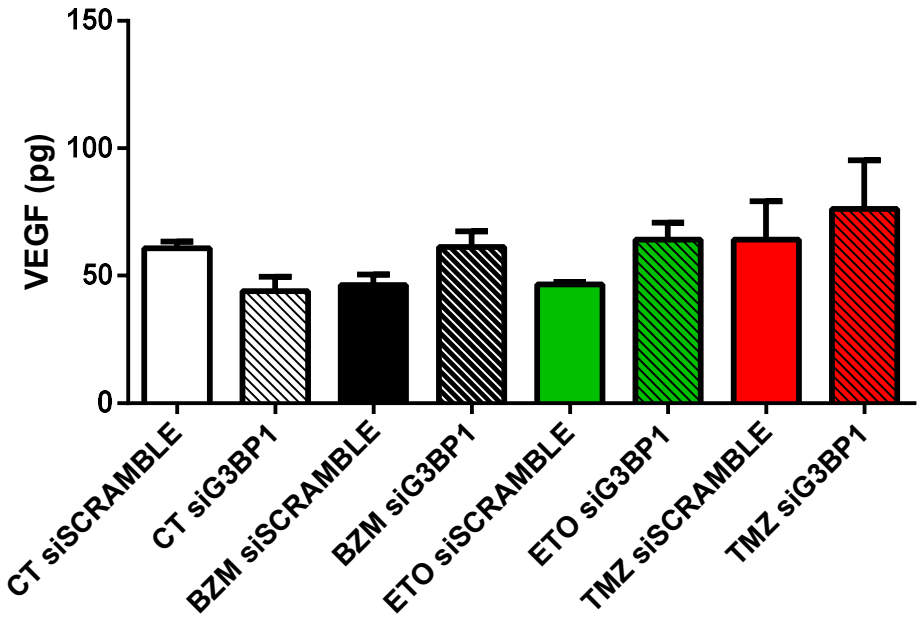

Figure 16. VEGF quantification reveals no significative differences amongst groups.

Graphical representation of VEGF quantification by ELISA assay of cultured media from U87 cell line treated with BZM, ETO and TMZ for 24 hours. Data is represented as pg of VEGF.

CD133+ content is high in U87 cell line

An important factor related to the angiogenic potential of GBM cell lines is the content of stem cells. In order to evaluate the percentage of steam cells in U87 cell line, we used flow cytometry to count CD133 (a classical hallmark membrane protein of steam cells) positive cells (VLASHI et al., 2009). Our results demonstrated a percentage of 15% in CD133+ cells in U87 population.

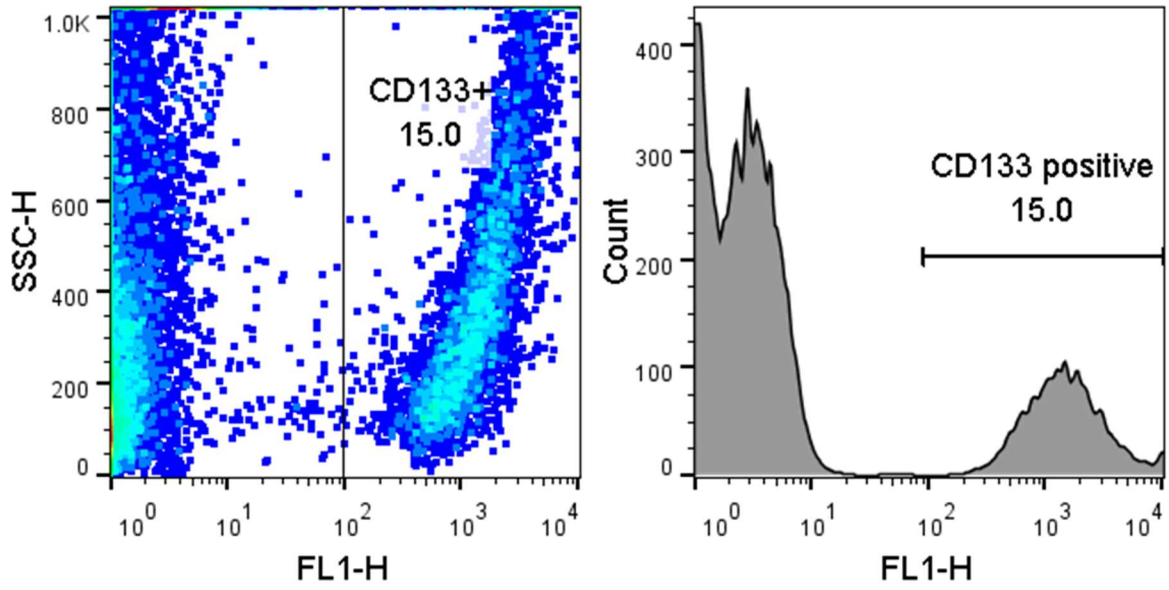

Figure 17. CD133+ cellular content in U87 cell line.

Representative dot-plot and histogram of CD133+ positive fluorescent marked cells in U87 cell line. Dot-plot is represented as cell size (SSC) x green fluorescence (FL1). Histogram is represented as count x green fluorescence (FL1).

Discussion

SGs play a vital role in the integrated stress response (ISR), that combine several information from stress sensors and coordinates adaptation to stress. The ISR detects several stressing factors such as amino acids deprivation via GCN2 (WEK; ZHU; WEK, 1995), reticulum stress via PERK (HARDING et al., 2000) and oxidative stress via HRI (MCEWEN et al., 2005). By doing so, tumor adapts to this aggressive microenvironment in order to maintain cell growth and resistance to chemotherapeutics.

Regarding cell growth, some cellular aspects such as hypoxia, hyperosmolarity and starvation are countered by inefficient and disorganized neovascularization of peritumoral area. Starved cells alternative is to uncouple glycolysis from oxidative phosphorylation to reduce dysregulation of protein synthesis that cause reticulum stress, an apoptotic trigger (PORPORATO et al., 2011). However, uncoupling glycolysis pathway from oxidative phosphorylation causes an important increase in oxidative stress, activating several antioxidative defense pathways such as NRF2/KEAP1, HIF1, HSF and p53 (GORRINI; HARRIS; MAK, 2013). Therefore, working with therapy-mimicking cell media (1% FBS) allowed us to better evaluate chemotherapeutic response as well as SGs role in a model closer to actual clinic reality.

It has been shown the redox imbalance caused by H_20_2 is able to induce SGs formation in a similar effect in cells as does sodium arsenite, the first described chemical able to induce SGs (ARIMOTO-MATSUZAKI; SAITO; TAKEKAWA, 2016; KEDERSHA et al., 1999). Different chemotherapeutic agents were described to also cause SG assembly like BZM (FOURNIER; GAREAU; MAZROUI, 2010) and from our previous article, Etoposide and Cisplatin (VILAS-BOAS et al., 2016). In doing so, cells acquire a drug-induced resistance to apoptosis dependent of SGs (GAREAU et al., 2011). This resistance is a very serious problem for patients as it renders chemotherapy not as potent as it should be. Hence, the importance of SGs formation inhibition to sensitize cancer cells to chemotherapeutic agents.

Using MTT, our results show important differences between cell lines IC50 as BZM U87 IC50 being 5-fold greater that T98 IC50 and T98 IC50 for ETO being 1,3-fold greater that IC50 of U87 cells. These data demonstrate cell line natural different sensitivity to treatments. Temozolomide is a special case, as U87 is a TMZ-sensitive cell line and T98 a TMZ-resistant cell lin. U87 IC50 is 13-fold greater than T98 IC50, confirming countless articles on the subject (ZHANG et al., 2011)(WANG et al., 2017)(JOHANNESSEN et al., 2013).

MTT has been widely utilized as a cytotoxicity test and even though its effectiveness and fidelity have been targeted in the past few years, few considerations should be stated. Being a metabolic-dependent assay, MTT reproducibility margin is higher in short-term treatments (24H) and non-DNA targeting drugs (BZM). As most chemotherapeutic agents tackle nuclear pathways, caution is required when interpreting MTT data prevenient from their usage. The drug TMZ has been tested in Glioblastoma cell lines such as U251 and for a 24-hour period of treatment, displayed no significative difference from manual trypan blue counting (STEPANENKO; DMITRENKO, 2015). For ETO, similar IC50 values have been reported from different cell viability assays, reassuring that in our case, MTT is a reliable test (AHMED et al., 2018).

SGs assembly occurs in a very dynamic way, initiating with nanoscopic SG seeds that are formed and recruit nearby seeds via weak electrostatic interactions, interactions with neighboring SG seeds, and coalescence to form irregular microscopically visible SGs. Microscopically visible SGs can fuse to produce larger SGs and after stress release, events that promote SG disassembly may include increase in concentrations of ternary complexes; phosphorylation of 4E-BP by mTOR, releasing the eIF4E block; and reactivation of eIF4A activities. As SGs shrink, the Laplace pressure increases to promote further fusion with adjacent SGs. Over time, fewer and larger SGs appear before they eventually disappear from the cytoplasm (PANAS; IVANOV; ANDERSON, 2016). The assembly and disassembly of SGs are controlled by several intracellular events such as inhibition RNA helicase eIF4A (KIM, Woo Jae; KIM; JANG, 2007), oxidative stress - promoting binding of 4EBP1 to eIF4E by promoting 4E-BP hypophosphorylation (EMARA et al., 2012) and situations where both eIF4F complex– and ph-eIF2α–mediated translation

inhibition contribute to SG assembly (treatment with antineoplastic vinca alkaloid drugs)(SZAFLARSKI et al., 2016).

In our case, we time-related SG dynamics with chemotherapeutic agents. SGs assembly occur earlier on U87 cell line, having its first score peak at 6 hours when treated with BZM and at 4 hours when treated with ETO and TMZ. Comparatively to T98 which shows later peaks at 8 hours for BZM and ETO. Temozolomide peak, however, occurred at the same time in both cell lines, indicating that despite the intrinsic differences between cell lines, TMZ activates stress response at the same time. Dynamically speaking, both cell lines showed a first fast and intense SGs assembly stress response followed by a minor later one. These results might be linked to different cellular downstream events of drugs influenced pathways.

The inhibition of G3BP1 mRNA levels using a short-interference RNA was challenging and brought us some insights. Not only G3BP1 mRNA levels were not diminishing with siRNA treatment at high concentration but we observed and increased expression. By lowering the final quantity of siRNA from 100pM to 0,1pM, inhibition of G3BP1 mRNA expression was achieved. The observed effect probably was caused by saturation of the RNAi machinery, which can happen in concentrations of 10–100 pM siRNA (corresponds to 10^3–10^4 dsRNA molecules). The transfection of exogenous siRNAs principally leads to competition for RISC binding between the endogenous microRNA (miRNA) pool and the exo-siRNAs. miRNA displacement influences the miRNA-mediated silencing and leads to an overall upregulation of miRNA-controlled genes. The preservation of robust silencing effects with lower dose is advantageous in terms of RISC competition (ALAGIA; ERITJA, 2016).

When siRNA inhibition of G3BP1 mRNA is employed, U87 cells demonstrate a clear negative viability ratio between drug treated cells that have been transfected with siG3BP1 and siSCRAMBLE ones, thus, evidencing the importance of this protein in chemotherapeutic resistance. These results corroborate with lung cancer (GAREAU et al., 2011), COS-7 cells, HeLa cells and HEK293 cell line (ARIMOTO, Kyoko et al., 2008) and others on literature that co-relate SGs presence/absence with drug potency.

Regarding cell cycle analysis, ETO was the only drug presenting statistic difference when compared to control groups. As it was previously described, ETO does cause an arrest in G2/M phase in U87, LN18 and U251 cells (DAS et al., 2007). This effect apparently is not G3BP1-dependent since no differences were observed between siG3BP1 and siSCRAMBLE groups.

The other two chemotherapeutic agents did not exhibit increased PS domains exposition, a possible explanation lies in TMZ as an alkylating agent mechanism, having a later (72 hours) effect in apoptotic induction in U87 and U251 cells (WU et al., 2018) Apoptotic secondary effects are time-dependent and are most commonly observed at 48 and 72 hours of treatment in other studies, in mice chondrosarcoma (BAO, Xing et al., 2017)and lymphoma cells (BEST et al., 2019). In this study, we were able to prove that by knocking down G3BP1 expression lead to an increased and significative apoptotic response observed as early as 24 hours. For the first time in literature, we describe that knocking down G3BP1 expression indeed sensitizes U87MG cells viability by potentializing and anticipating apoptotic response.

By analyzing number of vessels in CAM assay some interesting results were observed. Knocking down G3BP1 expression had an important role in the angiogenic capacity of U87 GBM cells, as comparative analysis clearly showed reduction in vessel numbers on control and BZM treated cells. The vessels number increase detected in comparing CT and BZM SCRAMBLE groups was prevented from happening when siG3BP1 was employed, thus demonstrating an angiogenic aspect of G3BP1 expression. Although an anti-angiogenic part of BZM has been described for myeloma cells (KIM, Choong et al., 2015) and myeloma microvesicles (GUO et al., 2018), GBM stem cells exposed to BZM have increased VEGF levels (BOTA et al., 2013). The mechanisms by which bortezomib evokes its antitumor activity may vary among tumor types, and the extent to which each affected pathway is critical to the inhibition of tumor growth could also differ (ADAMS, 2003). TMZ-resistance-induced stem cells, U251-MG and D54-MG (U251TR and D54TR) had high levels of VEGF in media when treated with BZM. Addition of bevacizumab - a VEGF blocking antibody which is now used as second-line GBM treatment was able to revert angiogenic increase in endothelial cells (BOTA et al., 2013). In this article we demonstrate an

unprecedented data that U87MG, a TMZ sensitive cell line also exerts anti-angiogenic effect when treated with BZM and this effect is abolished when G3BP1 protein expression is impaired. Even though our analyses conclude that there was no significative difference between groups in VEGF quantity, it is possible to modulate angiogenesis by other pathways. As SGs target RNA sequences, every mRNA is prone to regulation by this patwahy. The targeting efficiency varies from 1-95%, as extensively reviewed on the SG transcriptome (KHONG et al., 2017). Although many molecules can modulate angiogenesis like fibroblast growth factor (FGF), tumor necrosis factor-alpha (TNF-α), transforming growth factor-beta (TGF-β), and the angiopoietins (Ang) (UCUZIAN et al., 2010), we must consider miRNAs as a possible pathway influencing this event (BEYER et al., 2017). There are several "angio-mRNAs" described in literature: miR-7 a down-regulated miR that targets EGFR, IRS-1, IRS-2, FAK, OGR and inhibits angiogenesis which overexpression decreases cell proliferation and angiogenesis in U87 cells *in vitro* and in tumor xenograft model (MØLLER et al., 2013); miR-296 an up-regulated HGS targeting miR that promotes angiogenesis described which overexpression promotes angiogenesis *in vitro* and in a tumor xenograft model in vivo (ONISHI et al., 2011); and many other such as miR-15b (KARSY; ARSLAN; MOY, 2012) and miR-93 (SILBER; JAMES; HODGSON, 2009).

Another probable pathway involves glioma stem-cells, known as cancer stem cells (CSC). It has been observed that CD133 enriched CSC are located in proximity to blood vessels. Compared with CD133- CSC, CD133+ CSC generate tumors with increasing tumor vascularity, necrosis and hemorrhage (BAO, Shideng et al., 2006). The VEGF expression in CD133+ CSC is up-regulated, combined with a dramatically increased vascular density. Furthermore, therapy with VEGF neutralizing antibody (bevacizumab) can deplete CSC-induced vascular endothelial cell migration and tube formation (RIBATTI, 2012).

Most of published works to this date correlates indirect apoptotic modulation with altered SG dynamics. Some studies have demonstrated that SGs are responsible for inhibiting apoptosis by diminishing oxidative stress *in vivo* and therefore reducing overall cellular stress state (ARIMOTO, Suguru, 2008), or the increase in AIF, modulating the balance between NAD(P)H and glutathione (GSH) (CANDÉ et al.,

2004) and mutation of progranulin (PGRN) inflammatory gene, causing a mis-sorting in the protein angiogenin (ANG) a stress-response factor and neurodegenerative disease-related protein (LI, Siqi et al., 2018), for example.

Glioblastomas are characterized by extensive tissue hypoxia, which contributes to resistance to irradiation, the most effective therapeutic modality for patients with glioblastoma. Presence of low oxygen content in tumor tissues impedes radiation induced generation of free radicals that assert antitumor effect (SHEEHAN et al., 2010). Hypoxia may further contribute to tumor pathogenesis by promoting genomic instability. In certain mammalian cells, low oxygen environment can attenuate expression of DNA mismatch repair genes, which may then promote acquisition of additional gene mutations (COLWELL et al., 2017). Driven by these mechanisms, hypoxia is associated with a more aggressive tumor phenotype. The immediate adaptive cellular response to low levels of oxygen is the stabilization of transcription factors known as hypoxia inducible factors (HIFs) (MIHAYLOVA et al., 2003).

Autophagy plays a vital role in SGs dynamics, being responsible for SGs clearance after cellular stress, allowing SGs disassembly. Defective and inefficient SGs are observed when autophagy is inhibited (SEGUIN et al., 2014).

Results of cell granularity and size reveled a coincidental modulation of SGs expression e granularity in chemotherapeutic agents treated U87 cells. Increased granularity may be linked to augmented autophagic response as more autophagosomes are produced in cytoplasm (SHTEINGAUZ et al., 2018).

The role of autophagy in cancer is complex (HØYER-HANSEN; JÄÄTTELÄ, 2008). Autophagy can have a tumor suppressive function at early stages of cancer development and promote tumor cell survival in established tumors (APEL et al., 2009). Autophagy also facilitates the resistance of tumor cells to anticancer agents (SUI et al., 2013) and to radiation (CHAACHOUAY et al., 2011), causing malignant transformation and spontaneous tumors (DALBY et al., 2010). Recent studies have demonstrated that the inhibition of autophagy in cancer cells may be therapeutically beneficial in some circumstances, as it can

sensitize cancer cells to different therapies, including DNA-damaging agents, antihormone therapies (e.g., tamoxifen), and radiation therapy (DALBY et al., 2010).

Autophagy has either a pro-survival (oncogenic) or pro-death (tumor suppressive) role at different cancer stages, including cancer stem cell (CSC), initiation and progression, invasion and metastasis, and dormancy. Autophagy may modulate a series of oncogenic and tumor suppressive pathways in cancer, implicated in microRNA (miRNA) involvement. Targeting the oncogenic and tumor suppressive autophagic network would be a new promising therapeutic strategy (LIU; WEN; CHENG, 2013).

Our A.O. results demonstrate an increase in acidic vesicles at time-points with lower SG assembly. This data corroborate with SGs dynamics as autophagy is responsible for SG clearance/disassembly (SEGUIN et al., 2014). During autophagy, autophagosomes internalize cytoplasmic components such as cytosolic proteins and organelles. Concomitantly, a cytosolic form of LC3B (LC3-I) is conjugated to phosphatidylethanolamine to form LC3-phosphatidylethanolamine conjugate (LC3-II), which is recruited to autophagosome membranes. Autophagosomes fuse with lysosomes to form autolysosomes, and components are degraded by lysosomal hydrolases. At the same time, LC3-II in auto lysosomal lumen is degraded. Thus, lysosomes with LC3-II containing-membranes reflects starvation induced autophagic activity, and the detection of LC3B by immunoblotting or immunofluorescence has become a reliable method for monitoring autophagy and autophagy-related processes, including autophagic cell death (TANIDA; UENO; KOMINAMI, 2008). Being aware of this dynamic, we decided to evaluate LC3B levels in a time-point prior to observed peak in A.O. When analyzing LC3B we could clearly observe two peaks, one with low fluorescence and one with high fluorescence. LC3B measurement by flow cytometry has been utilized in Jurkat cells (WARNES, 2015). However, since we utilized a total LC3B antibody we cannot tell which fluorescence intensity represents which LC3B fraction, I or II. Additional experiments should be made in the future to address this technical limitation.

With AAU, a screening combined assay that combines 3 widely-used techniques MTT, neutral red and crystal violet staining to assess general autophagic response in cells (MARTINS et al., 2013, 2017) we

were able to observe increased autophagic response on U87 cells treated with TMZ. Chloroquine has a long history of human use and is currently being tested as a sensitizing agent for certain cancers, making understanding its mechanisms of action both topical and important (KIMURA et al., 2013). Chloroquine is a lysosomotropic weak base, which in the monoprotonated form diffuses into the lysosome, where it becomes deprotonated and becomes trapped. Protonated chloroquine then changes the lysosomal pH, thereby inhibiting autophagic degradation in the lysosomes (HOMEWOOD et al., 1972). As CQ did not revert TMZ autophagy induction, some questions have risen as: are TMZ-induced autophagosomes more resistant by G3BP1 inhibition? Does SG impairment also potentialize autophagy? These questions are important to better understand our observed data. Attempting to answer these questions a recent article concerning autophagy and SGs in Alzheimer disease found that environmental stress and glucocorticoid (GC) disturb cellular homeostasis and trigger the insoluble accumulation of different RBPs, such as PABP, G3BP1, TIA-1, and FUS, shown to form SGs and Tau aggregation. Interestingly, an mTOR-driven pharmacological stimulation of autophagy attenuates the GC-driven accumulation of Tau and SG-related proteins as well as the related cell death, suggesting a critical interface between autophagy and the response of the SG-related protein in the neurodegenerative potential of chronic stress and GC (SILVA et al., 2018).

Better understanding of underlying pathways concerning observed apoptotic increase are extremely important to a global vision of cellular events. Further autophagic and oxidative stress events will be tackled in future publications from our group.

Conclusion

- G3BP1 knockdown reduces U87MG cell viability when treated with BZM, ETO and TMZ
- Apoptosis is potentialized upon G3BP1 knockdown in U87MG cells treated with BZM
- Angiogenesis is diminished in U87MG cells treated with BZM and subjected do G3BP1 knockdown
- Autophagy is positively modulated in U87MG cells treated with TMZ

This work reveals new and exciting information that sure will help in developing new therapies and improve the ones already in use.

References

ADAMS, Julian. **Potential for proteasome inhibition in the treatment of cancer**. **Drug Discovery Today**. [S.l: s.n.]. , 2003

AHMED, Eroje M. et al. A HIF-independent, CD133-mediated mechanism of cisplatin resistance in glioblastoma cells. **Cellular Oncology**, 2018.

ALAGIA, Adele; ERITJA, Ramon. **siRNA and RNAi optimization**. **Wiley Interdisciplinary Reviews: RNA**. [S.l: s.n.]. , 2016

AMERICAN TYPE CULTURE COLLECTION. MTT Cell Proliferation Assay Instruction Guide. **Components**, v. 6597, p. 1–6, 2011.

APEL, Anja et al. **Autophagy - A double-edged sword in oncology**. **International Journal of Cancer**. [S.l: s.n.]. , 2009

ARIMOTO-MATSUZAKI, Kyoko; SAITO, Haruo; TAKEKAWA, Mutsuhiro. TIA1 oxidation inhibits stress granule assembly and sensitizes cells to stress-induced apoptosis. **Nature Communications**, v. 7, p. 1–10, 2016. Disponível em: <http://dx.doi.org/10.1038/ncomms10252>.

ARIMOTO, Kyoko et al. Formation of stress granules inhibits apoptosis by suppressing stress-responsive MAPK pathways. **Nature cell biology**, v. 10, n. 11, p. 1324–1332, 2008.

ARIMOTO, Suguru. **Control theory of multi-fingered hands: A modelling and analytical-mechanics approach for dexterity and intelligence**. [S.l: s.n.], 2008.

BAO, Shideng et al. Stem cell-like glioma cells promote tumor angiogenesis through vascular endothelial growth factor. **Cancer Research**, 2006.

BAO, Xing et al. Bortezomib induces apoptosis and suppresses cell growth and metastasis by inactivation

of Stat3 signaling in chondrosarcoma. **International Journal of Oncology**, v. 50, n. 2, p. 477–486, 2017.

BEST, Scott et al. Targeting ubiquitin-activating enzyme induces ER stress–mediated apoptosis in B-cell lymphoma cells. **Blood Advances**, v. 3, n. 1, p. 51–62, 2019. Disponível em: <http://www.bloodadvances.org/lookup/doi/10.1182/bloodadvances.2018026880>.

BEYER, Sasha et al. **The Role of miRNAs in angiogenesis, invasion and metabolism and their therapeutic implications in gliomas**. **Cancers**. [S.l: s.n.]. , 2017

BOTA, Daniela A et al. Proteasome inhibition with bortezomib induces cell death in GBM stem-like cells and temozolomide-resistant glioma cell lines, but stimulates GBM stem-like cells' VEGF production and angiogenesis. **Journal of Neurosurgery**, 2013.

BROWN, Ronald; MOTULSKY, Harvey. Detecting outliers when fitting data with nonlinear regression - a new method based on robust nonlinear regression and the false discovery rate. **BMC Bioinformatics**, v. 7, n. 1, p. 1–20, 2006. Disponível em: <http://dx.doi.org/10.1186/1471-2105-7-123>.

BUCHAN, J Ross. mRNP granules. Assembly, function, and connections with disease. **RNA biology**, v. 11, n. 8, p. 1019–30, 2014. Disponível em: <http://www.ncbi.nlm.nih.gov/pubmed/25531407%5Cnhttp://www.pubmedcentral.nih.gov/articlerender.fcgi?artid=PMC4615263>.

CANDÉ, Céline et al. AIF and cyclophilin A cooperate in apoptosis-associated chromatinolysis. **Oncogene**, 2004.

CHAACHOUAY, Hassan et al. Autophagy contributes to resistance of tumor cells to ionizing radiation. **Radiotherapy and Oncology**, 2011.

CHAN, Shu Ning; TANG, Bor Luen. Location and membrane sources for autophagosome formation-from ER-mitochondria contact sites to Golgi-endosome-derived carriers. **Molecular Membrane Biology**, 2013.

COLWELL, Nicole et al. Hypoxia in the glioblastoma microenvironment: Shaping the phenotype of cancer stem-like cells. **Neuro-Oncology**, 2017.

DALBY, Kevin N. et al. **Targeting the prodeath and prosurvival functions of autophagy as novel therapeutic strategies in cancer**. **Autophagy**. [S.l: s.n.]. , 2010

DAS, Chandra M. et al. Valproic acid induces p21 and topoisomerase-II (α/β) expression and synergistically enhances etoposide cytotoxicity in human glioblastoma cell lines. **Journal of Neuro-Oncology**, v. 85, n. 2, p. 159–170, 2007.

EMARA, Mohamed M. et al. Hydrogen peroxide induces stress granule formation independent of eIF2α phosphorylation. **Biochemical and Biophysical Research Communications**, 2012.

FOURNIER, Marie-Josée; GAREAU, Cristina; MAZROUI, Rachid. The chemotherapeutic agent bortezomib induces the formation of stress granules. **Cancer cell international**, v. 10, p. 12, 2010.

FURNARI, Frank B. et al. **Malignant astrocytic glioma: Genetics, biology, and paths to treatment**. **Genes and Development**. [S.l: s.n.]. , 2007

GAREAU, Cristina et al. P21waf1/cip1 upregulation through the stress granule-associated protein CUGBP1 confers resistance to bortezomib-mediated apoptosis. **PLoS ONE**, 2011.

GORRINI, Chiara; HARRIS, Isaac S.; MAK, Tak W. Modulation of oxidative stress as an anticancer strategy. **Nature Reviews Drug Discovery**, v. 12, n. 12, p. 931–947, 2013. Disponível em: <http://www.nature.com/doifinder/10.1038/nrd4002>.

GUO, Hui Mei et al. Microvesicles shed from bortezomib-treated or lenalidomide-treated human myeloma cells inhibit angiogenesis in vitro. **Oncology Reports**, 2018.

HARDING, Heather P. et al. Perk is essential for translational regulation and cell survival during the unfolded protein response. **Molecular Cell**, v. 5, n. 5, p. 897–904, 2000.

HOMEWOOD, C. A. et al. **Lysosomes, pH and the anti-malarial action of chloroquine [9]**. **Nature**. [S.l: s.n.]. , 1972

HØYER-HANSEN, Maria; JÄÄTTELÄ, Marja. **Autophagy: An emerging target for cancer therapy**. **Autophagy**. [S.l: s.n.]. , 2008

INCA. **Estimativa 2018: incidência de câncer no Brasil / Instituto Nacional de Câncer José Alencar Gomes da Silva. Coordenação de Prevenção e Vigilância. – Rio de Janeiro: INCA, 2017.** [S.l: s.n.], 2017.

JOHANNESSEN, Tor Christian Aase et al. The DNA repair protein ALKBH2 mediates temozolomide resistance in human glioblastoma cells. **Neuro-Oncology**, 2013.

KARSY, Michael; ARSLAN, Erol; MOY, Fred. **Current Progress on Understanding MicroRNAs in Glioblastoma Multiforme**. **Genes and Cancer**. [S.l: s.n.]. , 2012

KEDERSHA, Nancy L et al. eIF-2 to the Assembly of Mammalian Stress Granules. **The Journal of Cell biology**, v. 147, n. 7, p. 1431–1441, 1999.

KHONG, Anthony et al. The Stress Granule Transcriptome Reveals Principles of mRNA Accumulation in Stress Granules. **Molecular Cell**, 2017.

KIM, Choong et al. A quantitative microfluidic angiogenesis screen for studying anti-angiogenic therapeutic drugs. **Lab on a Chip**, 2015.

KIM, Woo Jae; KIM, Joon Hyun; JANG, Sung Key. Anti-inflammatory lipid mediator 15d-PGJ2 inhibits translation through inactivation of eIF4A. **EMBO Journal**, 2007.

KIMURA, Tomonori et al. **Chloroquine in cancer therapy: A double-edged sword of autophagy**. **Cancer Research**. [S.l: s.n.]. , 2013

KU, Sook Hee et al. Tumor-targeting multifunctional nanoparticles for sirna delivery: Recent advances in

cancer therapy. **Advanced Healthcare Materials**, v. 3, n. 8, p. 1182–1193, 2014.

LAVUT, Anna; RAVEH, Dina. Sequestration of highly expressed mrnas in cytoplasmic granules, p-bodies, and stress granules enhances cell viability. **PLoS Genetics**, v. 8, n. 2, 2012.

LI, Ping et al. MiR-181b suppresses proliferation of and reduces chemoresistance to temozolomide in U87 glioma stem cells. **Journal of Biomedical Research**, v. 24, n. 6, p. 436–443, 2010.

LI, Siqi et al. Angiogenin Prevents Progranulin A9D Mutation-Induced Neuronal-Like Cell Apoptosis Through Cleaving tRNAs into tiRNAs. **Molecular Neurobiology**, 2018.

LIU, B.; WEN, X.; CHENG, Y. **Survival or death: Disequilibrating the oncogenic and tumor suppressive autophagy in cancer**. **Cell Death and Disease**. [S.l: s.n.]. , 2013

MALHOTRA, Anshoo; MITTAL, Bhagwant Rai. SiRNA gene therapy using albumin as a carrier. **Pharmacogenetics and Genomics**, v. 24, n. 12, p. 582–587, 2014. Disponível em: <http://content.wkhealth.com/linkback/openurl?sid=WKPTLP:landingpage&an=01213011-201412000-00002>.

MARTINS, Waleska K. et al. Membrane damage by betulinic acid provides insights into cellular aging. **Biochimica et Biophysica Acta (BBA) - General Subjects**, v. 1861, n. 1, p. 3129–3143, 2017. Disponível em: <http://linkinghub.elsevier.com/retrieve/pii/S0304416516303932>.

_____. Rapid screening of potential autophagic inductor agents using mammalian cell lines. **Biotechnology Journal**, 2013.

MATSUKI, Hideaki et al. Both G3BP1 and G3BP2 contribute to stress granule formation. **Genes to Cells**, v. 18, n. 2, p. 135–146, 2013.

MCEWEN, Edward et al. Heme-regulated inhibitor kinase-mediated phosphorylation of eukaryotic translation initiation factor 2 inhibits translation, induces stress granule formation, and mediates survival upon arsenite exposure. **Journal of Biological Chemistry**, v. 280, n. 17, p. 16925–16933, 2005.

MIHAYLOVA, V. T. et al. Decreased Expression of the DNA Mismatch Repair Gene Mlh1 under Hypoxic Stress in Mammalian Cells. **Molecular and Cellular Biology**, 2003.

MØLLER, Heidi G. et al. **A systematic review of MicroRNA in glioblastoma multiforme: Micro-modulators in the mesenchymal mode of migration and invasion**. **Molecular Neurobiology**. [S.l: s.n.]. , 2013

OHGAKI, Hiroko. **Epidemiology of brain tumors**. **Methods in Molecular Biology**. [S.l: s.n.]. , 2009

OLIVEIRA, Amanda Gleyce de Lima et al. Chorioallantoic membrane assays (HET-CAM and CAM-TBS): alternative tests for performing toxicological evaluation of products with low potential for ocular irritation. **Revista do Instituto Adolfo Lutz**, v. 71, n. 1, p. 153–159, 2012.

ONISHI, Manabu et al. **Angiogenesis and invasion in glioma**. **Brain Tumor Pathology**. [S.l: s.n.]. , 2011

OSTROM, Quinn T. et al. The epidemiology of glioma in adults: A state of the science review. **Neuro-Oncology**, v. 16, n. 7, p. 896–913, 2014.

PANAS, Marc D.; IVANOV, Pavel; ANDERSON, Paul. **Mechanistic insights into mammalian stress granule dynamics**. **Journal of Cell Biology**. [S.l: s.n.]. , 2016

PIETRANI, Nathalia T. et al. Proresolving protein Annexin A1: The role in type 2 diabetes mellitus and obesity. **Biomedicine and Pharmacotherapy**, v. 103, n. April, p. 482–489, 2018. Disponível em: <https://doi.org/10.1016/j.biopha.2018.04.024>.

PORPORATO, Paolo E. et al. Anticancer targets in the glycolytic metabolism of tumors: A comprehensive review. **Frontiers in Pharmacology**, v. AUG, 2011.

RIBATTI, Domenico. Cancer stem cells and tumor angiogenesis. **Cancer Letters**, v. 321, n. 1, p. 13–17, 2012.

RICCARDI, Carlo; NICOLETTI, Ildo. Analysis of apoptosis by propidium iodide staining and flow cytometry. **Nature Protocols**, v. 1, n. 3, p. 1458–1461, 2006.

SCORRANO, Luca. **Keeping mitochondria in shape: A matter of life and death**. **European Journal of Clinical Investigation**. [S.l: s.n.]. , 2013

SEGUIN, S J et al. Inhibition of autophagy, lysosome and VCP function impairs stress granule assembly. **Cell Death and Differentiation**, v. 21, n. 12, p. 1838–1851, 2014. Disponível em: <http://www.nature.com/doifinder/10.1038/cdd.2014.103>.

SHEEHAN, Jason P. et al. **Improving the radiosensitivity of radioresistant and hypoxic glioblastoma**. **Future Oncology**. [S.l: s.n.]. , 2010

SHTEINGAUZ, Anna et al. AMPK-dependent autophagy upregulation serves as a survival mechanism in response to Tumor Treating Fields (TTFields). **Cell Death and Disease**, 2018.

SILBER, Joachim; JAMES, C. David; HODGSON, J. Graeme. **microRNAs in gliomas: small regulators of a big problem. Neuromolecular medicine**. [S.l: s.n.]. , 2009

SILVA, Joana Margarida *et al.* Dysregulation of autophagy and stress granule-related proteins in stress-driven Tau pathology. **Cell Death and Differentiation**, 2018.

STEPANENKO, A. A.; DMITRENKO, V. V. Pitfalls of the MTT assay: Direct and off-target effects of inhibitors can result in over/underestimation of cell viability. **Gene**, 2015.

SUI, X. et al. **Autophagy and chemotherapy resistance: A promising therapeutic target for cancer treatment**. **Cell Death and Disease**. [S.l: s.n.]. , 2013

SZAFLARSKI, Witold et al. Vinca alkaloid drugs promote stress-induced translational repression and stress granule formation. **Oncotarget**, 2016.

TANIDA, Isei; UENO, Takashi; KOMINAMI, Eiki. LC3 and autophagy. **Methods in Molecular**

Biology, 2008.

UCUZIAN, Areck A. et al. **Molecular mediators of angiogenesis**. **Journal of Burn Care and Research**. [S.l: s.n.]. , 2010

VILAS-BOAS, Fabrício de Almeida Souza et al. Impairment of stress granule assembly via inhibition of the eIF2alpha phosphorylation sensitizes glioma cells to chemotherapeutic agents. **Journal of Neuro-Oncology**, 2016.

VLASHI, Erina et al. In vivo imaging, tracking, and targeting of cancer stem cells. **Journal of the National Cancer Institute**, v. 101, n. 5, p. 350–9, 4 mar. 2009. Disponível em: <http://www.pubmedcentral.nih.gov/articlerender.fcgi?artid=2727141&tool=pmcentrez&rendertype=abstract>. Acesso em: 2 jun. 2013.

WANG, Hsiao Han et al. GADD45A plays a protective role against temozolomide treatment in glioblastoma cells. **Scientific Reports**, 2017.

WARNES, G. Flow cytometric assays for the study of autophagy. **Methods**, v. 82, n. April, p. 21–28, 2015. Disponível em: <http://dx.doi.org/10.1016/j.ymeth.2015.03.027>.

WEK, S A; ZHU, S; WEK, R C. The histidyl-tRNA synthetase-related sequence in the eIF-2 alpha protein kinase GCN2 interacts with tRNA and is required for activation in response to starvation for different amino acids. **Molecular and cellular biology**, v. 15, n. 8, p. 4497–506, 1995. Disponível em: <http://www.pubmedcentral.nih.gov/articlerender.fcgi?artid=230689&tool=pmcentrez&rendertype=abstract>.

WHEELER, Joshua R et al. Distinct stages in stress granule assembly and disassembly. **eLife**, 2016.

WU, Qinghua et al. Study on Therapeutic Action and Mechanism of TMZ Combined with RITA Against Glioblastoma. **Cellular physiology and biochemistry : international journal of experimental cellular physiology, biochemistry, and pharmacology**, v. 51, n. 6, p. 2536–2546, 2018. Disponível em:

<https://www.karger.com/Article/FullText/495923%0Ahttp://www.ncbi.nlm.nih.gov/pubmed/30562758>

.

ZHANG, Mengxian et al. Trimodal Glioblastoma Treatment Consisting of Concurrent Radiotherapy, Temozolomide, and the Novel TGF-β Receptor I Kinase Inhibitor LY2109761. **Neoplasia**, v. 13, n. 6, p. 537-IN14, 2011. Disponível em: <http://linkinghub.elsevier.com/retrieve/pii/S147655861180045X>.